INFORMATION TO USERS

This manuscript has been reproduced from the microfilm master. UMI films the text directly from the original or copy submitted. Thus, some thesis and dissertation copies are in typewriter face, while others may be from any type of computer printer.

The quality of this reproduction is dependent upon the quality of the copy submitted. Broken or indistinct print, colored or poor quality illustrations and photographs, print bleedthrough, substandard margins, and improper alignment can adversely affect reproduction.

In the unlikely event that the author did not send UMI a complete manuscript and there are missing pages, these will be noted. Also, if unauthorized copyright material had to be removed, a note will indicate the deletion.

Oversize materials (e.g., maps, drawings, charts) are reproduced by sectioning the original, beginning at the upper left-hand corner and continuing from left to right in equal sections with small overlaps. Each original is also photographed in one exposure and is included in reduced form at the back of the book.

Photographs included in the original manuscript have been reproduced xerographically in this copy. Higher quality 6" x 9" black and white photographic prints are available for any photographs or illustrations appearing in this copy for an additional charge. Contact UMI directly to order.

UMI

A Bell & Howell Information Company
300 North Zeeb Road, Ann Arbor MI 48106-1346 USA
313/761-4700 800/521-0600

Université d'Ottawa · University of Ottawa

EXPERIMENTAL AND THEORETICAL STUDIES OF THE EFFECTS OF BUOYANCY FORCES ON LIQUID/LIQUID DISPLACEMENT PROCESSES IN POROUS MEDIA

Tianle Guo

A thesis submitted to the School of Graduate Studies and Research
in partial fulfillment of the requirements for the
degree of
DOCTOR OF PHILOSOPHY
in the Department of Chemical Engineering
University of Ottawa

Abstract

When a higher-viscosity fluid is displaced by a lower-viscosity fluid in a porous medium, the displacing fluid tends to channel through the paths of lesser hydrodynamic resistance, thereby forming pronounced "fingers". The effects of buoyancy (gravity) forces on the stability of such displacement processes are of considerable importance in many practical situations, especially during the recovery of oil from underground reservoirs, or during the clean-up of subterranean toxic chemical spills, by means of aqueous fluid injection. The present work is confined to the former (i.e., oil recovery) situation.

In this work, the effects of buoyancy forces on immiscible water/oil displacement processes and miscible oil/oil displacement processes were studied for linear flows occurring in a two-dimensional, consolidated, transparent porous medium aligned in either the vertical or horizontal plane. Experiments were performed using three different flow modes, namely horizontal, vertical-upwards and vertical-downwards. A wide range of injection flow rates were employed in order to elucidate the relative effects of buoyancy forces, viscous forces and capillary forces. For each displacement, the breakthrough condition was measured, and photographs of the evolving fingering patterns were taken.

A mathematical analysis of the observed displacement phenomena produced an analytical relationship expressing the macroscopic water saturation profile as a function of dimensionless distance. The horizontal flow mode was employed as the reference condition for the prediction of the oil recovery efficiency in the two vertical flow modes, since buoyancy forces can be effectively neglected in horizontal flow. A reliable technique for measuring the saturation profile from the displacement photographs was developed in order to interpret the experimental data. Good agreement between the theoretical and experimental results was obtained, thereby permitting a reliable quantitative prediction of the effects of buoyancy forces on oil recovery during immiscible water/oil displacement processes.

The extent to which the viscosity ratio, interfacial tension, and flow rate influenced the relative effects of the buoyancy forces will be discussed in relation to measured breakthrough times and oil recoveries. Also, the instability theory of the displacement will be discussed. It is evident from the results obtained that buoyancy forces are capable of exerting very significant effects on the stability of liquid-liquid displacement processes occurring in porous media, on the formation of fingers, and on the ultimate oil recovery efficiency during practical oil recovery processes involving aqueous fluid injection.

Abstrait

Dans un milieu poreux, quand un fluide moins visqueux déplace un fluide plus visqueux, il tend à canaliser à travers des voies où la résistance hydrodynamique est moins élevée. De ce fait, ce fluide forme "des doigts" bien marqués. Les effets des forces de poussée (gravité) sur la stabilité de ces processus de déplacement ont une importance considérable dans plusieurs situations pratiques, surtout durant la récupération de pétrole des réservoirs souterrains, ou durant le nettoyage des déversements souterrains d'un produit chimique toxique, à l'aide de l'injection d'un fluide aqueux. Dans ce travail, on se limite à discuter seulement la dernière situation (c. à. d., la récupération de pétrole).

Dans cette ouvrage, on a étudié les effets des forces de poussée sur les processus de déplacement du systéme immiscible (eau/pétrole) et du systéme miscible (pétrole/pétrole) pour des écoulements linéaires, ayant lieu dans un milieu poreux à deux dimensions, consolidé, transparent et aligné soit en plan vertical ou horizontal. On a accompli les expériences en utilisant trois différents modes d'écoulement, à savoir horizontal, vertical ascendant et vertical descendant. On a utilisé de larges écarts de taux d'écoulement des injections afin d'élucider les effets relatifs des forces de poussée, des forces visqueuses et des forces capillaires. Pour chaque déplacement, on a mesuré les conditions de percée, et on a aussi photographié le développement des motifs en forme de doigts.

L'analyse mathématique du phénoméne de déplacement observé a produit une relation analytique exprimant le profile macroscopique de la saturation de l'eau en fonction de la distance adimensionnelle. On a utilisé le mode d'écoulement horizontal comme condition de référence pour prédire l'efficacité de la récupération de pétrole dans les deux modes d'écoulement vertical, puisque les forces de poussée peuvent effectivement être négligé dans l'écoulement horizontal. On a dévelopé une technique fiable pour mesurer le profil de saturation obtenu des photographies du déplacement afin d'interpréter les données expérimentaux. Ces résultats expérimentaux et théoriques s'accordaient bien. De ce fait, on a pu fiablement et quantativement prédire les effets des forces de poussée sur la récupération de pétrole durant les processus de déplacement du systém immiscible (eau/pétrole).

On discutera l'étendue à laquelle la proportion de viscosité, la tension interfacialle, et la taux d'écoulement ont relation avec les temps de percée et les récupérations de pétrole mesurés. De plus, on discutera la théorie d'instabilité du déplacement. Il est évident, des résultats obtenus, que les forces de poussée sont capables d'exercer des effets trés significatifs sur la stabilité des processus de déplacement liquide-liquide ayant lieu dans un milieu poreux, sur la formation des doigts, et sur l'efficacité ultime de la récupération de pétrole durant des processus pratiques de récupération de pétrole impliquant l'injection d'un fluide aqueux.

Acknowledgment

I would like to thank my research supervisor, Dr. G. Neale, for his invaluable guidance and assistance during the course of the experimental and theoretical work as well as during the preparation of this thesis.

I would like to thank Mr. Louis Tremblay, Mr. Frank Ziroldo and Mr. Gerard Nina for their helpful assistance during the fabrication and installation of the experimental equipment.

Claims to Original Research

This thesis contains experimental and theoretical studies of both immiscible and miscible displacement processes occurring in a porous medium. The immiscible displacement system comprised aqueous glycerol solution as the displacing fluid and heavy paraffin oil as the displaced fluid. The miscible displacement system comprised a mixture of heavy paraffin oil and tetrachloroethylene as the displacing fluid and light paraffin oil as the displaced fluid.

A brief summary of the claims to original research follows below.

1. *Development of a new experimental cell:*

A new consolidated porous medium cell was developed, which permits linear displacements to be performed and to be photographed in the three basic flow modes, namely horizontal, vertical-upwards and vertical-downwards. The linear flow was achieved by incorporating open reservoirs for the fluids at the inlet and outlet of the porous medium cell.

2. *Development of a new mathematical model:*

It has been well known for many years that there is no simple analytical solution to the immiscible displacement equation. In this study, the displacement equation has been reconstructed and reorganized; a simple analytical solution of this displacement

equation has been obtained based on several assumptions. Hence, it could be used to quantitatively determine the effects of the buoyancy forces on the displacements.

3. *Development of a new method of photographic process:*

A new scanning system for processing experimental photographs has been developed. This makes it possible to measure the average finger widths in the different flow orientations, compare experimental results with theoretical results, and verify the theory.

4. *Development of new fluid combinations:*

Immiscible Fluid System (i.e., non-zero interfacial tension):

In order to eliminate the effects of viscous forces, an immiscible system having a unity viscosity ratio was employed. The unity viscosity ratio was obtained by adjusting the viscosity of the displacing fluid (glycerol solution) to be equal to that of the displaced fluid (heavy paraffin oil). Thus, the immiscible system displacements were affected only by capillary forces and buoyancy forces.

Miscible Fluid System (i.e., zero interfacial tension):

In order to eliminate the effects of both capillary forces *and* viscous forces, a *miscible* system having a unity viscosity ratio was employed. The unity viscosity ratio was obtained by adjusting the viscosity of the displacing fluid (mixture of heavy paraffin oil and tetrachloroethylene) to be equal to that of the displaced fluid (light

paraffin oil). Thus, the miscible system displacements were affected solely by buoyancy forces.

Publications and Presentations

The work presented in this thesis has been submitted for publication, or is in the process of being published, as follows:

Full Refereed Journal Papers:

1- Thibodeau, L., Guo, T. and Neale, G. H.: *Effects of connate water on immiscible displacement processes in porous media*, Powder Technology (in press, accepted April 15, 1997).

2- Guo, T. and Neale, G. H.: *A new method for estimating the effects of buoyancy forces on linear immiscible displacement in a porous medium*, Society of Petroleum Engineers Journal, Paper Number 37379 (submitted June 1996).

3- Guo, T. and Neale, G. H.: *The effects of buoyancy forces on immiscible displacement processes in porous media in absence of viscous forces*, Journal of Petroleum Science and Engineering (submitted March 1997).

Conference Presentation:

1- Guo, T. and Neale, G. H.: *Experimental and theoretical studies of the effects of buoyancy forces on immiscible linear displacement processes occurring in porous media*, 46th Canadian Chemical Engineering Conference, Kingston, Ontario, September 29 - October 2, 1996.

Objectives

The principal objectives of this study were:

(i) to study the effects of buoyancy forces on the finger formation and oil recovery at the breakthrough condition in a water-wet porous medium over a wide range of injection flow rates.

(ii) to develop a mathematical model for describing the behaviour of immiscible liquid/liquid displacement in porous media.

(iii) to develop a reliable technique for scanning the experimental fingering photographs.

(iv) to develop a technique for adjusting the fluid/fluid viscosity ratio as required to eliminate significant viscous effects.

The first objective was achieved by carrying out detailed and extensive experimental work on horizontal and vertical liquid/liquid displacement processes occurring in a porous medium for both immiscible and miscible systems.

The second objective was achieved by predicting the saturation profile of the displacing phase in the direction of flow. This prediction demonstrates the effects of buoyancy

forces on the displacements, thereby making it easier to quantitatively predict the oil recovery and the effects of buoyancy forces.

The third objective was achieved by using a reliable scanning technique to process the experimental photographs. The necessary equipment consisted of a: scanner, computer and special software package. This made it possible to quantitatively analyze the oil recovery and fingering pattern, and to use this data to confirm the proposed mathematical model.

The last objective was achieved by preparing different fluid systems to illustrate both immiscible and miscible displacements. Thus, the effects of buoyancy forces were displayed more directly, whence one can easily study the buoyancy effects in both immiscible and miscible displacements.

Table of Contents

Abstract i

Acknowledgment v

Claims to Original Research vi

Publications and Presentations ix

Objectives x

Table of Contents xii

List of Tables xvii

List of Figures xviii

Nomenclature xxvii

1. Abbreviations xxvii

2. Greek Letters xxvii

3. Symbols xxviii

4. Superscripts and Subscripts xxxii

Chapter 1 Introduction 1

Chapter 2 Literature Survey 4

2.1 Linear Immiscible Displacement 4

2.2 Saturation Profiles 5

2.3 Effects of Buoyancy Forces 10

2.4 Instability of Immiscible Displacement 11

2.5 Instability of Miscible Displacement 14

2.6 Effects of Connate Water 16

Chapter 3 Theory 19

3.1 Modeling of Flow through Porous Media 19

3.1.1 Basic Equations 20

3.1.2 Derivations for the Immiscible Displacement Model 20

3.1.3 Solution of the Model 22

3.1.4 Relationship between R and N_{GN} 26

Chapter 4 Instability 27

4.1 Instability of Immiscible Displacement 27

4.2 Instability of Miscible Displacement 29

4.2.1 Vertical-Downward Case 30

4.2.2 Vertical-Upward Case 31

4.2.3 Horizontal Case 32

4.3 Critical Velocity for Different Flow Modes 32

Chapter 5 Dimensional Analysis 36

5.1 Determination of R 36

Chapter 6 Experimental 39

6.1 Materials 39

6.2 Porous Medium Cell 40

6.3 Specification of the System 42

6.4 Experimental Method 42

6.4.1 Saturation Processes 42

6.4.1.1 Saturation without Connate Water 42

6.4.1.2 Saturation with Connate Water 43

6.4.2 Displacement Processes 44

6.4.3 Cleaning and Drying Processes 45

6.4.4 Calculation of Breakthrough Oil Recovery 45

6.5 Experiments Performed 46

6.6 Measurement of Viscosity 46

6.7 Measurement of Density 49

6.8 Measurement of Porosity 50

6.9 Residual Saturation 51

6.9.1 Residual Water Saturation 51

6.9.2 Residual Oil Saturation 53

Chapter 7 Photographic Procedures 54

7.1 Principle of the Method 54

7.2 Precision of the Measurements 56

Chapter 8 Results and Discussions 57

8.1 Immiscible Displacements with Three Viscosity Ratios 57

8.1.1 Horizontal Displacements 59

8.1.2 Vertical-Upward Displacements 61

8.1.3 Vertical-Downward Displacements 63

8.1.4 Effects of Buoyancy Forces 65

8.1.5 Critical Condition of the Displacements 70

8.1.6 Effects of Viscosity Ratio 71

8.2 Immiscible Displacements with a Unity Viscosity Ratio 79

8.2.1 Effects of Buoyancy Forces 79

8.2.2 Low Injection Flow Rates 84

8.2.3 High Injection Flow Rates 87

8.3 Theoretical Results 91

8.3.1 Regression Analysis of R and Expressions for R and N_{GN} 91

8.3.2 Saturation Profiles and Comparisons 96

8.3.3 Comparison with Literature Results 114

8.3.4 Quantitatively Estimating the Buoyancy Effects 116

8.4 Combined Effects of Capillary Number and Bond Number.....120

8.4.1 Horizontal Flow Mode 122

8.4.2 Vertical-Upward Flow Mode 124

8.4.3 Vertical-Downward Flow Mode 126

8.5 Miscible Displacement with a Unity Viscosity Ratio 130

8.5.1 Horizontal Flow Mode 131

8.5.2 Vertical-Upward Flow Mode 133

8.5.3 Vertical-Downward Flow Mode 135

8.6 Immiscible Displacements with and without Connate Water 138

8.6.1 Horizontal Flow Mode 138

8.6.2 Vertical-Upward Flow Mode 144

8.6.3 Vertical-Downward Flow Mode 145

8.6.4 Instability Analysis 148

Chapter 9 Conclusions 150

9.1 Effects of Buoyancy Forces 150

9.2 Effects of Injection Flow Rates 150

9.3 Saturation Profile 151

9.4 Instability 152

Recommendations for Future Work 154

References 155

Appendices 164

Appendix I 164

Appendix II 165

Appendix III 167

Appendix IV 168

Appendix V 169

List of Tables

Table 6.1 Physical Properties of Heavy Paraffin Oil/Glycerol Solution at 25°C±0.5°C 40

Table 6.2 Physical Properties of Oils and Aqueous Solutions at 25°C±0.5°C 40

Table 6.3 Properties of the Porous Medium Cell 41

Table 6.4 Specification of the System Used in This Study 42

Table 8.1 Comparison of Breakthrough Time in Three Flow Modes at Q=2.0 mL/h 65

Table 8.2 Differences in Oil Recovery between the Vertical and the Horizontal Flow Modes for Different Injection Flow Rates.....81

Table 8.3 Results of Regression 94

Table 8.4 Results of Average Finger Width Ratio 119

Table 8.5 Physical Parameters for Calculating the Dimensionless Number, I_{gr}.....120

Table 8.6 Experimental and Calculated Data for the Horizontal Flow Mode.....122

Table 8.7 Experimental and Calculated Data for the Vertical-Upward Flow Mode 126

Table 8.8 Experimental and Calculated Data for the Vertical-Downward Flow Mode.....128

Table A-1 The Results of the Precision Calculations of the Experimental Data 171

List of Figures

Figure 2.1 Relative Permeability Curve and Fractional Flow Curves 7

Figure 2.2 Saturation Profile 7

Figure 6.1 Photograph of the Experimental Cell 41

Figure 6.2 Experimental Set-up 43

Figure 6.3 Scheme of Canon-Fenske Routine Viscometer Tubing 47

Figure 6.4 Relationship between the Concentration of the Glycerol Solution and the Viscosity of the Solution at 25°C±0.5°C 48

Figure 6.5 Relationship between the Concentration of the Heavy Paraffin Oil and the Viscosity of the Mixture of Tetrachloroethylene and Heavy Paraffin Oil 48

Figure 6.6 Relationship between the Concentration of the Glycerol Solution and the Density of the Glycerol Solution 50

Figure 7.1 Scheme of Interfaces before and after Adjustment 55

Figure 8.1 Relationship between the Injection Flow Rate and Breakthrough Oil Recovery in the Horizontal Flow Mode 57

Figure 8.2 Relationship between the Injection Flow Rate and Breakthrough Oil Recovery in the Vertical-Upwards Flow Mode 58

Figure 8.3 Relationship between the Injection Flow Rate and Breakthrough Oil Recovery in the Vertical-Downwards Flow Mode 58

Figure 8.4 Horizontal Immiscible Displacements. Dyed Distilled Water Displacing Paraffin Oil (μ_o/μ_w=152.02, ρ_o/ρ_w=0.876) at (a) Q=8.5 mL/h, R=28.19%; (b) Q=13.2 mL/h, R=23.06%; (c) Q=84.0 mL/h, R=11.56%; (d) Q=174.0 mL/h, R=10.11%. ...60

Figure 8.5 Vertical-Upward Immiscible Displacements. Dyed Distilled Water Displacing Paraffin Oil (μ_o/μ_w=152.02, ρ_o/ρ_w=0.876) at (a) Q=8.5 mL/h, R=28.38%; (b) Q=13.2 mL/h, R=26.72%; (c) Q=84.0 mL/h, R=7.27%; (d) Q=174.0 mL/h, R=8.05%. 62

Figure 8.6 Vertical-Downward Immiscible Displacements. Dyed Distilled Water Displacing Paraffin Oil (μ_o/μ_w=152.02, ρ_o/ρ_w=0.876) at (a) Q=8.5 mL/h, R=23.35%; (b) Q=13.2 mL/h, R=19.90%; (c) Q=84.0 mL/h, R=10.66%; (d) Q=174.0 mL/h, R=9.08%. 64

Figure 8.7 Relationship between Oil Recovery and Gravity Number in Vertical-Upward Mode 66

Figure 8.8a Effects of Capillary Number on Oil Recovery in Horizontal Mode 67

Figure 8.8b Effects of Capillary Number on Oil Recovery in Vertical-Upward Mode 67

Figure 8.8c Effects of Capillary Number on Oil Recovery in Vertical-Downward Mode 68

Figure 8.9 Relationship between Oil Recovery and Gravity Number in Vertical-Downward Mode 68

Figure 8.10 Horizontal Immiscible Displacements. Dyed 30% Glycerol Solution Displacing Paraffin Oil (μ_o/μ_w=52.13, ρ_o/ρ_w=0.808) at (a) Q=8.5 mL/h, R=29.64%;

(b) Q=13.2 mL/h, R=26.33%; (c) Q=84.0 mL/h, R=15.34%; (d) Q=174.0 mL/h, R=10.73% 73

Figure 8.11 Horizontal Immiscible Displacements. Dyed 75% Glycerol Solution Displacing Paraffin Oil (μ_o/μ_w=4.11, ρ_o/ρ_w=0.728) at (a) Q=8.5 mL/h, R=48.63%; (b) Q=13.2 mL/h, R=48.26%; (c) Q=84.0 mL/h, R=42.93%; (d) Q=174.0 mL/h, R=36.94%. 74

Figure 8.12 Vertical-Upward Immiscible Displacements. Dyed 30% Glycerol Solution Displacing Paraffin Oil (μ_o/μ_w=52.13, ρ_o/ρ_w=0.808) at (a) Q=8.5 mL/h, R=34.08%; (b) Q=13.2 mL/h, R=31.42%; (c) Q=84.0 mL/h, R=9.06%; (d) Q=174.0 mL/h, R=9.70%. 75

Figure 8.13 Vertical-Upward Immiscible Displacements. Dyed 75% Glycerol Solution Displacing Paraffin Oil (μ_o/μ_w=4.11, ρ_o/ρ_w=0.728) at (a) Q=8.5 mL/h, R=50.99%; (b) Q=13.2 mL/h, R=46.85%; (c) Q=84.0 mL/h, R=33.77%; (d) Q=174.0 mL/h, R=23.52%. 76

Figure 8.14 Vertical-Downward Immiscible Displacements. Dyed 30% Glycerol Solution Displacing Paraffin Oil (μ_o/μ_w=52.13, ρ_o/ρ_w=0.808) at (a) Q=8.5 mL/h, R=25.26%; (b) Q=13.2 mL/h, R=21.26%; (c) Q=84.0 mL/h, R=13.55%; (d) Q=174.0 mL/h, R=11.76%. 77

Figure 8.15 Vertical-Downward Immiscible Displacements. Dyed 75% Glycerol Solution Displacing Paraffin Oil (μ_o/μ_w=4.11, ρ_o/ρ_w=0.728) at (a) Q=8.5 mL/h, R=44.49%; (b) Q=13.2 mL/h, R=42.69%; (c) Q=84.0 mL/h, R=39.25%; (d) Q=174.0 mL/h, R=36.32%. 78

Figure 8.16 Relationship between Injection Flow Rate and Breakthrough Oil Recovery in All Three Different Flow Modes 80

Figure 8.17 Displacement Patterns at a Low Injection Flow Rate of Q=2.1 mL/h in All Three Different Flow Modes. (a) Horizontal Flow Mode, (b) Vertical-Upward Flow Mode, (c) Vertical-Downward Flow Mode 82

Figure 8.18 Displacement Patterns at a Low Injection Flow Rate of Q=4.4 mL/h in All Three Different Flow Modes. (a) Horizontal Flow Mode, (b) Vertical-Upward Flow Mode, (c) Vertical-Downward Flow Mode 83

Figure 8.19 Different Finger Shapes That Occurred in the Different Flow Orientations. (a) Dendritic Shape in Miscible, Vertical-Upward Displacement, (b) Mushroom Shape in Immiscible, Horizontal Displacement, (c) Cactus Shape in Immiscible, Vertical-Downward Displacement 85

Figure 8.20 Displacement Patterns at a High Injection Flow Rate of Q=59.4 mL/h in All Three Different Flow Modes. (a) Horizontal Flow Mode, (b) Vertical-Upward Flow Mode, (c) Vertical-Downward Flow Mode 89

Figure 8.21 Displacement Patterns at a High Injection Flow Rate of Q=126.0 mL/h in All Three Different Flow Modes. (a) Horizontal Flow Mode, (b) Vertical-Upward Flow Mode, (c) Vertical-Downward Flow Mode 90

Figure 8.22 Residual Plot for Horizontal Flow Mode 92

Figure 8.23 Residual Plot for Vertical-Upward Flow Mode 92

Figure 8.24 Residual Plot for Vertical-Downward Flow Mode 93

Figure 8.25(I) Comparison between Predicted and Measured Saturation Profiles in Horizontal Flow Mode. For (μ_o/μ_w=152.02, ρ_o/ρ_w=0.876), (a) Q=8.5 mL/h, (b) Q=13.2 mL/h 97

Figure 8.25(II) Comparison between Predicted and Measured Saturation Profiles in Horizontal Flow Mode. For (μ_o/μ_w=152.02, ρ_o/ρ_w=0.876), (c) Q=84.0 mL/h, (d) Q=174.0 mL/h 98

Figure 8.26(I) Comparison between Predicted and Measured Saturation Profiles in Horizontal Flow Mode. For (μ_o/μ_w=52.13, ρ_o/ρ_w=0.808), (a) Q=8.5 mL/h, (b) Q=13.2 mL/h 99

Figure 8.26(II) Comparison between Predicted and Measured Saturation Profiles in Horizontal Flow Mode. For (μ_o/μ_w=52.13, ρ_o/ρ_w=0.808), (c) Q=84.0 mL/h, (d) Q=174.0 mL/h 100

Figure 8.27(I) Comparison between Predicted and Measured Saturation Profiles in Horizontal Flow Mode. For (μ_o/μ_w=4.11, ρ_o/ρ_w=0.728), (a) Q=8.5 mL/h, (b) Q=13.2 mL/h.....101

Figure 8.27(II) Comparison between Predicted and Measured Saturation Profiles in Horizontal Flow Mode. For (μ_o/μ_w=4.11, ρ_o/ρ_w=0.728), (c) Q=84.0 mL/h, (d) Q=174.0 mL/h 102

Figure 8.28(I) Comparison between Predicted and Measured Saturation Profiles in Vertical-Upward Flow Mode. For (μ_o/μ_w=152.02, ρ_o/ρ_w=0.876), (a) Q=8.5 mL/h, (b) Q=13.2 mL/h 103

Figure 8.28(II) Comparison between Predicted and Measured Saturation Profiles in Vertical-Upward Flow Mode. For (μ_o/μ_w=152.02, ρ_o/ρ_w=0.876), (c) Q=84.0 mL/h, (d) Q=174.0 mL/h 104

Figure 8.29(I) Comparison between Predicted and Measured Saturation Profiles in Vertical-Upward Flow Mode. For (μ_o/μ_w=52.13, ρ_o/ρ_w=0.808), (a) Q=8.5 mL/h, (b) Q=13.2 mL/h 105

Figure 8.29(II) Comparison between Predicted and Measured Saturation Profiles in Vertical-Upward Flow Mode. For (μ_o/μ_w=52.13, ρ_o/ρ_w=0.808), (c) Q=84.0 mL/h, (d) Q=174.0 mL/h 106

Figure 8.30(I) Comparison between Predicted and Measured Saturation Profiles in Vertical-Upward Flow Mode. For (μ_o/μ_w=4.11, ρ_o/ρ_w=0.728), (a) Q=8.5 mL/h, (b) Q=13.2 mL/h 107

Figure 8.30(II) Comparison between Predicted and Measured Saturation Profiles in Vertical-Upward Flow Mode. For (μ_o/μ_w=4.11, ρ_o/ρ_w=0.728), (c) Q=84.0 mL/h ...108

Figure 8.31(I) Comparison between Predicted and Measured Saturation Profiles in Vertical-Downward Flow Mode. For (μ_o/μ_w=152.02, ρ_o/ρ_w=0.876), (a) Q=8.5 mL/h, (b) Q=13.2 mL/h 109

Figure 8.31(II) Comparison between Predicted and Measured Saturation Profiles in Vertical-Downward Flow Mode. For (μ_o/μ_w=152.02, ρ_o/ρ_w=0.876), (c) Q=84.0 mL/h, (d) Q=174.0 mL/h 110

Figure 8.32(I) Comparison between Predicted and Measured Saturation Profiles in Vertical-Downward Flow Mode. For (μ_o/μ_w=52.13, ρ_o/ρ_w=0.808), (a) Q=8.5 mL/h, (b) Q=13.2 mL/h 111

Figure 8.32(II) Comparison between Predicted and Measured Saturation Profiles in Vertical-Downward Flow Mode. For (μ_o/μ_w=52.13, ρ_o/ρ_w=0.808), (c) Q=84.0 mL/h, (d) Q=174.0 mL/h 112

Figure 8.33(I) Comparison between Predicted and Measured Saturation Profiles in Vertical-Downward Flow Mode. For (μ_o/μ_w=4.11, ρ_o/ρ_w=0.728), (a) Q=8.5 mL/h, (b) Q=13.2 mL/h 113

Figure 8.33(II) Comparison between Predicted and Measured Saturation Profiles in Vertical-Downward Flow Mode. For (μ_o/μ_w=4.11, ρ_o/ρ_w=0.728), (c) Q=84.0 mL/h 114

Figure 8.34 Comparison between Predicted Saturation Profile and Experimentally Measured Saturation Profile of Sarma and Bentsen 115

Figure 8.35 Relationship between the Dimensionless Number and Oil Recovery in the Horizontal Flow Mode 124

Figure 8.36 Scheme of Different Flow Regions at μ_r=1.0 in Horizontal Flow Mode.....124

Figure 8.37 Relationship between the Dimensionless Number and Oil Recovery in Vertical-Upward Flow Mode 127

Figure 8.38 Relationship between the Dimensionless Number and Oil Recovery in Vertical-Downward Flow Mode.....129

Figure 8.39 Relationship between the Injection Flow Rate and Oil Recovery in All Three Different Flow Modes 131

Figure 8.40 Horizontal Miscible Displacement. Dyed Tetrachloroethylene-Heavy Paraffin Oil Mixture Displacing Light Paraffin Oil (μ_o/μ_w=1.0, ρ_o/ρ_w=0.8496) at (a) Q=2.1 mL/h, R=81.06%; (b) Q=4.4 mL/h, R=80.85%; (c) Q=59.8 mL/h, R=75.76%; (d) Q=126.0 mL/h, R=78.24%. 132

Figure 8.41 Vertical-Upward Miscible Displacement. Dyed Tetrachloroethylene-Heavy Paraffin Oil Mixture Displacing Light Paraffin Oil (μ_o/μ_w=1.0, ρ_o/ρ_w=0.8496) at (a) Q=2.1 mL/h, R=95.15%; (b) Q=4.4 mL/h, R=92.24%; (c) Q=59.8 mL/h, R=79.21%; (d) Q=126.0 mL/h, R=82.57%. 134

Figure 8.42 Vertical-Downward Miscible Displacement. Dyed Tetrachloroethylene-Heavy Paraffin Oil Mixture Displacing Light Paraffin Oil (μ_o/μ_w=1.0, ρ_o/ρ_w=0.8496) at (a) Q=2.1 mL/h, R=24.10%; (b) Q=4.4 mL/h, R=52.37%; (c) Q=59.8 mL/h, R=73.71%; (d) Q=126.0 mL/h, R=74.11%. 136

Figure 8.43 Scheme of the Connate Water Film, the Particles, and the Oil in the Porous Medium 139

Figure 8.44 Relationship between Injection Flow Rate and Oil Recovery in the Presence and Absence of Connate Water in the Horizontal Flow Mode 140

Figure 8.45 Fingering Patterns in the Horizontal Flow Modes with μ_o/μ_w=152.02, ρ_o/ρ_w=0.876 at (I) Q=2.1 mL/h. (a) t_{br}=7855 s, R=25.74%; (b) t_{br}=7080 s, R=23.20%; (II) Q=126.0 mL/h. (c) t_{br}=49 s, R=9.63%; (d) t_{br}=65 s, R=12.79% 141

Figure 8.46 Relationship between the Injection Flow Rate and Oil Recovery in the Presence and Absence of Connate Water in the Vertical-Upward Flow Mode 143

Figure 8.47 Fingering PatternS in Vertical-Upward Flow Mode with μ_o/μ_w=152..20, ρ_o/ρ_w=0.876 at (I) Q=2.1 mL/h. (a) t_{br}=6093 s, R=19.96%; (b) t_{br}=3954 s, R=12.95%; (II) Q=126.0 mL/h. (c) t_{br}=57 s, R=11.21%; (d) t_{br}=79 s, R=15.53%. 144

Figure 8.48 Relationship between the Injection Flow Rate and Oil Recovery in the Presence and Absence of Connate Water in the Vertical-Downward Flow Mode...146

Figure 8.49 Fingering Patterns in the Vertical-Downward Flow Modes with μ_o/μ_w =152.02, ρ_o/ρ_w=0.876 at (I) Q=2.1 mL/h. (a) t_{br}=2619 s, R=8.58%; (b) t_{br}=3646 s, R=11.95%; (II) Q=126.0 mL/h. (c) t_{br}=60 s, R=11.80%; (d) t_{br}=80 s, R=15.73%...147

Nomenclature

1. Abbreviations

EOR: Enhanced Oil Recovery.

IFT: InterFacial Tension.

2. Greek Symbols

$\alpha, \beta, \gamma, \lambda, \Lambda, \theta$: regression constants.

δ: ratio of the finger width between vertical and horizontal or vertical and vertical orientation [dimensionless].

$\varepsilon = TC_1+C_2-\Phi\Lambda T/t_{br}$, defined in Equation (3.27).

Φ: porosity of porous media cell [dimensionless].

μ : viscosity [mPa.s].

μ_r : viscosity ratio [dimensionless].

μ_v : viscosity of sample measured [mPa.s].

ν_1, ν_2: degrees of freedom associated with the pooled estimate of variance [dimensionless].

ρ: density [g/cm^3].

ρ_v: density of sample measured [g/cm^3].

$\Delta\rho$: density difference between displacing and displaced fluids [g/cm^3].

σ: interfacial tension [mN/m].

$\hat{\sigma}_p^2$: estimated variance of response [dimensionless].

$\hat{\sigma}_i^2$: individual estimated variance of replicate response [dimensionless].

ξ : dimensionless distance [dimensionless].

ψ: dip angle [degree].

3. Symbols

a, b, c, d, e, f, i, j: exponents [constant].

A: cross-section area [cm^2].

A_s: the area under saturation curve [dimensionless].

C_1, C_2, C_4 : constant [dimensionless].

C_c : variable defined by Equation (21) [cm/s].

C_v : viscometer constant [dimensionless].

C^*: a dimensionless parameter [dimensionless].

d_p: average diameter of particle [cm].

F: value of probability density function [dimensionless].

f_w : fractional flow function [dimensionless].

g: gravitational acceleration [cm/s^2].

h: thickness of porous medium cell [cm].

I_{sr}: instability number [dimensionless].

K: absolute permeability [mm^2].

k: phase permeability [dimensionless].

k_{wor} : permeability to water at residual oil saturation [mm^2].

k_{oiw} : permeability to oil at connate water saturation [mm^2].

k_{rw} : relative permeability of water [dimensionless].

k_{ro} : relative permeability of oil [dimensionless].

L: length of porous media [cm].

L_x: width of the experimental cell [cm].

L_y: thickness of the experimental cell [cm].

m_i: individual number of replications [dimensionless].

M : mobility [mm^2/mPa.s].

M_{water} : weight of water [g].

M_{cell} : weight of cell [g].

$M_{cell\text{-}water}$: weight of water and cell [g].

$M_{cell\text{-}water\text{-}oil}$: weight of cell, residual water (connate water) and oil [g].

n: number of experimental runs [dimensionless].

N_B: Bond number [dimensionless].

N_c: capillary number [dimensionless].

N_F: Froude number [dimensionless].

N_g: gravity number [dimensionless].

N_{GN}: comprehensive coefficient [dimensionless].

P: phase pressure [mPa].

p: number of variables [dimensionless].

P_C : capillary pressure [mPa].

R: oil recovery [dimensionless].

R^2_{adj}: adjusted coefficient of determination (square of correlation between the dependent variables and the predicted values) [dimensionless].

R^2: coefficient of determination [dimensionless].

R_s: a ratio used in quantitative lack of fit test [dimensionless].

r: radius of particles [cm].

ΔR: oil recovery difference between horizontal flow mode and vertical flow mode [dimensionless].

ΔR^u: oil recovery difference between horizontal flow mode and vertical-upward flow mode [dimensionless].

ΔR^d: oil recovery difference between horizontal flow mode and vertical-downward flow mode [dimensionless].

Q: total injection volumetric flow rate [cm^3/s].

s_{max}: maximum saturation of water [dimensionless].

s_{or}: residual saturation of oil [dimensionless].

s (s_w): saturation of water [dimensionless].

$\bar{s}_{wi}$: average initial water saturation [dimensionless].

$\bar{s}_{or}$: average residual oil saturation [dimensionless].

s_{wi}: residual water saturation [dimensionless].

s^*: a certain saturation of water [dimensionless].

$s_c = \frac{s_w - \bar{s}_{wi}}{1 - \bar{s}_{wi} - \bar{s}_{or}}$ [dimensionless].

t: time [s].

t_{br}: at breakthrough time [s].

t_v: efflux time of measuring viscosity by Cannon-Fenske Viscometer [s].

t^*: a certain time [s].

T: dimensionless time [dimensionless].

U: total injection flow rate [cm/s].

U_c: critical velocity [cm/s].

V: volume of porous medium [cm^3].

W: width of porous medium [cm].

W_f: average finger width [cm].

x: distance [cm].

Δx: an elemental distance [cm].

$\bar{Y}$: mean observed response value [dimensionless].

$\hat{Y}$: estimated response value [dimensionless].

y: mathematical transform [dimensionless].

z: a combined variable [dimensionless].

4. Superscripts and Subscripts

a. Superscripts:

V: denotes vertical flow mode.

H: denotes horizontal flow mode.

b. Subscripts:

1: denotes water

2: denotes oil.

w: denotes water.

o: denotes oil.

p: denotes pore volume.

Chapter 1

Introduction

Petroleum is one of the most important sources of energy for industry and for our everyday life. In the early days of the petroleum industry, conventional methods of oil production relied largely on the internal reservoir pressure, whereby intrisic pressure associated with the reservoir was used to recover a portion of the oil. Mechanisms such as liquid expansion and rock compaction initially help drive the reservoir fluids into the wellbores as the natural pressure declined. This stage is called the primary recovery. In the past, most reservoirs produced oil by primary recovery mechanisms until an uneconomical oil flow rate was eventually reached.

Traditional methods of oil production are unsuitable to meet the high current rate of petroleum comsumption. As continuous oil production necessarily results in a decreasing reservoir pressure, new techniques for increasing oil recovery, such as displacement methods, must be developed to facilitate recovery. However, the displacement of oil from the pores of a reservoir rock formation by means of an injected fluid (usually water) is a very complicated process that depends on the interaction of several different types of forces, in particular viscous forces, capillary forces, and buoyancy forces.

Viscous Fingering: During the displacement of one fluid by another in a porous medium, a variety of instabilities in the displacement front can arise that reduce the displacement efficiency; i.e., the fractional recovery of the displaced phase. Considerable attention has been paid to the fundamental phenomenon known as *viscous fingering.* Viscous fingering is closely associated with viscous forces, and occurs whenever a lower-viscosity phase (water in the present context) displaces a higher-viscosity phase (oil in the present context). The water tends to channel or "finger" through the paths of lesser hydrodynamic resistance, leaving large amounts of oil surrounded uncontacted and hence unrecovered in the oil reservoir. It is therefore important to study and develop an improved understanding of these effects.

Capillary Forces: The existence of a tension force at the interface between two immiscible fluids is witnessed daily by most people. In conjunction with the wettability, size and geometry of the porous medium, capillary (or interfacial tension) forces can exert significant, or even dominant, effects on fingering behaviour during water/oil displacement processes in a porous medium. Generally speaking, the higher the interfacial tension, the lower the oil recovery. Capillary forces can be reduced to very low values by using surfactants to diminish forces and enhance oil recovery.

Buoyancy Forces: Buoyancy (gravity) forces can also exert very significant effects on the recovery efficiency when one fluid (oil) is being displaced by another (water) in a porous medium. Buoyancy forces come into play because of the difference in density

between the displaced and displacing fluids. They are capable of significantly affecting the geometry of the displacement front and the oil recovery efficiency; especially when the displacement process is occurring in the vertical mode. Depending on the displacement mode (e.g., vertical upward or vertical downward), buoyancy forces will either tend to stabilize the displacement process (with a consequent increase in oil recovery) or destabilize it (with a consequent decrease in oil recovery).

The principal focus of the present research is on the affects of buoyancy forces, although the effects of viscous and capillary forces will also be addressed. To make effective use of the positive effects of the buoyancy forces in real petroleum reservoir recovery situations, a clear understanding of the relative interactions between the buoyancy, viscous and capillary forces is imperative.

Chapter 2

Literature Survey

2.1 Linear Immiscible Displacement

Viscous fingering on water flooding processes has become one of the most important area of study in the field of Enhanced Oil Recovery (EOR) because of its significant impact on oil recovery. Numerous laboratory studies have been conducted to elucidate fingering phenomenon, including experiments in the radial, semi-radial, linear, and other flow modes. Previous work involving radial flow [Hu et al. 1985, Ni et al. 1986, Nasr-el-Din et al. 1987] and linear flow [van Meurs and van der Poel 1958, McEven 1959, Paterson et al. 1984a, 1984b] focused on the viscous fingering phenomenon, with or without buoyancy (gravity) forces and the capillary forces were neglected. For semi-radial flow (i.e., point source to point sink) displacements [Page et al. 1993, Thirunavu and Neale 1995, Guo and Neale 1996], the stream lines are partially diverging and partially converging. This makes it troublesome to calculate a meaningful superficial velocity of the displacing fluid, whence it is difficult to calculate the traditional capillary number and gravity number, thereby precluding direct comparisons with the data of other workers. For these reasons, linear displacement (i.e., line source to line sink) experiments were conducted in the present work, to study

the effects of buoyancy forces and to facilitate comparison with the data of other researchers.

2.2 Saturation Profiles

For single-phase fluid flow through a homogeneous porous medium, Darcy (1856) proposed an empirical equation relating the volumetric flow rate to the pressure gradient and the permeability of the porous medium. The relation is often written in differential form as:

$$\frac{Q}{A} = -\frac{K}{\mu}\frac{dP}{dx} \tag{2.1}$$

where Q is total injection volumetric flow rate, A is cross-section area, K is absolute permeability, μ is viscosity, and dP/dx is the pressure grdient. The extension of Darcy's Law to multiphase flow through a homogeneous porous medium was first suggested by Muskat et al. (1937), as:

$$U_w = -(\frac{Kk_{rw}}{\mu_w})(\nabla P_w - \rho_w g) \tag{2.2}$$

$$U_o = -(\frac{Kk_{ro}}{\mu_o})(\nabla P_o - \rho_o g) \tag{2.3}$$

where U_w and U_o are the Darcy's velocities of water and oil. k_{rw} and k_{ro} are relative permeabilities to water phase and oil phase. μ_w and μ_o are viscosities of water and oil. ∇P_w and ∇P_o are pressure gradient to water and oil, ρ_w and ρ_o are densities of water

and oil, and g is gravitational acceleration. The equations of continuity for each fluid are:

$$\frac{\partial U_o}{\partial x} = -\Phi \frac{\partial s_o}{\partial t} \tag{2.4}$$

$$\frac{\partial U_w}{\partial x} = -\Phi \frac{\partial s_w}{\partial t} \tag{2.5}$$

wher Φ is porosity of porous medium, s_w and s_o are the saturations to water and oil. The pressures in the two phases at any macroscopic point in the porous medium are assumed to be related to each other via the capillary pressure, P_c. Hence, the two pressure gradients are related by the gradient of the capillary pressure [Leverett 1941]:

$$\frac{\partial P_c}{\partial x} = \frac{\partial P_o}{\partial x} - \frac{\partial P_w}{\partial x} \tag{2.6}$$

Equation (2.6) indicates that the two pressure gradients are equal only if the capillary pressure has zero gradient. Based on Equations (2.2 ~ 2.6), a mathematical model for describing immiscible displacement in porous media can be formulated. However, due to the complexity of this model, it does not have an analytical solution [Bentsen and Saeedi 1981].

In endeavouring to solve this equation, Buckley and Leverett (1942) introduced a fractional flow function, $f_w = U_w/U$, for situation where the displacement was carried out in a horizontal one-dimensional porous medium with insignificant gravity forces. With the further assumption that the water-oil capillary pressure is insignificant, it becomes possible to eliminate the capillary pressure gradient and obtain a single equation with a single unknown, s_w, as:

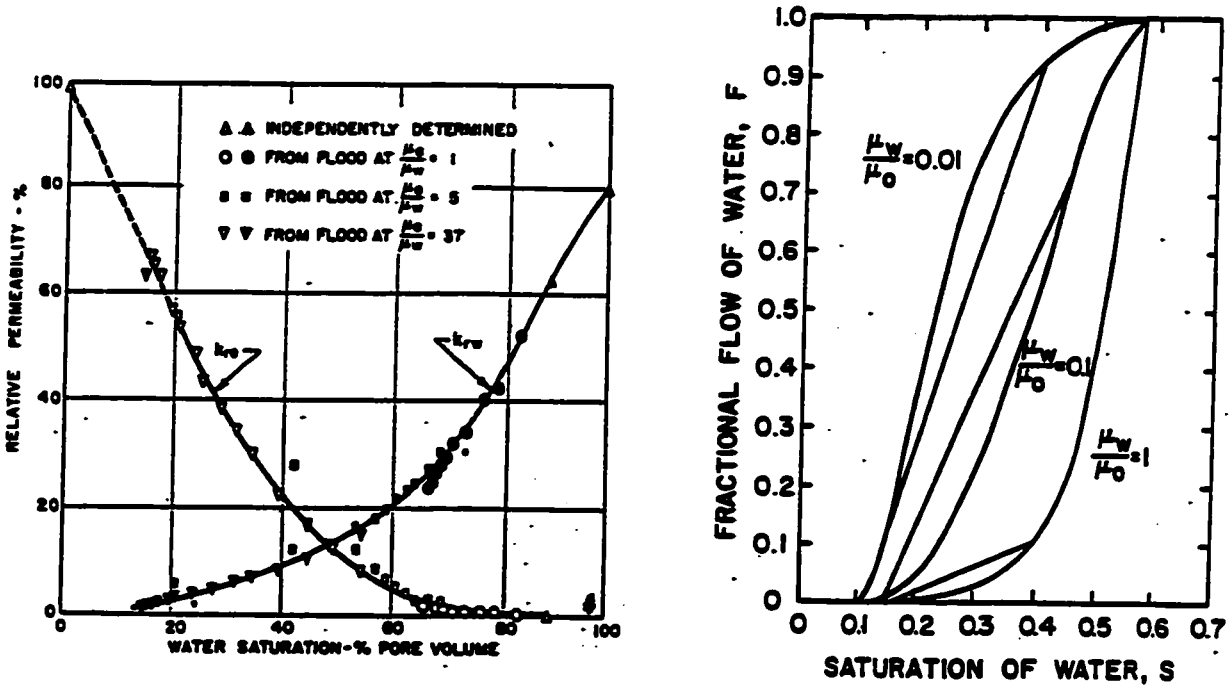

Fig.2.1. Relative permeability curve [Johnson et al. 1959] and fractional flow curves [Jerauld et al. 1984].

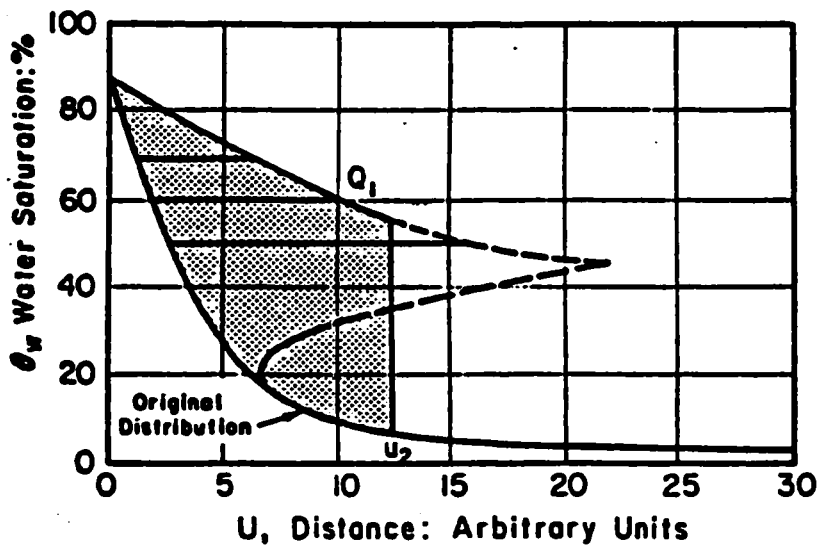

Fig.2.2. Saturation profile [Wooding and Morel-Seytoux 1976].

$$\frac{\partial s_w}{\partial t} + U\frac{\partial f_w(s_w)}{\partial x} = 0 \tag{2.7}$$

where $f_w(s_w) = [1+(k_{ro}/k_{rw})(\mu_w/\mu_o)]^{-1}$. If the typical curves of relative permeability and f_w for different viscosity ratios as a function of s_w are given (see Fig.2.1) [Johnson et al. 1959, Jerauld et al. 1984], Equation (2.7) can be written in a characteristic form and integrated to obtain [van Meurs and van der Poel 1958]:

$$\int dx = -\int U\frac{df_w(s_w)}{ds_w}dt \tag{2.8}$$

A problem associated with Buckley-Leverett's approach is that Equation (2.8) generally leads to a profile that is multiple-valued in s_w as a function of x because of the omission of capillary forces (see Fig.2.2) [Wooding and Morel-Seytoux 1976]. Hence, it becomes necessary to introduce the concept of a discontinuity or "front" [Buckley and Leverett 1942, Morel-Seytoux 1969, Wooding and Morel-Seytoux 1976].

Due to the impossibility of analytically solving the displacement equation, Douglas and Wagner (1958) and McEven (1959) proposed numerical solutions to the one-dimensional linear displacement equation, but only for the case in which the gravity term was neglected. The role of both the capillary pressure and gravitational forces on two-phase fluid flow in a porous medium has been investigated by Fayers and Sheldon (1959). They concluded that the capillary term does indeed eliminate the triple-valued saturation behaviour that appears in the Buckley-Leverett saturation profiles. The addition of gravitational forces and capillary pressure will cause significant changes to the Buckley-Leverett profile curves for just low displacement rates. Gottfried et al.

(1966) employed a numerical method to solve the equation for one-dimensional, multiphase flow in porous media. In their study, both the capillary pressure and gravitational forces were neglected. However, their numerical method could solve this equation with the help of a relative permeability curve for oil and water phases and a capillary pressure curve. Unfortunately, the method used is not practical for real engineering use since the relative permeability to both phases is not generally known and not easy to measure.

Sarma and Bentsen (1988) gained an experimental understanding of how one fluid displaces another in a one-dimensional porous medium by measuring saturation as a function of time and distance using microwave instrumentation. A comparison was made between numerical results and experimental results at favourable mobility ratios and unfavourable mobility ratios. The difference between these results were attributed to end effects, since Kyte and Rapoport (1958) had previously explained that both inlet and outlet end effects would be affected by the length of the flood system, the rate of injection, and the fluid viscosities. In practice, a simple analytical formulation is necessary to predict the saturation profile. Unfortunately, no simple analytical solution for the general displacement equation is currently available to plot a saturation profile with respect to capillary and gravity terms [Bentsen and Saeedi 1981].

2.3 Effects Of Buoyancy Forces

A very large amount of work has been conducted on the subject of water/oil displacement in porous media. Unfortunately, only a few of the studies have dealt with the effects of the buoyancy forces. Richardson and Perkins (1957) investigated the effect of the injection flow rate on the oil recovery efficiency and concluded that decreasing the flow rate will increase the tendency of the water to under-ride the oil because of the water's greater density. At about the same time, Craig et al. (1957) conducted experiments to study the effects of gravity segregation during water, gas and solvent flooding. They observed that gravity segregation could result in a significant decrease in the oil recovery at breakthrough. Spivak (1974) studied gravity segregation in two-phase displacement processes, and concluded that gravity segregation effects will increase with: (1) an increase in permeability, (2) an increase in density difference, and (3) an increase in mobility ratio. Hornof and Morrow (1987) studied the effects of gravity during the displacement of oil by surfactant solutions. They found that the observed instabilities could be attributed to gravity segregation, which occurs when the capillary and viscous forces are insufficient to overcome the buoyancy forces. A more recent consideration of the effects of buoyancy forces was presented by Page et al. (1993). In their preliminary study, the effects of buoyancy forces were observed for three fundamentally different flow modes; i.e., horizontal, vertically-upward or vertically-downward. Thirunavu and Neale (1995) and Guo and Neale (1996) extended Page et al.'s experiments in order to study the effects of buoyancy forces

during immiscible and miscible displacements, respectively. Their experiments revealed that buoyancy forces can significantly affect the fingering pattern and oil recovery. However, all of the preceding studies were of a qualitative nature, and they did not address the more important quantitative aspect of the degree by which the buoyancy forces can affect the fingering pattern and oil recovery efficiency.

2.4 Instability of Immiscible Displacement

In describing the liquid-liquid displacement in a porous medium, three dimensionless numbers are commonly utilized to analyze the interaction between the viscous, capillary and buoyancy forces; namely: (i) the capillary number, N_c (the ratio of viscous forces to capillary forces), (ii) the Bond number, N_B (the ratio of gravity forces to capillary forces), and (iii) the gravity number, N_g (the ratio of viscous forces to gravity forces) These numbers are defined as follows:

$$N_c = \frac{\mu_w U}{\sigma} \tag{2.9}$$

$$N_B = \frac{\Delta\rho g d_p^{\,2}}{\sigma} \tag{2.10}$$

$$N_g = \frac{\mu_w U}{\Delta\rho g d_p^{\,2}} = \frac{N_c}{N_B} \tag{2.11}$$

It should be noted that the gravity number is not independent of the capillary number and Bond number.

On account of the complexity of the interactions between the viscous, capillary and buoyancy forces in immiscible liquid-liquid displacement processes, Morrow and Songkran (1981) proposed a combined dimensionless number involving the capillary number, Bond number and several physical parameters relating to the structure of the porous media. They showed that when the capillary number is lower than about 10^{-6}, the oil trapping mechanism is dominated by capillary forces, and the residual oil saturation is essentially constant. Whenever this combined dimensionless number increases, the trapped residual saturation is decreased. This indicates that increasing this number will diminish the capillary forces and promote the buoyancy forces. Once the buoyancy forces become dominant, and positively oriented to the displacement, they will benefit oil recovery. However, a theoretical derivation of this dimensionless number was not presented in Morrow and Songkran's study.

Based on the stability theory of Chuoke et al. (1959), Peters and Flock (1981) developed a dimensionless number, I_m, and provided its critical value for predicting the onset of instability during immiscible displacement in a porous medium at an unfavorable viscosity ratio. They reported that when this dimensionless number is greater than 13.56 (for a cylindrical system), or π^2 (for a rectangular system), the displacement in the horizontal flow mode will be unstable. Characteristically, this unstable displacement is the result of viscous forces, and could be called viscous instability. In the present study, however, it was found that the situation is somewhat different, and the existence of a simple critical value is an oversimplification of the

problem. Even if the viscosity ratio is favorable (i.e., $\mu_w > \mu_o$), instability can still develop, depending on the relative magnitude of the viscous, capillary and buoyancy forces.

When the viscosity ratio is set to unity, van Meurs and van der Poel (1958) found that the low oil/water viscosity ratio is very favourable to the water-drive process, and it is reasonable to expect a higher oil recovery. However, they neglected the effects of the capillary forces and buoyancy forces, since these forces could also make the displacement become unstable. Several researchers [Ni et al. 1986, Scott et al. 1965, Nasr-el-Din et al. 1987] presented a scheme of different regions to exhibit the relationship between oil recovery and the injection flow rate. Three regions were indicated for horizontal flow: (i) the capillary region, (ii) the stable region, and (iii) the viscous regions. Unfortunately, the vertical orientation was not considered, for which buoyancy forces could exert significant effects on the displacement instabillity. It is believed, however, that observations of the unstable region caused by capillary forces and buoyancy forces in both the horizontal and vertical cases have not been reported by previous researchers [Ni et al. 1986, van Meurs and van der Poel 1958, Scott et al. 1965, Nasr-el-Din et al. 1987]. In the present study, experiments will be carried out in all three different flow modes. Hence, the effects of the buoyancy forces on the fingering pattern, the instability of the displacements, and the oil recovery efficiency can be assessed.

2.5 Instability of Miscible Displacement

It is well known that the displacement of a fluid of higher viscosity (μ_2) by one of lower viscosity (μ_1) leads to an unstable displacement process and to the phenomenon known as viscous fingering. When the density of the two fluids is different, buoyancy (gravity) forces can come into play and can modify the observed fingering behavior via the phenomenon of gravity segregation. Therefore, both viscous fingering and gravity segregation should be considered as the consequence of displacement instability. from the early experimental study of Hill, many studies [Koval 1963, Perkins et al. 1965, Fayers 1988, Page et al. 1993] have focused on viscous fingering for liquids possessing an unfavorable viscosity ratio ($\mu_2/\mu_1>1$), because this situation is of the most practical interest; e.g. the displacement of oil by water from an underground petroleum reservoir. Craig et al. (1957) conducted experiments to study gravity segregation by employing a viscosity ratio of unity for both horizontal and vertical orientations. They concluded that gravity segregation would tend to reduce oil recovery, often significantly, and that gravity segregation could be significantly influenced by the injection flow rates. Gardner et al. (1962) studied the gravity segregation of miscible liquids with a viscosity ratio of unity and obtained analytical formulas for the motion of a narrow transition zone between the fluids; the results were in good agreement with those of Craig et al (1957). In the vertical-downward flow mode, a sharp interface between the fluids was observed, but no photographic evidence was published. Slobod and Howlett (1964) also studied

the effects of gravity segregation on miscible displacement in vertical unconsolidated porous media, and they deduced that the length of the mixing zone, which develops between phases, depends upon the viscosity ratio, density difference and the injection flow rate.

Any study of miscible unstable displacement processes is ultimately aimed at eliminating or controlling the viscous fingering phenomenon. Dumoré (1964) observed that under a suitable combination of buoyancy and viscous forces, transition zones that are either stable or unstable could develop. He postulated a well-known critical velocity relation for stable downward displacement by considering a small hypothetical protrusion of the displacing fluid into the displaced fluid. When the injection flow rate is greater than a certain critical velocity, the displacement becomes unstable. However, it was found that this critical velocity relation tends to become infinity when the viscosity ratio is set equal to unity. In other words, the displacement will absolutely be stable. However, the present study has found that unstable phenomenon can still occur in the case of a unity viscosity ratio, and that gravitational-induced fingers can be observed; provided buoyancy forces are very significant. It will be seen later that gravitational fingers were produced and that these fingers caused the displacements to be unstable in the vertical-downward flow mode. On the other hand, the displacements were stable in the vertical-upward flow mode.

2.6 Effects of Connate Water

Viscous fingering is a manifestation of frontal instability, which is a function of the properties of the porous medium and of the fluids employed. This fingering phenomena can severely decrease oil recovery efficiency. The oil in a reservoir is generally associated with a small amount of native water, which is randomly or uniformly distributed within the oil phase. This connate water covers the surface of particles of the porous medium. Thus, the size of the channels and the wettability of the porous media is changed at different magnitudes. The displacement instability is an important factor determining the oil recovery efficiency of the water-drive process. Chuoke et al. (1959) and Peters and Flock (1981) used the same formulation of the critical velocity for different flow orientations. They treated the critical velocity as zero for the horizontal case. However, they found that there is no physical critical velocity for the horizontal flow mode; only a theoretical critical velocity exists. As found in the present study, this critical velocity has a negative value, and this consequently has no physical meaning. Chuoke et al. (1959) and Peters and Flock (1981) did not discuss the case in the vertical-downward flow mode. The present study has concluded that there is no critical velocity for linear immiscible displacements aligned in the horizontal and vertical-downward direction, and it is possible that there is a critical velocity only for the vertical-upward flow mode.

A number of researchers [Outmans 1962a, Outmans 1962b, Dumoré 1964] have studied the instability of liquid-liquid displacements with and without connate water. In which the interface of the liquid/liquid displacement was horizontal for any flow rate below the critical velocity in the vertical case. They found that the first-order theory cannot be used to derive the shape and growth of the viscous fingers because the equations for describing the fingers are incomplete. Rachford (1964) extended the previous analysis of frontal instabilities, using relation for parallel plate models, by including the effects of the saturation transition zone observed behind the front in water floods for a water-wet system. He concluded that the instability of such water floods in relatively homogeneous porous media can successfully be predicted. Hagoort (1974) pointed out the important effects of capillary forces on the wavelength of the instabilities. Gravitational forces were excluded for the horizontal case, but the capillary forces were thought to determine the wavelength of the instabilities. In the vertical case, Hagoort (1980) has shown that gravity drainage in water-wet, connate water-bearing reservoirs can be a very effective process of enhanced oil recovery, and the oil relative permeability is a key factor in the process.

Vizika and Lombard (1996) studied the effects of wettability and spreading coefficient on the oil recovery in the presence of connate water. They found that the existence of connate water in a porous medium is very sensitive factor on the recovery of oil, because of the spreading film of connate water. Paterson et al. (1984b) found that the fingers become more irregular in an oil-wet porous medium

when a non-wetting fluid displaces a wetting fluid with residual fluid (connate water) present. They proposed two distinct mechanisms for the irregularities of the fingers: (i) the inherent irregularity of the porous medium, and (ii) the irregularity of the size and distribution of residual ganglia. The present study will focus on these irregularities of the fingers by conducting linear immiscible displacements with a high viscosity ratio in the presence and absence of connate water in three different flow modes to elucidate the important effects of buoyancy forces on the displacement pattern and the instability of immiscible displacements.

Chapter 3

Theory

3.1 Modeling of Flow through Porous Media

Before deriving the fundamental displacement equation, several assumptions must be made:

a) The fluids employed are incompressible.

b) The porous medium is homogeneous.

c) There are no end effects at the beginning of the displacement (i.e., the displacing fluid can fill the entire inlet cross-section of the porous medium).

d) The effects of buoyancy forces and capillary forces are considered to be independent.

The displacement equation representing two-phase flow in a porous medium in the presence of capillary pressure and gravity (buoyancy) forces is obtained by applying Darcy's law and the material balance condition for each phase [Muskat 1942, Douglas and Wagner 1957, Gottfried et al. 1966].

3.1.1. Basic equations

Equations (2.2) ~ (2.6) in Chapter 2 are the basic equations used to derive the displacement equation.

3.1.2 Derivations for the Immiscible Displacement Model

Combining Equations (2.4) and (2.5) leads to the fundamental observation that the sum of the water velocity and the oil velocity must be constant throughout the porous medium. Moreover, if the cross-sectional area, A, of the porous medium remains constant, the sum of these two velocities must be equal to the water injection velocity, U, (assumption (a) above), i.e.

$$\frac{Q}{A} = \frac{Q_o}{A} + \frac{Q_w}{A} \tag{3.1}$$

where Q is the total volumetric injection flow rate, whence

$$U = U_o + U_w \tag{3.2}$$

By eliminating P_o , P_w , and U_o from Equations (2.2), (2.3), (2.6) and (3.2), it follows that:

$$U_w^V = f_w(U \mp M_o \Delta\rho g + M_o \frac{\partial P_c}{\partial x}) \tag{3.3}$$

(Vertical Case)

$$U_w^H = f_w(U + M_o \frac{\partial P_c}{\partial x}) \tag{3.4}$$

(Horizontal Case)

where

$$M_w = \frac{Kk_{rw}}{\mu_w} \quad M_o = \frac{Kk_{ro}}{\mu_o} \quad \Delta\rho = \rho_w - \rho_o \tag{3.5}$$

$$f_w = \frac{M_w}{M_w + M_o}, \tag{3.6}$$

and the minus sign in Equation (3.3) is employed for vertical-upward displacements and the plus sign for vertical-downward displacements, and where the superscripts V and H denote vertical flow and horizontal flow, respectively. The gravity term has been neglected in the horizontal case. Combinating of the continuity of mass equation with the following expansion equation

$$\frac{\partial P_c}{\partial x} = \frac{dP_c}{ds}\frac{\partial s}{\partial x} \tag{3.7}$$

yields:

$$\frac{dU^V}{ds}\frac{\partial s}{\partial x} + \frac{dC_c}{ds}\left(\frac{\partial s}{\partial x}\right)^2 + C_c\frac{\partial^2 s}{\partial x^2} = -\Phi\frac{\partial s}{\partial t} \tag{3.8}$$

(Vertical Case)

$$\frac{dU^H}{ds}\frac{\partial s}{\partial x} + \frac{dC_c}{ds}\left(\frac{\partial s}{\partial x}\right)^2 + C_c\frac{\partial^2 s}{\partial x^2} = -\Phi\frac{\partial s}{\partial t} \tag{3.9}$$

(Horizontal Case)

where:

$$U^V = f_w(U \mp M_o\Delta\rho g), \quad U^H = f_w U, \quad C_c = f_w M_o\frac{dP_c}{ds} \tag{3.10}$$

To afford a better comparison with results reported in the literature, Equations (3.8) and (3.9) were changed into dimensionless form using the following definitions:

$$\xi = \frac{x}{L} \Rightarrow dx = Ld\xi \Rightarrow dx^2 = L^2 d\xi^2 \tag{3.11}$$

$$T = \frac{t}{t_{br}} \Rightarrow dT = \frac{1}{t_{br}} dt \Rightarrow dt = t_{br} dT \tag{3.12}$$

Substitution of Equations (3.11) and (3.12) into Equations (3.8) and (3.9) yields:

$$\frac{1}{L}\frac{dU^V}{ds}\frac{\partial s}{\partial \xi} + \frac{1}{L^2}\frac{dC_c}{ds}\left(\frac{\partial s}{\partial \xi}\right)^2 + \frac{C_c}{L^2}\frac{\partial^2 s}{\partial \xi^2} = -\frac{\Phi}{t_{br}}\frac{\partial s}{\partial T} \tag{3.13}$$

(Vertical Case)

$$\frac{1}{L}\frac{dU^H}{ds}\frac{\partial s}{\partial \xi} + \frac{1}{L^2}\frac{dC_c}{ds}\left(\frac{\partial s}{\partial \xi}\right)^2 + \frac{C_c}{L^2}\frac{\partial^2 s}{\partial \xi^2} = -\frac{\Phi}{t_{br}}\frac{\partial s}{\partial T} \tag{3.14}$$

(Horizontal Case)

These are the final governing equations used to describe vertical and horizontal immiscible displacement flow in porous media. The mathematical forms of both equations are the same, the only difference being that Equation (3.13) includes a gravity term, whereas Equation (3.14) does not.

3.1.3 Solution of the Model

In Appendix I it is demonstrated that in the absence of the capillary pressure term the functional relationship between the dimensionless distance, ξ, time, T, and saturation, s, of the displacing fluid will be of the general form:

$$\xi = F(s)T \tag{3.15}$$

which may be rewritten as:

$$s = s(z) = s(\frac{\xi}{T}) \tag{3.16}$$

Differentiating Equation (3.16) with respect to ξ and T, and then substituting into Equation (3.13) yields:

$$T\frac{dU^V}{ds}\frac{ds}{dz}+\frac{1}{L}\frac{dC_c}{ds}(\frac{ds}{dz})^2+\frac{C_c}{L}\frac{d^2s}{dz^2}=\frac{LT\Phi z}{t_{br}}\frac{ds}{dz} \tag{3.17}$$

Since the final mathematical forms for both the vertical and horizontal cases are the same, we deal only with the vertical case here. Also, from Appendix I it can be seen that the first term on the left-hand side in Equation (3.17) is equal to the right-hand side in the absence of capillary forces. Thus, based on assumption (d) above, it is reasonable to assume that:

$$\frac{dU^V}{ds} = C_1 z \tag{3.18}$$

where C_1 is a constant. Insertion of Equation (3.18) into Equation (3.17) then yields:

$$[C_1Tz-\frac{\Phi LT}{t_{br}}z+\frac{1}{L}\frac{dC_c}{ds}(\frac{ds}{dz})]\frac{ds}{dz}+\frac{C_c}{L}\frac{d^2s}{dz^2}=0 \tag{3.19}$$

Equation (3.19) can be rewritten as:

$$[C_1Tz-\frac{\Phi LT}{t_{br}}z+C_2f(z)]\frac{ds}{dz}+\frac{C_c}{L}\frac{d^2s}{dz^2}=0 \tag{3.20}$$

where:

$$C_2f(z)=\frac{1}{L}\frac{dC_c}{ds}(\frac{ds}{dz}) \tag{3.21}$$

Integrating Equation (3.21) yields:

$$\frac{1}{L}C_c = C_2\int f(z)dz + C \tag{3.22}$$

and substitution of Equation (3.22) into (3.20) yields:

$$[C_1Tz - \frac{\Phi LT}{t_{br}}z + C_2 f(z)]\frac{ds}{dz} + [C_2\int f(z)dz + C]\frac{d^2s}{dz^2} = 0 \tag{3.23}$$

By letting y = ds /dz, Equation (3.23) becomes:

$$\frac{[C_1Tz - \frac{\Phi LT}{t_{br}}z + C_2 f(z)]}{[C_2\int f(z)dz + C]}dz = -\frac{dy}{y} \tag{3.24}$$

For a specific time, say $t = t^*$, Equation (3.24) may be integrated to yield:

$$y = N_{GN}e^{-\int \frac{[C_1Tz - \frac{\Phi LT}{t_{br}}z + C_2 f(z)]}{[C_2\int f(z)dz + C]}dz} \tag{3.25}$$

where N_{GN} is a constant that will be discussed later. Upon replacing y by ds/dz, and then integrating, we obtain:

$$s = \int N_{GN}e^{-\int \frac{[C_1Tz - \frac{\Phi LT}{t_{br}}z + C_2 f(z)]}{[C_2\int f(z)dz + C]}dz}dz + C_4 \tag{3.26}$$

where C_4 is another constant. Since Equation (3.26) contains an unknown function, f (z), we cannot obtain an explicit analytical expression. Thus, we assume that $f(z) \propto z$ (see Appendix II), so that C may be zero by using Equation (3.22), and Equation (3.26) may be integrated to give:

$$s = \frac{N_{GN}}{1 - \frac{2\varepsilon}{C_2}}z^{1 - \frac{2\varepsilon}{C_2}} + C_4 \tag{3.27}$$

where: $\varepsilon = TC_1 + C_2 - \Phi LT/t_{br}$. We then apply the two prevailing boundary conditions, namely:

(i) at $z = 0$, $s = s_{max}$

(ii) at $z = 1$, $s = s_{wi}$

Boundary condition (i) represents the inlet condition, boundary condition, (ii) represents the outlet condition, s_{max} denotes the water saturation at the inlet side, and s_{wi} the connate water saturation of the displacing fluid. Thus, the final result is:

$$\xi = T[\frac{(s - s_{max})}{(s_{wi} - s_{max})}]^{\frac{s_{wi} - s_{max}}{N_{GN}}} \tag{3.28}$$

For the case without connate water, the connate water saturation will be zero (s_{wi}=0), because the porous medium cell is perfectly dry before the oil is fed into the cell. Also, according to assumption (c) above, the maximum water saturation will be 1.0 (s_{max}=1). Hence, Equation (3.28) may be simplified to:

$$\xi = T[(1 - s)]^{-\frac{1}{N_{GN}}} \tag{3.29}$$

Equation (3.29) is the final analytical solution of the displacement equation. The difference between vertical and horizontal displacements will be determined mainly by the value of N_{GN}. In other words, different flow orientations are associated with different values of N_{GN}, and different values of N_{GN} will give rise to different saturation profiles. We therefore describe N_{GN} as a *comprehensive coefficient*, since it is the reflection of all the various factors, such as the buoyancy effects (in the vertical mode), the capillary effects, the viscous effects, injection flow rate, and geometry of the porous medium.

3.1.4 Relationship between R and N_{GN}

It has been reported in the literature [van Meurs & van der Poel 1958, Dullien 1979] that the area under the saturation curve multiplied by the thickness of the porous medium is equal to the cumulative volume of the displacing fluid. Thus, the oil recovery can be determined from the following expression:

$$A_s = \int_0^1 \xi ds \tag{3.30}$$

where A_s denotes the area (dimensionless) under the saturation curve. Substituting Equation (3.29) into Equation (3.30) and then integrating yields:

$$A_s = \frac{N_{GN}}{N_{GN} - 1} \tag{3.31}$$

Since the total area of the $\xi \sim s$ coordinate is 1, the final percentage oil recovery will be:

$$R = \frac{N_{GN}}{N_{GN} - 1} \times 100\% \tag{3.32}$$

The oil recovery can be obtained either by experiment or by other methods to be discussed later. Hence, the comprehensive coefficient N_{GN} can be calculated as:

$$N_{GN} = -\frac{R}{1 - R} \tag{3.33}$$

Chapter 4

Instability

4.1 Instability of Immiscible Displacement

The traditional method for studying the displacement instability is to investigate the individual dimensionless numbers, such as the capillary number, gravity number and Bond number. In the present study, a combined dimensionless number was derived, which governs the interaction between these numbers. Hence, it gives a relatively close study of these effects on the displacements. Chuoke et al. (1959) and later Peters and Flock (1981) have presented a formula for a stability index in terms of various physical parameters relating to the porous media. In Peters and Flock's study, a dimensionless number, I_{sr}, was presented to describe the onset of instability:

$$I_{sr} = \frac{(\frac{k_{wor}\mu_o}{k_{oiw}\mu_w} - 1)[U - \frac{k_{wor}(\rho_w - \rho_o)g\cos\psi}{\mu_w(\frac{k_{wor}\mu_o}{k_{oiw}\mu_w} - 1)}]\mu_w L_x^2 L_y^2}{C^* \sigma k_{wor}(L_x^2 + L_y^2)} \qquad (4.1)$$

For displacements in the vertical direction, since buoyancy forces have significant effects on the fingering pattern and the oil recovery efficiency, this dimensionless number must be modified to take buoyancy forces into account. Thus, we have:

$$I_{sr} = \frac{L_x^2 L_y^2 (\frac{k_{wor}\mu_o}{k_{oiw}\mu_w} - 1)}{(L_x^2 + L_y^2)C^* k_{wor}} [\frac{\mu_w U}{\sigma} - \frac{\Delta\rho g k_{wor} \cos\psi}{\sigma(\frac{k_{wor}\mu_o}{k_{oiw}\mu_w} - 1)}] \tag{4.2}$$

In conjunction with the deifnition of the capillary number and Bond number, Equation (4.2) could be rewriten as:

$$I_{sr} = \frac{L_x^2 L_y^2 (\frac{k_{wor}\mu_o}{k_{oiw}\mu_w} - 1)}{(L_x^2 + L_y^2)C^* k_{wor}} [N_c - \frac{N_B k_{wor} \cos\psi}{d_p^2(\frac{k_{wor}\mu_o}{k_{oiw}\mu_w} - 1)}] \tag{4.3}$$

where the definitions of Nc and N_B are the same as Equations (2.9) and (2.11). For linear immiscible displacement, the relative permeability to water and oil can be approximately expressed as [Christle 1989]:

$$k_{rw}(s_w) = s_w^2 \qquad k_{ro}(s_w) = (1 - s_w)^2 \tag{4.4}$$

A combination of Equations (4.3) and (4.4) could yield the final form of this dimensionless number. By inserting the basic parameters, such as viscosity for both fluids, radius of the particles, length and width of the experimental cell, etc., this number could be used to analyze the interaction between the viscous forces, capillary forces and buoyancy forces.

Equation (4.3) has the same mathematical form as Morrow and Songkran's (1981). The only difference is the coefficient attached to this dimensionless number. Morrow and Songkran's dimensionless number was obtained from the experimental results,

whereas the present dimensionless number is the result of a theoretical derivation. The dip angle, ψ, is designated for the three different flow modes as:

$\psi=0^{\circ}$ for the vertical-upward case;

$\psi=90^{\circ}$ for the horizontal case;

$\psi=180^{\circ}$ for the vertical-downward case.

Hence, this effective number could be used to analyze the relative interaction between the viscous forces, capillary forces and buoyancy forces in all three different flow modes, respectively.

4.2 Instability of Miscible Displacement

In miscible displacements, the situation presented here is somewhat different from previous work [Dumoré 1964]. Because the viscosity ratio has been fixed at unity as a special case in the miscible displacements, the viscous forces could be eliminated. Thus, the buoyancy forces are the only factors acting on the displacements. Due to the buoyancy effects, the instability of the linear miscible displacement in vertical cases (vertical-upward and vertical-downward) could result in two extreme situations: stable in the vertical-upward flow mode, unstable in the vertical-downward flow mode. This can be proved by extending Dumoré's theory, as the following subsection demonstrates:

4.2.1 Vertical-Downward Case

In the vertical-downward case, the criterion of a stable displacement is: (i) the *interface* (the contact boundary between the displacing and the displaced fluids) is horizontal, and (ii) the velocity is uniform. Then, applying Darcy's law, the result is:

$$U = -\frac{k_1}{\mu_1}[(\frac{dp}{dz})_1 - \rho_1 g] = -\frac{k_2}{\mu_2}[(\frac{dp}{dz})_2 - \rho_2 g] \tag{4.5}$$

Subscripts 1 and 2 indicate the displacing phase and the displaced phase, respectively. The necessary and sufficient condition for a stable displacement is that the pressure gradient for the displaced phase must be greater than that of the displacing phase [Dumoré 1964]; thus

$$-\frac{U\mu_1}{k_1} + \rho_1 g < -\frac{U\mu_2}{k_2} + \rho_2 g \tag{4.6}$$

If the phase permeability for both displacing and displaced phases could be approximately expressed by the end point permeability [Peters and Flock, 1981], Equation (4.6) becomes:

$$-\frac{U\mu_1}{K} + \rho_1 g < -\frac{U\mu_2}{K} + \rho_2 g \tag{4.7}$$

By observing Equation (4.7), one notes that this inequality is unsatisfied, since the viscosity of both fluids is the same ($\mu_1=\mu_2$), and the density of the displacing phase (a mixture of heavy paraffin oil and tetrachloroethylene), ρ_1, is always greater than that of the displaced phase (light paraffin oil), ρ_2 (i.e., $\rho_1>\rho_2$). Therefore, it can be

concluded that this linear miscible displacement will never be stable in the vertical-downward case when the viscosity ratio is unity.

4.2.2 Vertical-Upward Case

In the vertical-upward case, Equation (4.5) will become the following:

$$U = -\frac{k_1}{\mu_1}[(\frac{dp}{dz})_1 + \rho_1 g] = -\frac{k_2}{\mu_2}[(\frac{dp}{dz})_2 + \rho_2 g] \tag{4.8}$$

Still, the critical condition for a stable displacement is the same as that applied above:

$$-\frac{U\mu_1}{k_1} - \rho_1 g < -\frac{U\mu_2}{k_2} - \rho_2 g \tag{4.9}$$

Also, we approximately employ the end point permeability, instead of the phase permeability, for both displacing and displaced fluids. Thus, Equation (4.9) could be rewritten as:

$$-\frac{U\mu_1}{K} - \rho_1 g < -\frac{U\mu_2}{K} - \rho_2 g \tag{4.10}$$

In Equation (4.10), one can see that this inequality equation is always satisfied, because the density of the displacing fluid (mixture of heavy paraffin oil and tetrachloroethylene), ρ_1, is always greater that of displaced fluid (light paraffin oil), ρ_2 (i.e., $\rho_1 > \rho_2$). Therefore, we can conclude that this linear miscible displacement will always be stable in the vertical-upward case when the viscosity ratio is unity.

4.2.3 Horizontal Case

The above two cases are valid only at low injection flow rates. Once the injection flow rate has increased up to the point at which the pressure gradient (dp/dz term) between the two sides of the cell overshadows the buoyancy (gravity) forces (ρg term), Equation (4.5) for both vertical-upward and vertical-downward flow modes at criterion conditions becomes:

$$U = -\frac{k_1}{\mu_1}(\frac{dp}{dz})_1 = -\frac{k_2}{\mu_2}(\frac{dp}{dz})_2 \tag{4.11}$$

This is also the stability criterion for the horizontal flow mode, since buoyancy forces can effectively be neglected in horizontal flow mode. Equation (4.11) indicates that the displacement can be treated as a single-phase flow situation as long as the viscosity of the two liquids is equal. As a consequence, the displacement will be absolutely stable. Experimental visualization of the displacement patterns for the three different flow modes at high injection flow rates confirms this assertion.

4.3 Critical Velocity for Different Flow Modes

Muskat et al. (1937) were the first to suggest the extension of Darcy's law to multiphase flow through a homogeneous porous medium. Equations (2.2) and (2.3) could be modified as the following forms for both vertical-upward and vertical-downward flow modes:

$$U_w = -\frac{k_w}{\mu_w}\left(\frac{\partial P_w}{\partial x} \pm \rho_w g\right) \tag{4.12}$$

$$U_o = -\frac{k_o}{\mu_o}\left(\frac{\partial P_o}{\partial x} \pm \rho_o g\right) \tag{4.13}$$

The plus sign indicates the vertical-upward case, and the minus sign indicates the vertical-downward case. The pressure gradient for both phases would be writen as:

$$\frac{\partial P_w}{\partial x} = -\frac{U_w \mu_w}{k_w} \mp \rho_w g \tag{4.14}$$

$$\frac{\partial P_o}{\partial x} = -\frac{U_o \mu_o}{k_o} \mp \rho_o g \tag{4.15}$$

The definition of the capillary pressure, P_C, in the two phases at any macroscopic point in the porous medium is presented in Equation (2.6) as:

$$\frac{\partial P_c}{\partial x} = \frac{\partial P_o}{\partial x} - \frac{\partial P_w}{\partial x} \tag{4.16}$$

The necessary and sufficient condition for the stable displacement in the immiscible condition [Dumoré, 1964] is:

$$\frac{\partial P_o}{\partial x} > \frac{\partial P_c}{\partial x} + \frac{\partial P_w}{\partial x} \tag{4.17}$$

The combination of Equations (4.14), (4.15) and (4.17) with the approximate replacement of permeability [Peters and Flock 1981] produces:

$$U < \frac{(\pm \Delta\rho g - \frac{\partial P_c}{\partial x})K}{(\mu_o - \mu_w)} \tag{4.18}$$

Equation (4.18) gives the critical condition for the immiscible displacement aligned in the vertical direction. In other words, the displacement will be stable if the flow rate has a value lower than this critical velocity, U_c, where

$$U_c = \frac{(\pm\Delta\rho g - \frac{\partial P_c}{\partial x})K}{(\mu_o - \mu_w)} \tag{4.19}$$

The capillary pressure model was expressed as [Bentsen and Saeedi 1981]:

$$P_c = -\sigma \ln s_c \tag{4.20}$$

Thus, the differentiation of the capillary pressure with respect to saturation of the displacing fluid will yield:

$$\frac{dP_c}{ds} = -\frac{\sigma}{s_c} \tag{4.21}$$

Equation (3.29) shows the relationships between ξ, T and s. The frontal instability of the displacement was accounted for at the breakthrough condition. Therefore, rearranging and differentiating Equation (3.28) with respect to x yields:

$$\frac{\partial s}{\partial x} = \frac{N_{GN}}{L}\left(\frac{s - s_{\max}}{s_{wi} - s_{\max}}\right)^{1-\frac{s_{wi}-s_{\max}}{N_{GN}}} \tag{4.22}$$

Hence, with the help of Equation (3.7), we have:

$$\frac{\partial p_c}{\partial x} = -\frac{\sigma N_{GN}}{s_c L}\left(\frac{s_c - s_{\max}}{s_{wi} - s_{\max}}\right)^{1-\frac{s_{wi}-s_{\max}}{N_{GN}}} \tag{4.23}$$

Insertion of Equation (4.23) into Equation (4.19) produces the final form of the critical velocity for both vertical cases, which is:

$$U_c = \frac{[\pm\Delta\rho g + \frac{\sigma N_{GN}}{s_c L}(\frac{s_c - s_{max}}{s_{wi} - s_{max}})^{1-\frac{s_{wi}-s_{max}}{N_{GN}}}]K}{(\mu_o - \mu_w)} \tag{4.24}$$

This is the equation for describing the critical condition of the displacement in the three different flow modes. Individually, they are:

(a) Vertical-Upward Case

$$U_c = \frac{[\Delta\rho g + \frac{\sigma N_{GN}}{s_c L}(\frac{s_c - s_{max}}{s_{wi} - s_{max}})^{1-\frac{s_{wi}-s_{max}}{N_{GN}}}]K}{(\mu_o - \mu_w)} \tag{4.25a}$$

(b) Horizontal Case

$$U_c = \frac{\frac{\sigma N_{GN}}{s_c L}(\frac{s_c - s_{max}}{s_{wi} - s_{max}})^{1-\frac{s_{wi}-s_{max}}{N_{GN}}} K}{(\mu_o - \mu_w)} \tag{4.25b}$$

(c) Vertical-Downward Case

$$U_c = \frac{[-\Delta\rho g + \frac{\sigma N_{GN}}{s_c L}(\frac{s_c - s_{max}}{s_{wi} - s_{max}})^{1-\frac{s_{wi}-s_{max}}{N_{GN}}}]K}{(\mu_o - \mu_w)} \tag{4.25c}$$

Chapter 5

Dimensional Analysis

5.1 Determination of R

Oil recovery is known to be controlled by viscous forces, capillary forces, buoyancy forces, injection flow rate, and the physical properties of the porous medium. A dimensional analysis approach, in conjunction with a linear regression to estimate the relevant parameters, was employed in the present study to predict the oil recovery, R, as a function of various dimensionless groups. It was assumed that:

$$R = function(\Delta\rho, \mu_o, \mu_w, \sigma, U, d_p, g, L) \tag{5.1}$$

(Vertical Case)

$$R = function(\mu_o, \mu_w, \sigma, U, d_p, L) \tag{5.2}$$

(Horizontal Case)

When written in terms of the fundamental dimensions (mass, length and time), Equations (5.1) and (5.2) become:

$$[1] = [ML^{-3}]^a [ML^{-1}T^{-1}]^b [ML^{-1}T^{-1}]^c [MT^{-2}]^d [LT^{-1}]^e [L]^f [LT^{-2}]^i [L]^j \tag{5.3}$$

(Vertical Case)

$$[1] = [ML^{-1}T^{-1}]^a [ML^{-1}T^{-1}]^b [MT^{-2}]^c [LT^{-1}]^d [L]^e [L]^f \tag{5.4}$$

(Horizontal Case)

Since the exponents of the dimensions M, L and T must be equal on both sides of these equations, in order to ensure dimensionless consistency, we have:

(1) the vertical case

[M]: 0=a+b+c+d

[L]: 0=-3a-b-c+e+f+i+j

[T]: 0=-b-c-2d-e-2i

(2) the horizontal case

[M]: 0=a+b+c

[L]: 0=-a-b+d+e+f

[T]: 0=-a-b-2c-d

Solving the above equations in (1) and (2) and rearranging Equations (5.1) and (5.2) leads to:

$$\ln R = \ln \Lambda + \alpha \ln(N_g) + \beta \ln(\mu_r) + \gamma \ln(N_c) + \lambda \ln(\frac{d_p}{L}) + \theta \ln(N_F) \qquad (5.5)$$

(Vertical Case)

$$\ln R = \ln \Lambda + \beta \ln(\mu_r) + \gamma \ln(N_c) + \lambda \ln(\frac{d_p}{L}) \qquad (5.6)$$

(Horizontal Case)

where $\mu_r = \frac{\mu_o}{\mu_w}$, $N_c = \frac{\mu_w U}{\sigma}$, and $N_g = \frac{\mu_w U}{\Delta \rho g d_p^2}$, $N_F = \frac{gL}{U^2}$.

For the vertical case, Equation (5.5) shows that the oil recovery, R, is influenced by the following dimensionless groups: (i) the ratio of the buoyancy forces to the viscous

forces (i.e., the gravity number); (ii) the viscosity ratio; (iii) the ratio of the capillary forces to the viscous forces (i.e., the capillary number), (iv) a group characterizing the geometry of the porous medium, and (v) a group involving the flow rate (the Froude number). Since (iv) remains constant, it will be combined into $\ln\Lambda$, and since the factor in (v) has a linear relationship with the previous three groups, this group will be omitted when the regression analysis is performed.

In the horizontal case (Equation (5.6)), the oil recovery, R, is a function only of the viscosity ratio, capillary number and geometry of the porous medium. Because the last term is constant in a certain porous medium, it will be combined into $\ln\Lambda$. Thus, N_{GN} can then be determined using these equations.

Chapter 6

Experimental

6.1 Materials

In the present study, the fluid system contained two distinct fluids: the displaced fluid and the displacing fluid. For immiscible displacement processes, heavy paraffin oil was used as the displaced fluid, while distilled water (and/or glycerol solution) dyed with methylene blue was used as the displacing fluid. For miscible displacement processes, light paraffin oil was used as the displaced fluid, and a mixture of heavy paraffin oil and tetrachloroethylene dyed with oil red was used as the displacing fluid. The physical properties of heavy paraffin oil against various aqueous solutions are listed in Table 6.1. Table 6.2 lists the physical properties of the basic fluids employed in this study.

Table 6.1 Physical Properties of Heavy Paraffin Oil/Glycerol Solution at 25°C±0.5°C

Glycerol Solution Concentration (vol. %)	ρ_o/ρ_w	μ_o/μ_w	σ (mN/m)	
			Non-Dyed	Dyed
0.0	0.876	152.02	50.56	49.53
30.0	0.808	52.13	40.81	39.88
75.0	0.728	4.11	31.43	30.90

Table 6.2 Physical Properties of Oils and Aqueous Solutions at 25°C±0.5°C

Fluid	Viscosity (mPa.s)	Density (g/cm^3)
Heavy Paraffin Oil	135.82	0.874
Light Paraffin Oil	20.50	0.852
67% Glycerol Solution	20.50	1.171
Dyed Distilled Water	0.89	0.998

6.2 Porous Medium Cell

A linear consolidated porous medium cell of nominal dimensions 20 cm × 10 cm × 0.3 cm was produced by lightly sintering glass beads (diameter 0.040 ~ 0.045 cm) between two parallel glass plates at about 575°C. This cell contained two separate reservoirs at either end of the cell. These two reservoirs were incorporated so as to avoid any end effects. Table 6.3 lists the properties of the porous medium cell, and Fig.6.1 shows a photograph of the experimental cell.

Table 6.3. Properties of Porous Medium Cell

Pore Volume (cm^3)	Porosity (%)	Dimension (L×W×h) (cm^3)
31.483	34.98	20.0×15.0×0.3
23.424	37.18	20.0×10.0×0.3

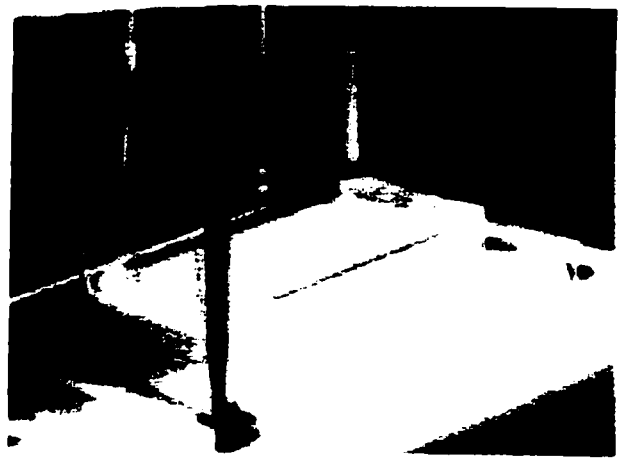

Fig.6.1 Photograph of the Experimental Cell.

6.3 Specification of the System

Table 6.4 Specification of the Components and Fluids Used in the Experiments

Item	Specification
Water	Distilled
Glycerol Solution	BDH
Heavy Paraffin Oil	BDH
Light Paraffin Oil	BDH
Tetrachloroethylene	BDH
Glass Beads (0.040~0.0445 cm)	Rouville Inc.
White Silicon Epoxy	Lepage Inc.
Acetone	BDH
Propanol-2	BDH
Syringe Pump	Sage Instrument Model 341A
Syringe	Fisher Scientific Co.
Methylene Blue Dye	Fisher Scientific Co.
Oil Red	Fisher Scientific Co.
Timer	Precision Scientific Co.
Camera	Minolta XG-M
HP ScanJet 3p Scanner	Hewlett Packard
486DX33-Computer	Compustar

6.4 Experimental Method

6.4.1 Saturation Processes

6.4.1.1 Saturation without Connate Water

To completely saturate the porous medium, the cell was first connected to a vaccum pump at the inlet side. When the vacuum pressure was established, the burette was

opened and the oil was introduced into the cell. Meanwhile, both reservoirs were also fully filled with oil. Otherwise, if the reservoirs contained any air, the displacement process would become a three-phase displacement rather than a two-phase displacement. Fig.6.2 shows the experimental set-up.

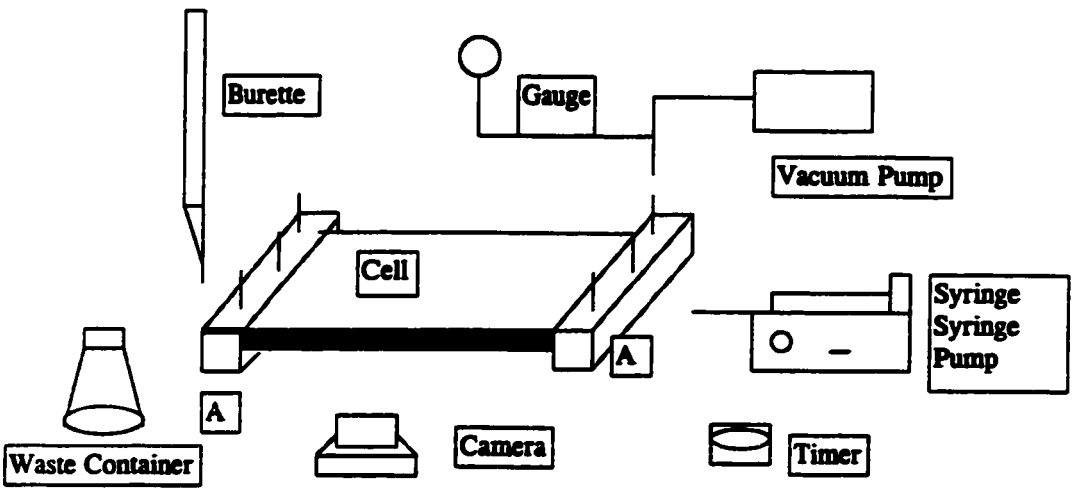

Fig.6.2 Experimental Set-Up. A = reservoir.

6.4.1.2 Saturation with Connate Water

To establish the connate water in the porous medium cell, the cell was first saturated with water (non-dyed), and then flushed many times with volumes of heavy paraffin oil, until the water ceased to be mobilized. Thus, the water left in the cell existed as water drops surrounded by the heavy paraffin oil. Due to the high capillary forces, the water could not move, and is called connate water. The saturation of this connate water

is called the residual saturation of water. The residual saturation of water in the present study was about 5%.

6.4.2 Displacement Processes

The reservoir was installed at the inlet side to keep the same pressure anywhere inside the reservoir. The reservoir at the outlet side collected the oil across the entire cross-section of the porous medium cell, rather than at only one or several points, so that the flow streamlines could go directly from the inlet side to the outlet side. Before the displacement started, the reservoir at the inlet side had to be slowly filled with displacing fluid, so that the linear displacement could be conducted. After the filling process at the inlet reservoir was completed, the displacement started at a certain injection flow rate. The syringe and syringe pump were used to inject the displacing fluid into the porous medium, to displace the displaced fluid. Meanwhile, the timer was turned on to record the displacement time. Photographs were taken at different displacement times, up to and including the breakthrough time, to record the fingering pattern.

6.4.3 Cleaning and Drying Processes

Cleaning and drying of the cell had to be done after each run. 100mL Propanol-2, 100mL acetone and 250mL water were used to clean the cell. Finally, nitrogen gas was slowly passed through the porous medium cell until the cell was completely dry.

6.4.4 Calculation of Breakthrough Oil Recovery

For each experimental run, the breakthrough oil recovery was calculated. Based on assumption (a) in Chapter 3, the fractional oil recovery at the breakthrough condition, R, was equal to the cumulative volume of water injected up to the breakthrough, divided by the initial volume of oil in the porous medium cell [Guo and Neale, 1996]; that is,

$$R = \frac{Qt_{br}}{V_p} \tag{6.1}$$

All of the oil recoveries, including replicate experiments, had an accuracy of ±3% [Appendix IV].

6.5 Experiments Performed

The experiments performed in this study included: (i) those immiscible displacements, and (ii) miscible displacements. Part (i) consisted of three sets of experiments:

(1) three different viscosity ratios;

(2) a unity viscosity ratio; and

(3) with and without connate water.

In part (ii), the experiments were conducted only with a unity viscosity ratio. All experiments were carried out in all three different flow modes, and the operation temperature was 25°C±0.5°C.

6.6 Measurement of Viscosity

The fluid viscosities were measured using the Cannon-Fenske Routine Viscometer, provided by Cannon Instrument Corporation. This viscometer works by measuring the efflux time required for the meniscus to flow freely down from mark C to mark E (see Fig.6.3), and using this time measurement and the coefficient of the U-tube to calculate the viscosity of the fluid, as follows:

$$\mu = t_v C_v \rho_v \tag{6.2}$$

where t_v is efflux time of measuring viscosity, C_v is viscometer constant, and ρ_v is density of sample measured. All measurements were taken after equilibrium was reached. Fig.6.3 shows a schematic of the viscometer tubing and Figs.6.4 and 6.5 show results for different fluid systems.

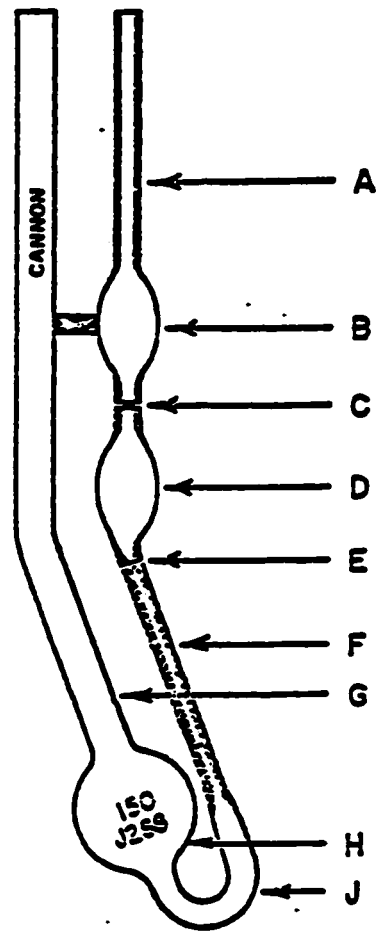

Fig.6.3 Scheme of Cannon-Fenske Routine Viscometer tubing [Cannon Instrument Co.].

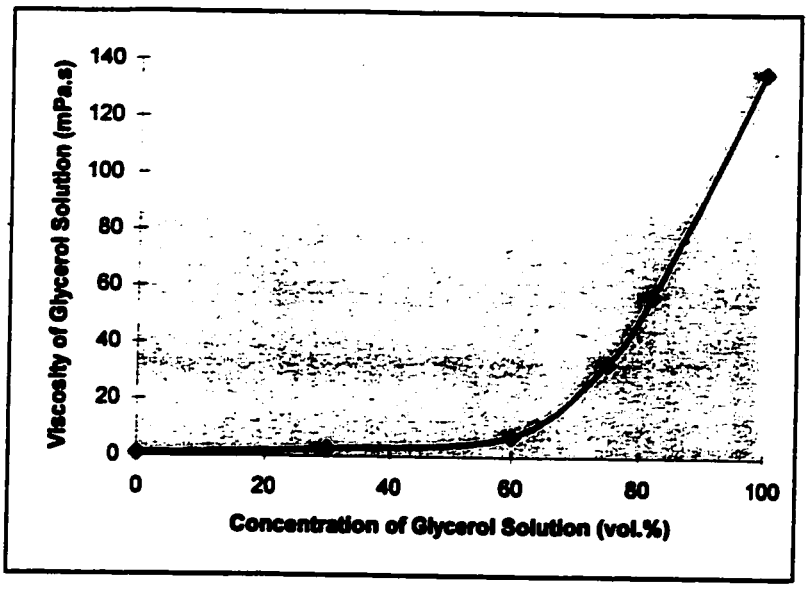

Fig.6.4 Relationship between the Concentration of the Glycerol Solution and the Viscosity of the Solution at 25°C±0.5°C.

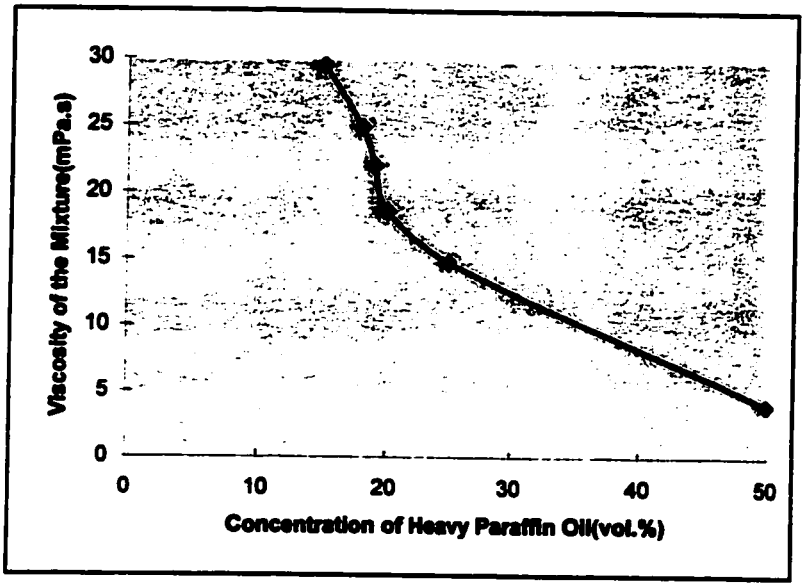

Fig.6.5 Relationship between the Concentration of the Heavy Paraffin Oil and the Viscosity of the Mixture of Tetrachloroethylene and Heavy Paraffin Oil.

6.7 Measurement of Density

A DMA 48 density meter, manufactured by PAAR in Austria, was used to measure the density for all the fluids employed in this study. The principle of this density meter is to measure the period of oscillation of a glass-U tube to determine the density of liquids and gases. After the sample is injected into the U-tube, the oscillation is influenced by the mass of the sample. The tube is called the oscillation cell. The volume of the cell is fixed. Therefore, once the calibration with known substances, such as air or water, is performed, the mass of the sample can be taken to be proportional to its density. The specifications of this density meter are:

(i) The measuring range is from 0 to 3 g/cm^3. Accuracy is $\pm 1 \times 10^{-4} g/cm^3$.

(ii) The temperature accuracy is 0.1°C, and the temperature range for the measurement is from -10°C to + 70°C.

(iii) The sample size of the cell is approximately 0.7 cm^3.

All measurements in this study were done at a temperature of 25°C. Fig.6.6 shows the relationship between the density and the concentration of the glycerol solution.

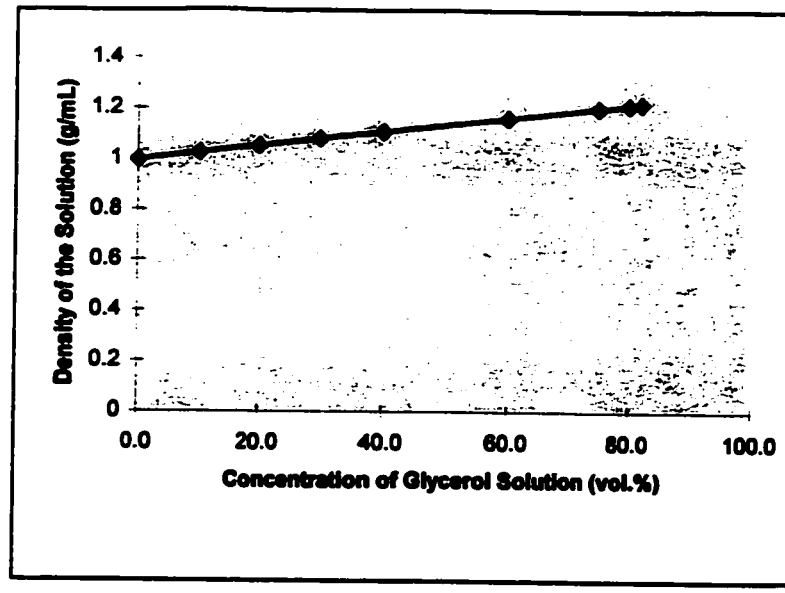

Fig.6.6 Relationship between the Concentration of the Glycerol Solution and the Density of the Glycerol Solution.

6.8 Measurement of Porosity

The procedures for measuring the porosity of the experimental cell are:

- the cell was weighed (M_{cell}) when completely dry.
- the cell was filled slowly with water until it was completely saturated, and then the cell was weighed again ($M_{cell\text{-}water}$).
- the pore volume and porosity of the cell could be calculated as:

$$M_{water} = M_{cell-water} - M_{cell} \tag{6.3}$$

$$V_p = V_w = \frac{M_{water}}{\rho_w} \tag{6.4}$$

Combination of Equations (6.3) and (6.4) yields the formula for calculating the pore volume:

- the volume of the cell is calculated as:

$$V = L \times W \times h \tag{6.5}$$

- the porosity of the cell is calculated as:

$$\Phi = \frac{V_p}{V} \tag{6.6}$$

6.9 Residual Saturation

The procedure for measuring and calculating the residual water saturation (connate water saturation) and residual oil saturation is decribed in the following subsection:

6.9.1 Residual Water Saturation

- The cell was weighed (M_{cell}) when completely dry.
- After the cell was completely saturated with the water, oil was introduced into the cell to displace the water until the water ceased to mobilize. It should be remembered that most of the water will be displaced because the viscosity of oil is

greater than that of water. The cell was weighed again, yielding the quantity $M_{cell\text{-}water\text{-}oil}$.

- The two measurements obtained above were used to calculate the weight of the water and the oil:

$$M_{water} + M_{oil} = M_{cell-water-oil} - M_{cell} \tag{6.7}$$

where

$$M_{water} = V_w \rho_w \qquad M_{oil} = V_o \rho_o \tag{6.8}$$

and the pore volume of the cell is equal to the sum of volume of the water and the oil, as follows:

$$V_p = V_w + V_o \tag{6.9}$$

Inserting Equations (6.8) and (6.9) into Equation (6.7) and rearranging it yields:

$$V_w = \frac{M_{cell-water-oil} - M_{cell} - V_p \rho_o}{(\rho_w - \rho_o)} \tag{6.10}$$

From Equation (6.10) we can calculate the volume of residual water (connate water); then the residual water saturation (connate water saturation) can easily be calculated as:

$$s_{wi} = \frac{V_w}{V_p} \tag{6.11}$$

6.9.2 Residual Oil Saturation

The method for measuring residual oil saturation differed slightly from that for residual water saturation:

- The cell was weighed (M_{cell}) when completely dry.
- After the cell was completely saturated with oil, water was very slowly introduced into the cell to displace the oil in a vertical-upward direction, until the oil stopped moving; most of the oil was displaced, because the density of water is greater than that of oil. The cell was weighed again ($M_{cell\text{-}water\text{-}oil}$).
- The two measurements obtained above were used to calculate the weight of the oil and the water (Equation (6.7)).
- Equations (6.7), (6.8) and (6.9) were used to obtain the formula to calculate the residual volume of the oil:

$$V_o = \frac{V_p \rho_o - (M_{cell-water-oil} - M_{cell})}{(\rho_w - \rho_o)} \tag{6.12}$$

- The residual oil saturation can be calculated as:

$$s_{or} = \frac{V_o}{V_p} \tag{6.13}$$

Chapter 7

Photographic Procedures

7.1 Principle of the Method

During the displacement experiments, photographs were taken prior to and at the final breakthrough time. To process these photographs, a commerical computer software package, known as *Mocha,* was used to measure the surface area occupied by the fingers. However, there is some difficulty in interpreting the photographs, since the experimental data (breakthrough time, oil recovery, etc.) relate to the actual three-dimensional porous medium, whereas the fingering patterns shown in the photographs are necessarily two-dimensional in nature. To overcome this difficulty, the photographs were processed using the following procedure:

(1) a Scanjet 3P scanner was used to scan the pictures and savthem for future use;

(2) the *Mocha* software was used to adjust the two-dimensional area covered by the fingers so that this adjusted area, when multiplied by the thickness of the porous medium, became equal to the volume of the displacing fluid (Fig.7.1);

(3) this adjusted area and the area corresponding to the entire cell were measured;

(4) the widths (W_f) of the fingers at different lateral distances, x, were then measured, and the saturation profile was obtained from:

$$s = \frac{W_f h \Delta x}{W h \Delta x} = \frac{W_f}{W} \; ; \tag{7.1}$$

(5) the computer output was printed out and recorded.

The basic tools used to perform this procedure were the software *Mocha, Windows 3.1* and *Axum 3.0,* a 486sx-33 personal computer, and a Hewlett-Packard Scanjet 3P scanner.

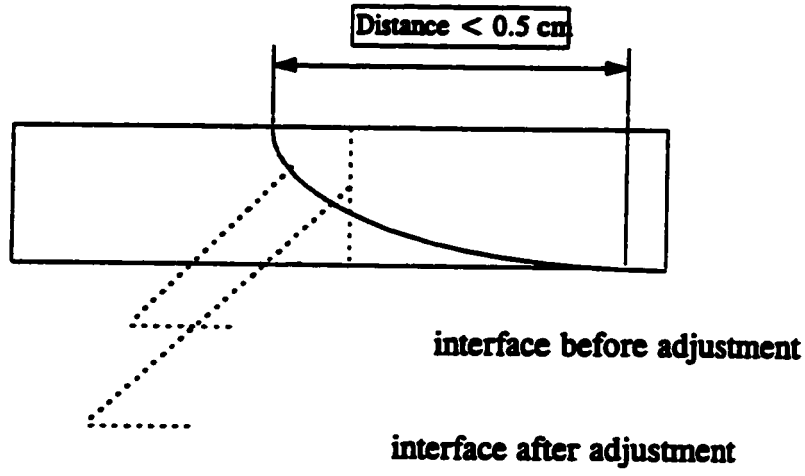

Fig.7.1 Scheme of Interfaces before and after Adjustment.

7.2 Precision of the Measurement

Before *Mocha* was used to perform the measurements, the calibration of the measurements had to be made [see Appendix V]. The length of the photo shown on the screen was 644 pixels, and this 644 pixels was calibrated to be equal to 20 cm long, which is the length of the experimental cell. After calibration, the measurements could be started.

First, the threshold function was used to make a clear boundary of the fingering pattern, so that the three-dimensional fingering pattern could be expressed by a two-dimensional fingering pattern. Next, the average finger width at each interval (such as 1 cm), along with the x-axis, was measured. Because the boundary was clear after the adjustment, the error produced by the measurements was only one pixel, which is 0.031 cm. If it is assumed that the maximum finger width is 10 cm (the width of the experimental cell), then the precision of the measurements could be considered to be 0.31%. This is acceptable precision in these measurements.

Chapter 8

Results and Discussions

8.1 Immiscible Displacements with Three Viscosity Ratios

Three sets of experiments (in the *horizontal, vertical-upwards* and *vertical-downwards* flow modes) with three different viscosity ratios (μ_r=152.02, μ_r=52.13 and μ_r=4.11) were performed. Photographs were taken at the breakthrough time. Fig. 8.1, 8.2, and 8.3 show the general nature of the relationship between the injection flow rate and breakthrough oil recovery.

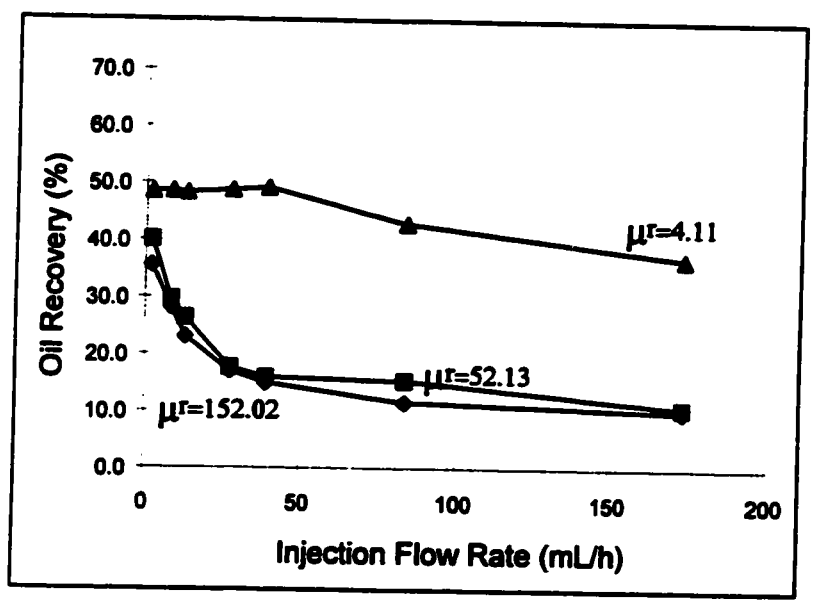

Fig.8.1 Relationship between the Injection Flow Rate and Breakthrough Oil Recovery in the Horizontal Flow Mode.

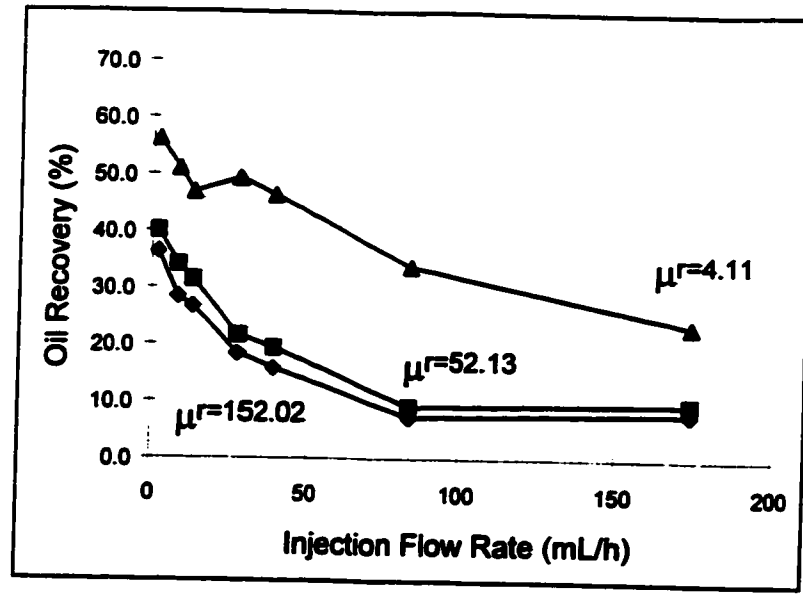

Fig.8.2 Relationship between the Injection Flow Rate and Breakthrough Oil Recovery in the Vertical-Upward Flow Mode.

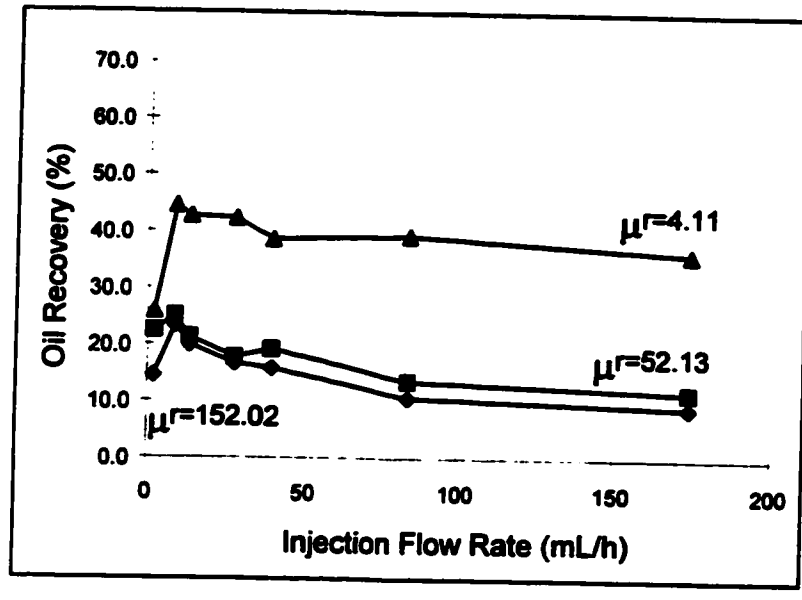

Fig.8.3 Relationship between the Injection Flow Rate and Breakthrough Oil Recovery in the Vertical-Downward Flow Mode.

8.1.1 Horizontal Displacements

In the horizontal displacement mode, the oil recovery basically decreases with increasing injection flow rate, and these results agree well with those of Scott et al. (1965). At low injection flow rates, where capillary forces play a key role [Fayers and Sheldon, 1959, Perkins and Johnston, 1969], invading fluid (water) displaces more oil not only in the smaller channels, but also in the larger ones. Relatively speaking, viscous forces do not affect the displacement very much in this flow regime. It may be seen from Figs.8.4a and b that only a few fingers developed, but they almost filled the entire porous medium, whence a relatively higher oil recovery can be expected. However, when the injection flow rate was increased, the fingering pattern displayed significant differences (Figs. 8.4c and d). Numerous small fingers developed early during the injection, particularly near the entrance of the cell. These fingers soon broke up into a fine dendritic network of channels. These observations indicate that the viscous forces are much more important than the capillary forces in this region [Spivak 1974, Ni et al. 1986]. The extensive fingering resulted in only part of the oil being displaced, thereby causing a large amount of oil to be left behind in the porous medium, and a low percentage of oil to be recovered.

Horizontal immiscible displacement

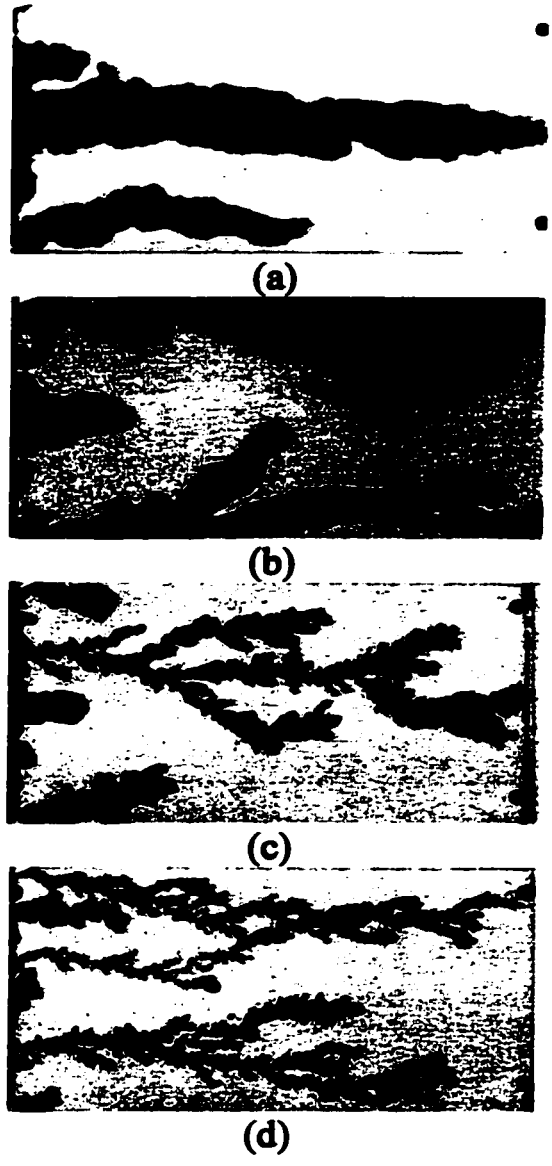

Fig.8.4. Horizontal immiscible displacements. Dyed distilled water displacing paraffin oil (μ_o/μ_w=152.02, ρ_o/ρ_w=0.876) at (a) Q=8.5 mL/h, R=28.19%; (b) Q=13.2 mL/h, R=23.06%; (c) Q=84.0 mL/h, R=11.56%; (d) Q=174.0 mL/h, R=10.11%.

8.1.2 Vertical-Upward Displacements

The fingering patterns in vertical-upward displacements differ from those in horizontal displacements, especially at low injection flow rates, even though the general trends of the oil recovery-injection flow rate relationship are similar to each other (see Fig.8.1 and 8.2). At low injection flow rates, because of the significant effects of the buoyancy forces, the fingers appeared to be much stronger (Figs.8.5a and b). Also, the capillary forces performed an important role at this low injection flow rate, as the channels in contact with the displacing fluid were fully filled. On the other hand, viscous forces did not show significant effects on these displacements. Therefore, large fingers indicate that higher oil recoveries can be obtained. In this situation, the influence of buoyancy forces on the displacement process is more significant than in the case of horizontal displacement (R=48.59% in horizontal case, R=56.25% in vertical-upward case at μ_r=4.11 and Q=2.0 mL/h). Moreover, these effects play a positive role in the vertical-upward displacements. As a result, at the same low injection flow rate, the oil recovery in the vertical-upward case is higher than in the horizontal case. However, the results are completely different as the injection flow rate increases. Increasing the injection flow rate will greatly promote viscous forces, whence buoyancy forces and capillary forces will have no time to exert their full effects on the displacement process. Hence, the fingering pattern becomes similar to that obtained for the horizontal case, since the factors affecting the displacement are almost the same. This hypothesis can be

Vertical-upward immiscible displacement

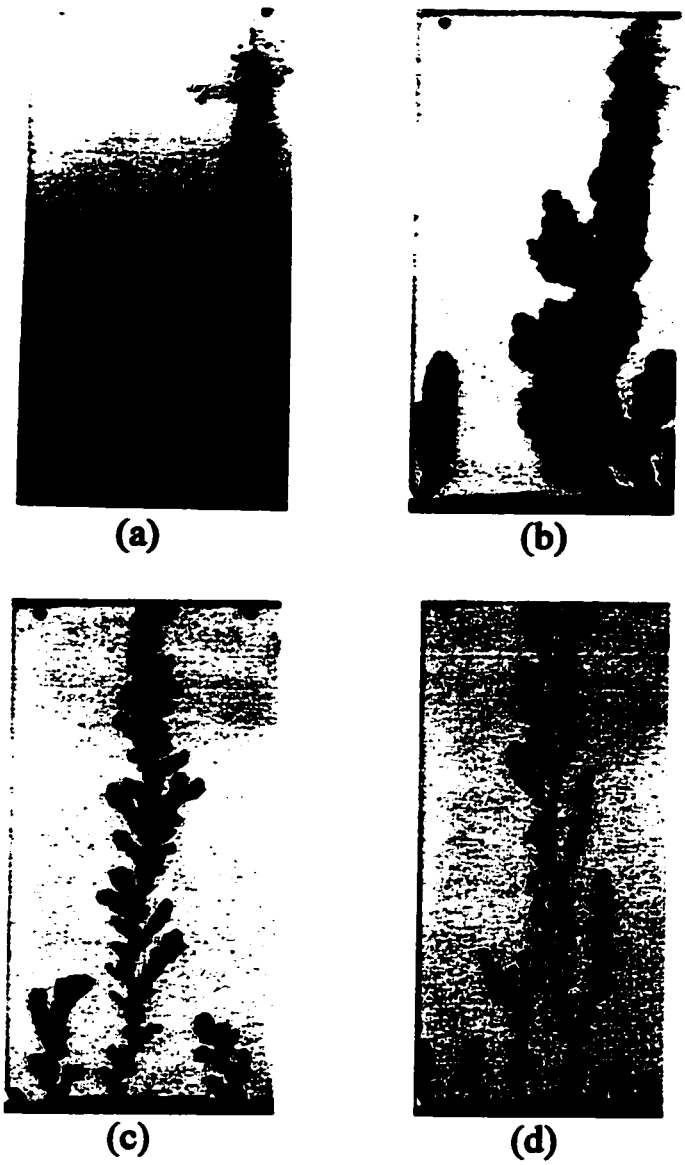

Fig.8.5. Vertical-upward immiscible displacements. Dyed distilled water displacing paraffin oil (μ_o/μ_w=152.02, ρ_o/ρ_w=0.876) at (a) Q=8.5 mL/h, R=28.38%; (b) Q=13.2 mL/h, R=26.72%; (c) Q=84.0 mL/h, R=7.27%; (d) Q=174.0 mL/h, R=8.05%.

confirmed by comparing the pictures in Figs.8.4c and d with those in Figs.8.5c and d, in which the final oil recoveries are apparently close to each other.

8.1.3 Vertical-Downward Displacements

In the vertical-downward displacement mode, the fingering pattern will be different yet again. At low injection flow rates, buoyancy forces and capillary forces dominate the displacement. The buoyancy forces play a negative role, since they speed up the downward movement of the displacing fluid on account of the higher density of the displacing aqueous phase than that of the oil. Thus, the displacing fluid moves much faster than in the horizontal and vertical-upward cases (see Table 8.1), and a larger uncontacted area is established. This leads to a drastically reduced oil recovery due to premature breakthrough of the displacing fluid. Figs.8.6a and b show that the colour density of the fingering pattern is lighter, indicating that the displacing fluid only partially filled the porous medium. The oil recovery is lower (R=21.99% at Q=2.0 mL/h, μ_r=4.11) than in either the horizontal or the vertical-upward displacements; further demonstrating the negative role played by buoyancy. With increasing injection flow rate, the fingering pattern gradually becomes close to those in the horizontal and vertical-upward cases, since viscous forces are significantly increased and come to dominant both the buoyancy forces and capillary forces. Also, the effects of both buoyancy forces and capillary forces are reduced. Dynamically speaking, no matter which displacement orientation is involved, only the viscous forces have a dominant influence on the displacements when the injection flow rate and viscosity ratio are high.

Vertical-downward immiscible displacement

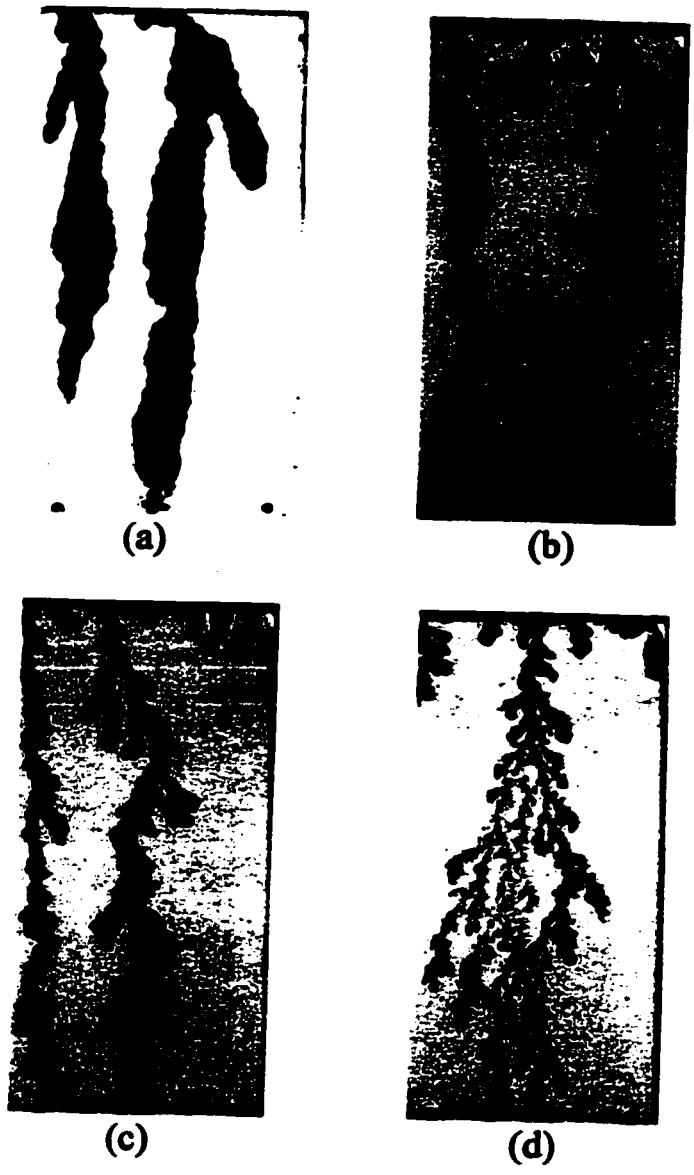

Fig.8.6. Vertical-downward immiscible displacements. Dyed distilled water displacing paraffin oil μ_o/μ_w=152.02, ρ_o/ρ_w=0.876) at (a) Q=8.5 mL/h, R=23.35%; (b) Q=13.2 mL/h, R=19.90%; (c) Q=84.0 mL/h, R=10.66%; (d) Q=174.0 mL/h, R=9.08%.

In view of this fact, all of the fingering patterns look quite similar at high injection flow for all three flow modes (compare Figs.8.4c and d, 8.5c and d and 8.6c and d) and the final oil recoveries are virtually the same.

Table 8.1 Comparison of Breakthrough Time in Three Flow Modes at Q=2.0 mL/h

Flow Mode	Viscosity Ratio	Breakthrough Time (s)
Horizontal Mode	4.11	20448
Vertical-Upward Mode	4.11	23717
Vertical-Downward Mode	4.11	10201
Horizontal Mode	52.13	10259
Vertical-Upward Mode	52.13	16874
Vertical-Downward Mode	52.13	9946
Horizontal Mode	152.02	9274
Vertical-Upward Mode	152.02	15322
Vertical-Downward Mode	152.02	6131

8.1.4 Effects of Buoyancy Forces

Since the gravity number is defined as the ratio of viscous forces and buoyancy forces, it is easy to plot the relationship between this number and oil recovery. Fig.8.7 shows the volumetric oil recovery efficiency at the breakthrough condition vs. gravity number in the vertical-upward flow mode. On the basis of these results, the oil recovery increases with a decrease in the gravity number [van Meurs and van der Poel 1958, Richardson and Perkins 1957]. A decrease in the gravity number means increasing the

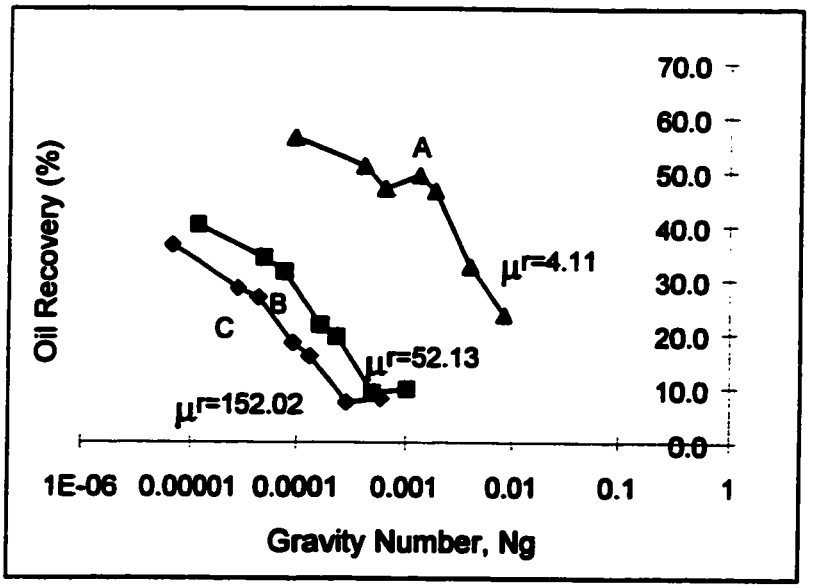

Fig.8.7 Relationship between Oil Recovery and Gravity Number in Vertical-Upward Mode.

buoyancy effects on the displacement, which results in an increasing tendency for displacing fluid to linger at the bottom of the porous medium, or for the displaced fluid to float upwards. This can be established by either increasing the difference in density between two fluids or slowing down the injection flow rate. The lower the gravity number, the more stable the displacement, and the higher the oil recovery. On the other hand, capillary forces also play a significant role in the displacement. Oil recovery increases with increasing capillary number (see Figs.8.8a, b and c), since an increase in the capillary number means a decrease in the interfacial tension. This further confirms that both the capillary and buoyancy forces are extremely important at low injection flow rates.

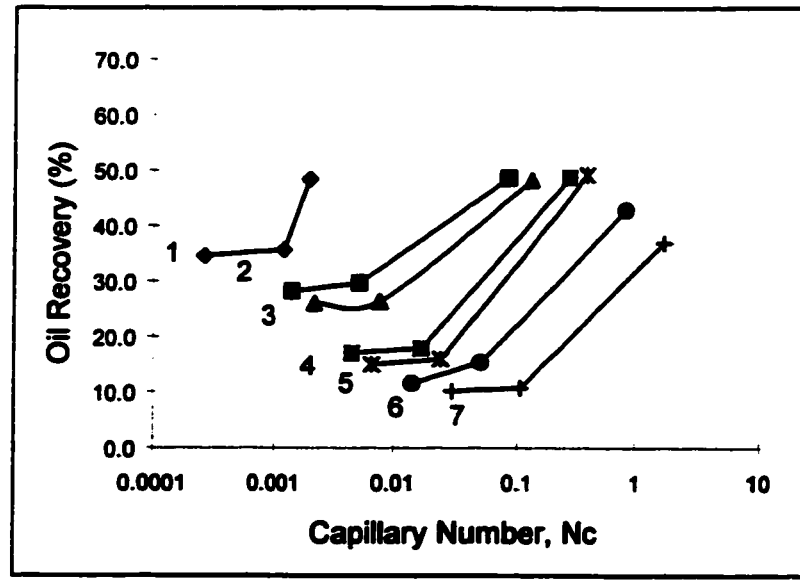

Fig.8.8a. Effects of Capillary Number on Oil Recovery in Horizontal Mode. 1. Q=2.0 mL/h; 2. Q=8.5 mL/h; 3. Q=13.2 mL/h; 4. Q=27.6 mL/h; 5. Q=39.0 mL/h; 6. Q=84.0 mL/h; 7. Q=174.0 mL/h.

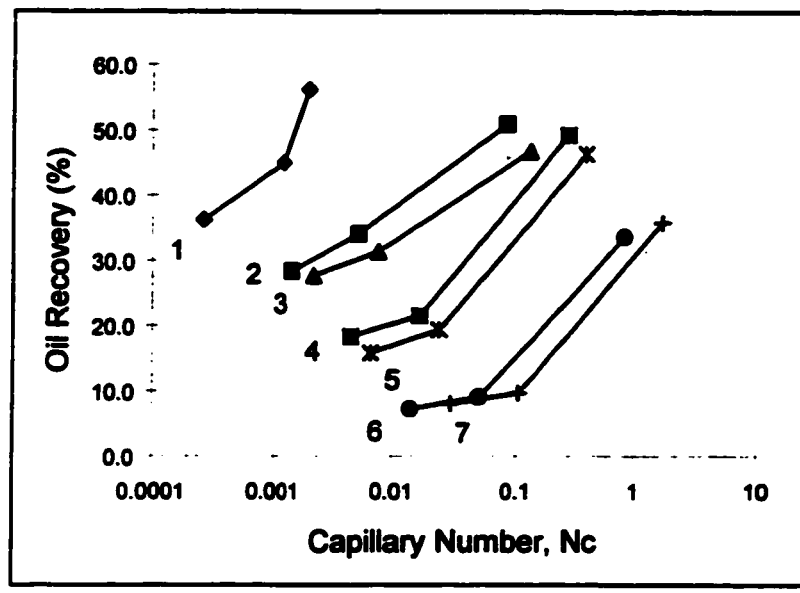

Fig.8.8b. Effects of Capillary Number on Oil Recovery in Vertical-Upward Mode. 1. Q=2.0 mL/h; 2. Q=8.5 mL/h; 3. Q=13.2 mL/h; 4. Q=27.6 mL/h; 5. Q=39.0 mL/h; 6. Q=84.0 mL/h; 7. Q=174.0 mL/h.

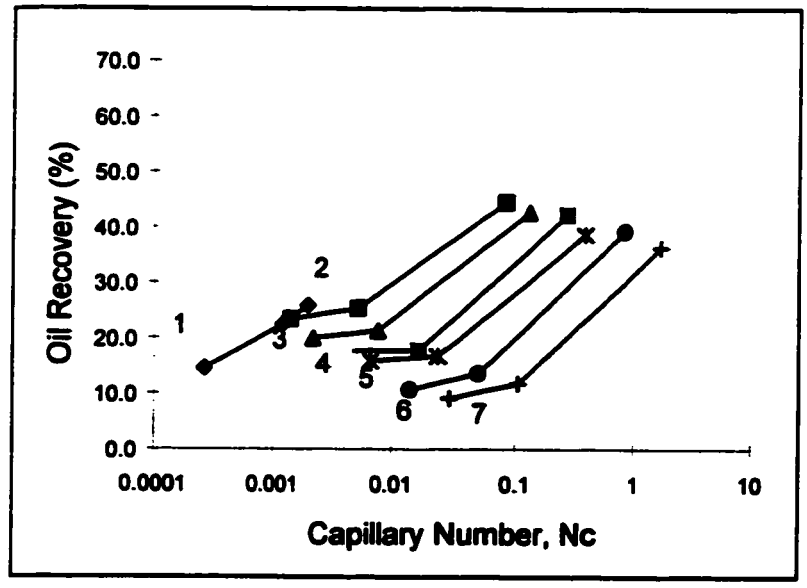

Fig.8.8c. Effects of Capillary Number on Oil Recovery in Vertical-Downward Mode. 1. Q=2.0 mL/h; 2. Q=8.5 mL/h; 3. Q=13.2 mL/h; 4. Q=27.6 mL/h; 5. Q=39.0 mL/h; 6. Q=84.0 mL/h; 7. Q=174.0 mL/h.

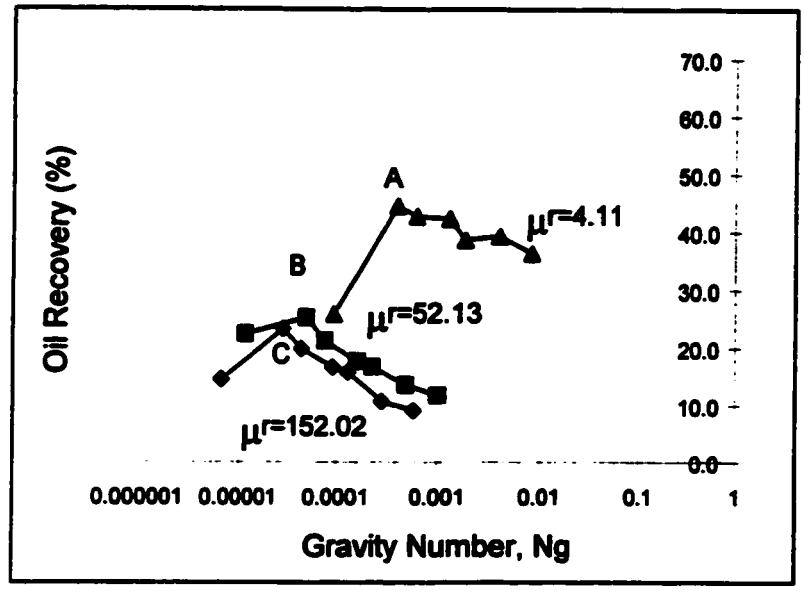

Fig.8.9 Relationship between Oil Recovery and Gravity Number in Vertical-Downward Mode.

Fig.8.9 depictes the volumetric oil recovery efficiency at the breakthrough condition vs. gravity number in the vertical-downward flow mode. In contrast to the vertical-upward flow mode, the oil recovery in the vertical-downward flow mode is much lower at the same flow rates. It can be concluded that buoyancy forces acted inversely in this particular case. However, the competition between the capillary forces, buoyancy forces and viscous forces may be changed by varying the injection flow rates. At very low gravity numbers, oil recovery increased with increasing gravity number. This is because the viscous forces began to compete with both the capillary and buoyancy forces as the injection flow rate increased, leading to slightly wider fingers. As a consequence, little gain in the oil recovery was obtained. Continuously increasing the gravity number will largely enhance viscous forces. With the help of buoyancy forces, the displacing fluid will go downwards much faster and the fingers will grow even wider. However, capillary imbibition is still effective in the displacement. Thus, oil recovery is increased to the maximum (points A, B and C).

The situations will be similar for both the vertical-upward and downward cases at high gravity numbers. As mentioned above, increasing the injection flow rate will drastically increase the effects of viscous forces. In this situation, viscous forces will completely dominate both the capillary forces and buoyancy forces, and capillary imbibition will no longer be effective. Numerous viscous fingers resulted in greatly reduced oil recovery, as expected. Because the key factors are the same at high

injection flow rates in both vertical-upward and vertical-downward flow modes, the fingering patterns looked very similar to each other.

8.1.5 Critical Condition of the Displacements

There is a relative equilibrium point for the balance of these three forces (viscous forces, capillary forces and buoyancy forces). Passing through this point, the oil recovery changed suddenly (see points in Figs.8.7 and 8.9). In general, these curves could be divided into two distinct regions, namely (i) the capillary and buoyancy region (at low injection flow rates), and (ii) the viscous region (at high injection flow rates).

In the vertical-upward flow mode the critical points are: $N_g \approx 0.001299$ for $\mu_o/\mu_w = 4.11$ (point A), $N_g \approx 0.000078$ for $\mu_o/\mu_w = 52.13$ (point B), and $N_g \approx 0.000044$ for $\mu_o/\mu_w = 152.02$ (point C). An explanation for this is as follows: (a) In the capillary and buoyancy region: both capillary imbibition and buoyancy effects are large enough to overcome viscous forces. This makes the displacing fluid stay underneath the oil and penetrate different size of channels. Increasing the injection flow rate will reduce the effects of both the capillary and buoyancy forces, but the viscous forces are still not capable of competing with those forces. From the plot (Fig.8.7) one can see that oil recovery is slightly decreased. (b) In the viscous region: after the critical points (points A, B and C), the viscous forces are very high and become the dominant factor in the

displacement. The effects of both the capillary and buoyancy forces have been diminished during the displacement. As a result, oil recovery decreased sharply.

In the vertical-downward flow mode the critical points are: $N_g \approx 0.000402$ for $\mu_o/\mu_w = 4.11$ (point A), $N_g \approx 0.000050$ for $\mu_o/\mu_w = 52.13$ (point B), and $N_g \approx 0.000029$ for $\mu_o/\mu_w = 152.02$ (point C). (a) In the capillary and buoyancy region: capillary imbibition could be considered to be the same as in the above case, but the buoyancy effects are different, since the direction of the buoyancy forces is the same as that of the velocity of the displacing fluid, and this may make the displacing fluid move downwards faster. Less viscous effects are observed. On the other hand, (b) in the viscous region: after points A, B and C, the viscous forces are highly promoted and become the dominant factor in the displacement. The capillary forces no longer affect the displacement, but the buoyancy forces make the displacement become even worse. Thus, the oil recovery decreased after these critical points.

8.1.6 Effects of Viscosity Ratio

In general, no matter which mode is employed, increasing the viscosity ratio will drastically decrease oil recovery. Fig. (a) and (b) in (8.4 ~ 8.6) and (8.10 ~ 8.15) showed the fingering patterns for different viscosity ratios at low injection flow rate in three different modes. The number and size of the fingers increase at the entrance of

the porous medium with decreasing viscosity ratio, since a decrease of this ratio made the rheological characterization of both fluids close to each other. Hence, the effects of viscous forces are decreased. Meanwhile, the end effect is diminished; the photographs show the entrance saturation to be close to 100%.

On the other hand, when the viscosity ratios are changed at high injection flow rates (see Fig.(c) and (d) in (8.4 ~ 8.6) and (8.10 ~ 8.15), the fingering patterns are completely different from the previous ones. Increasing the injection flow rate will greatly strengthen the viscous forces and reduce the effects of both the capillary and buoyancy forces. This phenomena has been specially shown at a high viscosity ratio (see Figs. (c) and (d)). For the low viscosity ratios, however, the fingering patterns do not change very much, because of the closing rheological characterization of both fluids.

Horizontal Immiscible Displacement

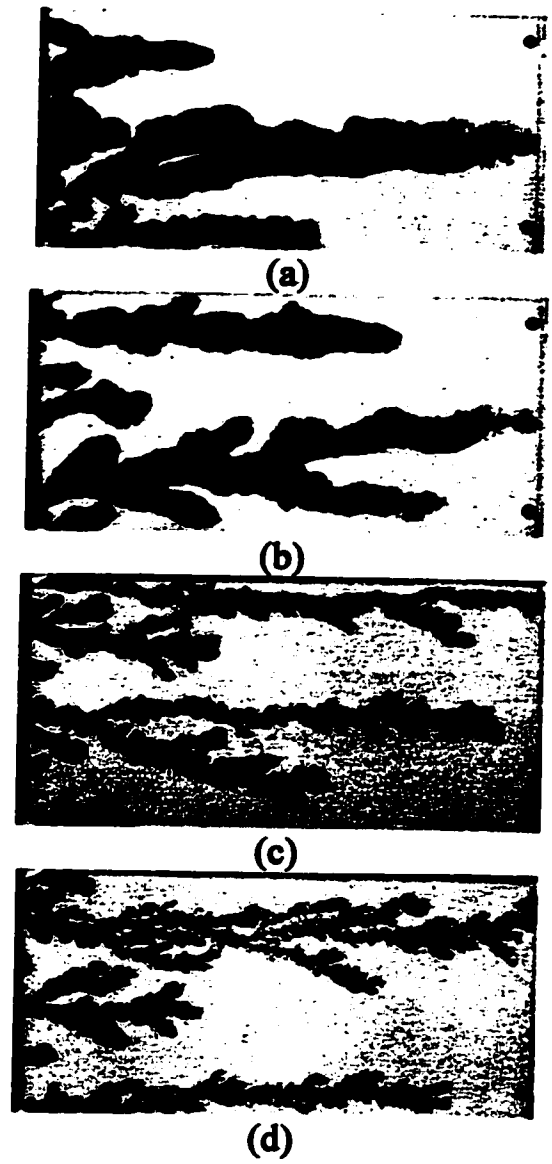

Fig.8.10. Horizontal Immiscible Displacements. Dyed 30% Glycerol Solution Displacing Paraffin Oil (μ_o/μ_w=52.13, ρ_o/ρ_w=0.808) at (a) Q=8.5 mL/h, R=29.64%; (b) Q=13.2 mL/h, R=26.33%; (c) Q=84.0 mL/h, R=15.34%; (d) Q=174.0 mL/h, R=10.73%.

Horizontal Immiscible Displacement

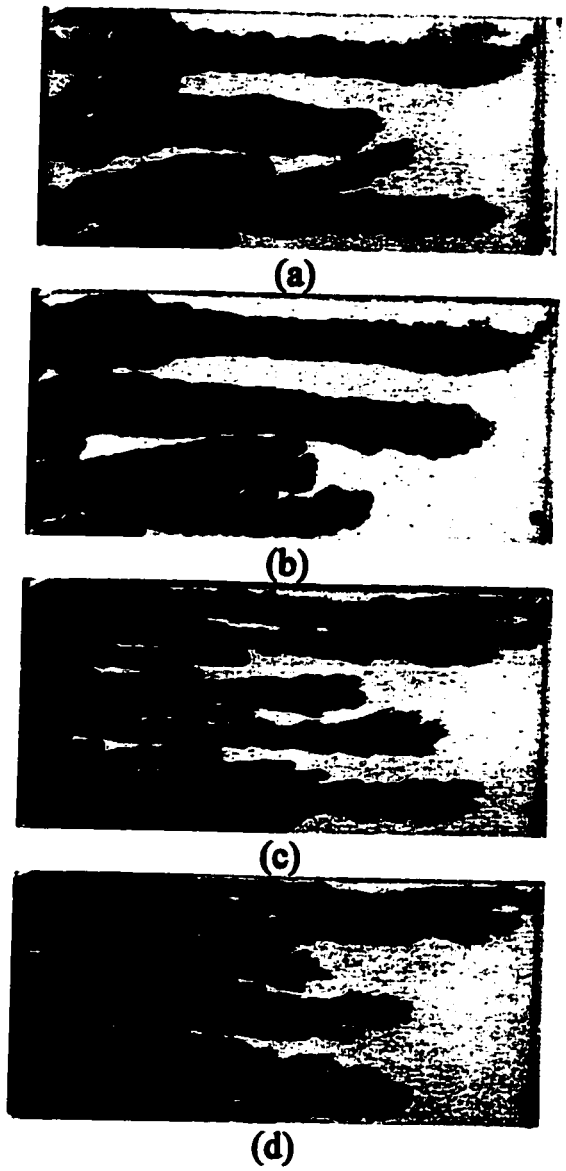

Fig.8.11. Horizontal Immiscible Displacements. Dyed 75% Glycerol Solution Displacing Paraffin Oil (μ_o/μ_w=4.11, ρ_o/ρ_w=0.728) at (a) Q=8.5 mL/h, R=48.63%; (b) Q=13.2 mL/h, R=48.26%; (c) Q=84.0 mL/h, R=42.93%; (d) Q=174.0 mL/h, R=36.94%.

Vertical-Upward Immiscible Displacement

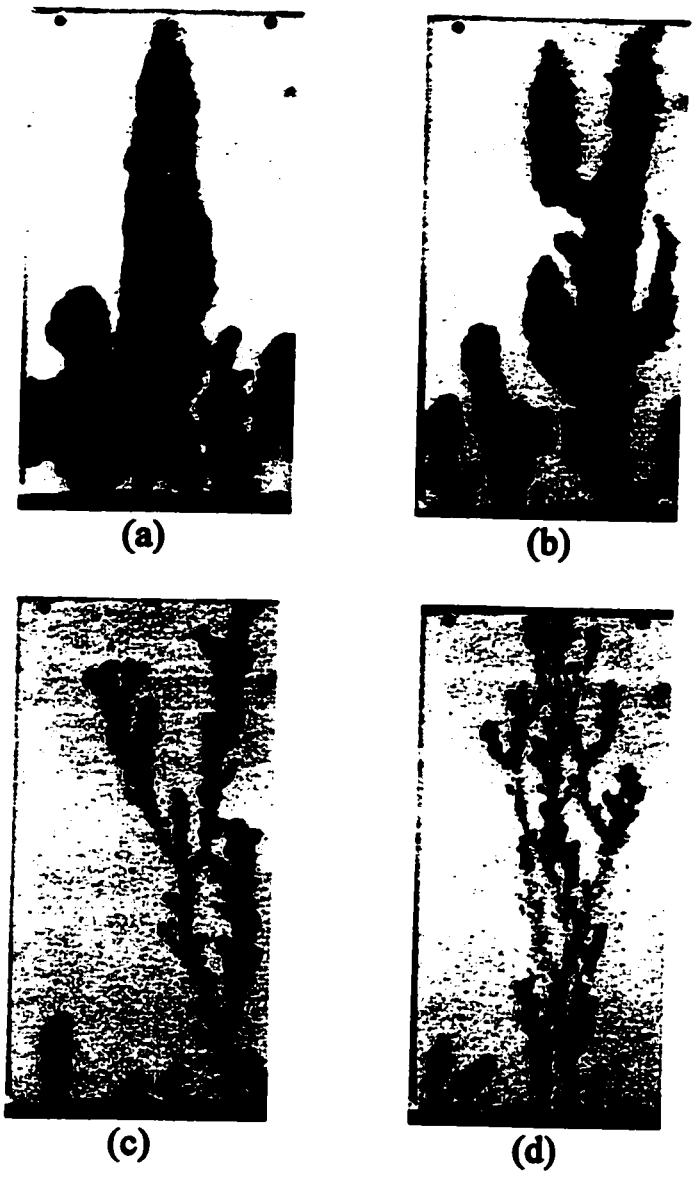

Fig.8.12. Vertical-Upward Immiscible Displacements. Dyed 30% Glycerol Solution Displacing Paraffin Oil (μ_o/μ_w=52.13, ρ_o/ρ_w=0.808) at (a) Q=8.5 mL/h, R=34.08%; (b) Q=13.2 mL/h, R=31.42%; (c) Q=84.0 mL/h, R=9.06%; (d) Q=174.0 mL/h, R=9.70%.

Vertical-Upward Immiscible Displacement

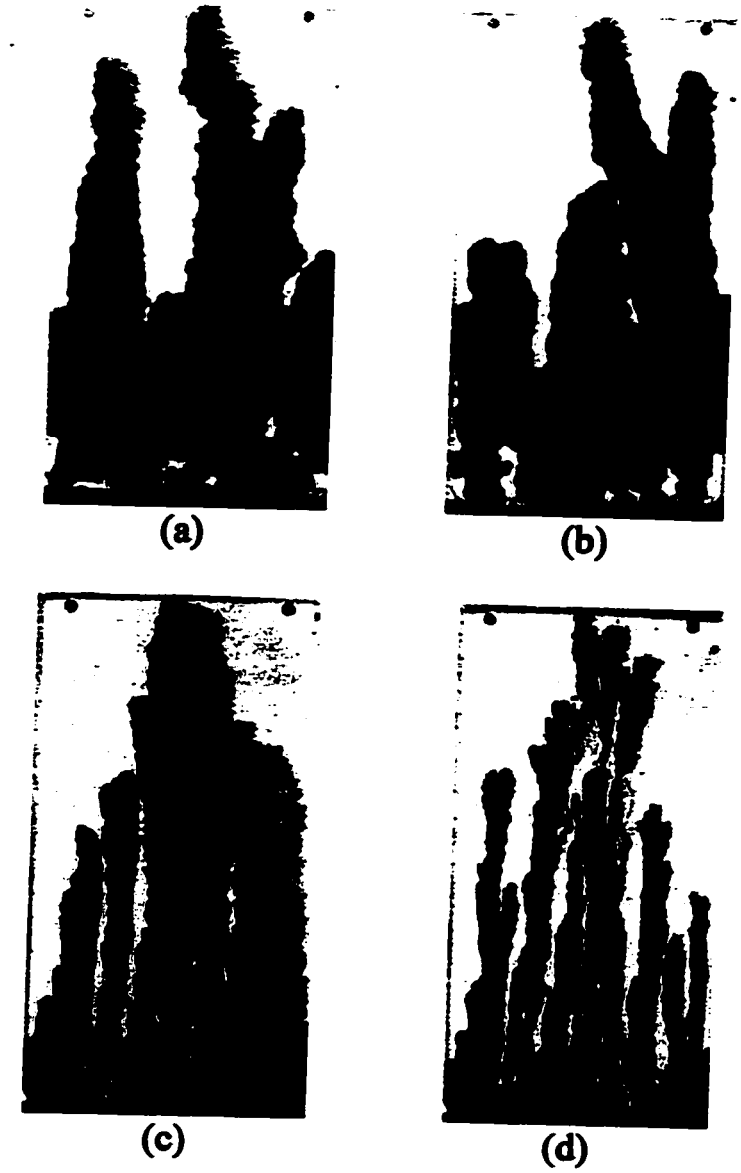

Fig.8.13. Vertical-Upward Immiscible Displacements. Dyed 75% Glycerol Solution Displacing Paraffin Oil (μ_o/μ_w=4.11, ρ_o/ρ_w=0.728) at (a) Q=8.5 mL/h, R=50.99%; (b) Q=13.2 mL/h, R=46.85%; (c) Q=84.0 mL/h, R=33.77%; (d) Q=174.0 mL/h, R=23.52%.

Vertical-Downward Immiscible Displacement

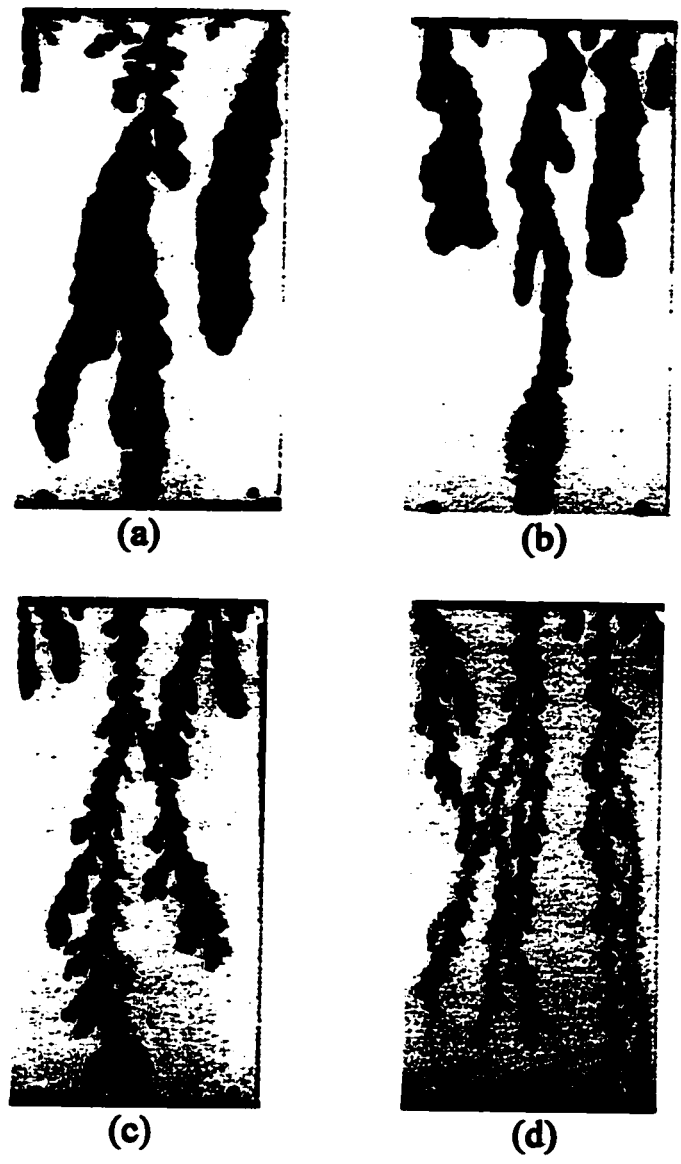

Fig.8.14. Vertical-Downward Immiscible Displacements. Dyed 30% Glycerol Solution Displacing Paraffin Oil (μ_o/μ_w=52.13, ρ_o/ρ_w=0.808) at (a) Q=8.5 mL/h, R=25.26%; (b) Q=13.2 mL/h, R=21.26%; (c) Q=84.0 mL/h, R=13.55%; (d) Q=174.0 mL/h, R=11.76%.

Vertical-Downward Immiscible Displacement

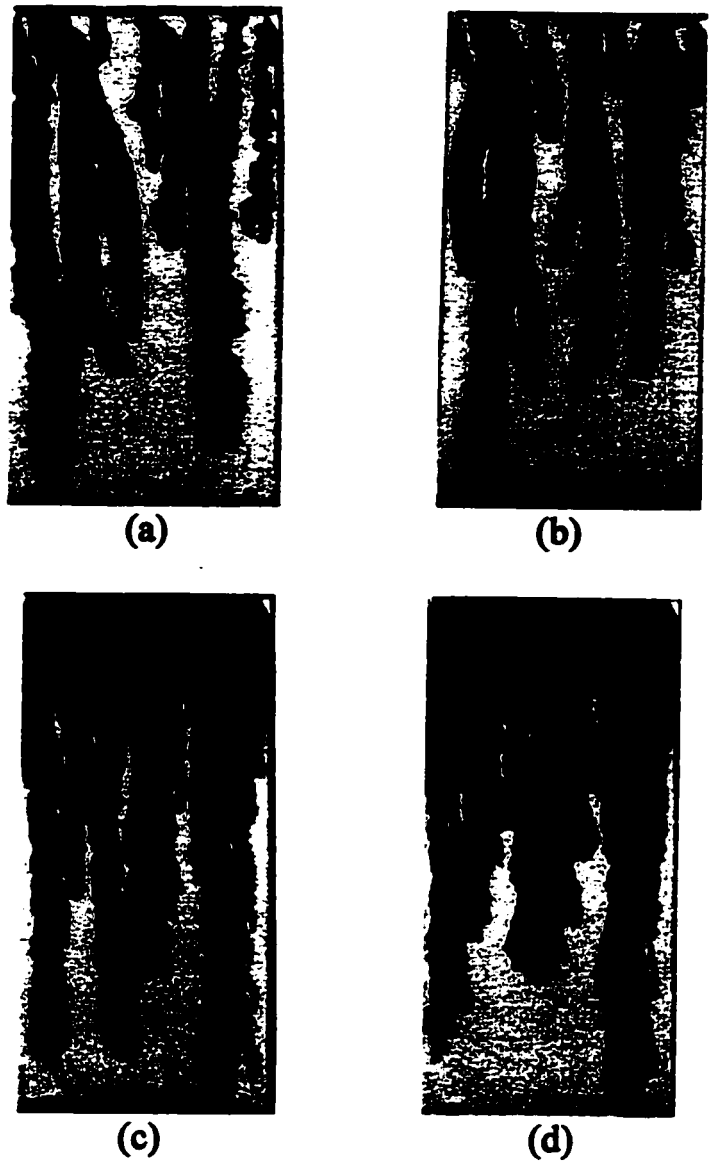

Fig.8.15. Vertical-Downward Immiscible Displacements. Dyed 75% Glycerol Solution Displacing Paraffin Oil (μ_o/μ_w=4.11, ρ_o/ρ_w=0.728) at (a) Q=8.5 mL/h, R=44.49%; (b) Q=13.2 mL/h, R=42.69%; (c) Q=84.0 mL/h, R=39.25%; (d) Q=174.0 mL/h, R=36.32%.

8.2 Immiscible Displacements with a Unity Viscosity Ratio

Three sets of experiments with an identical viscosity ratio were carried out. The effects of the viscous forces were therefore eliminated. The effects of the capillary forces, buoyancy forces and injection flow rates are discussed below.

8.2.1 Effects of Buoyancy Forces

To better understand the effects of the buoyancy forces, viscous forces were eliminated by selecting a unity viscosity ratio to unity (i.e., $\mu_w=\mu_o$). Thus, any observed effects will be the result of the interplay between the capillary forces and buoyancy forces, as well as the inertial (pressure gradient) forces. Furthermore, since the effects of buoyancy forces can be effectively neglected for the horizontal displacement mode in the case of thin, two-dimensional porous media (Appendix III), the experimental data obtained in this mode were employed as a reference for comparison with those for the vertical-upward and vertical-downward modes. Also, because of the elimination of viscous forces, the system was simplified so that the principal controlling factors in the horizontal case were the capillary forces. In both vertical cases, the main factors involved were the buoyancy forces and capillary forces. Fig.8.16 shows the relationship between the injection flow rate and the oil recovery efficiency for the three

different flow modes. Assuming that the effects of the capillary forces will be the same in all three basic flow modes under the same experimental conditions (i.e., the same injection flow rate, fluid system, and experimental cell), a comparison between each pair of experiments (i.e., horizontal and vertical-upward or horizontal and vertical-downward) can be made to quantitatively determine the effects of the buoyancy forces on the displacements, and the increase or decrease in the oil recovery can be evaluated by Equation (8.1) as follows:

$$\Delta R = R^{v} - R^{h} \tag{8.1}$$

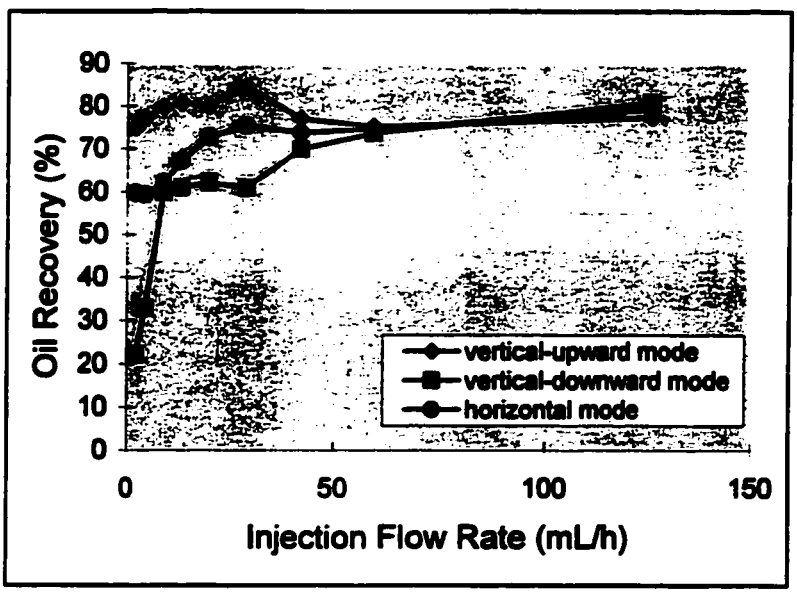

Fig.8.16 Relationship between Injection Flow Rate and Breakthrough Oil Recovery in All Three Different Flow Modes.

As an example of the comparison between the horizontal and the vertical flow modes using Equation (8.1), two pairs of experimental runs were used as to show the significant buoyancy effects. The oil recovery in the horizontal flow mode is 59.78%;

the oil recovery was increased by 15.26% in the vertical-upward flow mode and was decreased by 37.60% in the vertical-downward flow mode at the same injection flow rate of Q=2.1 mL/h (see Table 8.2 for more extensive comparisons). This larger difference confirmed, as expected, that the buoyancy forces performed a beneficial role in the vertical-upward mode and a detrimental role in the vertical-downward mode.

Table 8.2. Differences in Oil Recovery between the Vertical and the Horizontal Flow Modes for Different Injection Flow Rates

Flow Rate, Q (mL/h)	R^h	ΔR^u (%)	ΔR^d (%)
2.1	59.78	+15.26	-37.60
4.4	59.39	+18.01	-26.49
8.8	62.18	+17.60	-2.37
13.0	67.13	+13.63	+0.74
19.8	72.75	+3.95	-0.34
28.8	75.40	+9.07	-14.46
42.0	73.78	+3.35	-3.80
59.4	74.70	+0.55	-0.93
126.0	79.22	-1.77	+1.58

Displacement Patterns

(a)

(b) **(c)**

Fig.8.17 Displacement Patterns at a Low Injection Flow Rate of Q=2.1 mL/h in All Three Different Flow Modes. (a) Horizontal Flow Mode; (b) Vertical-Upward Flow Mode; (c) Vertical-Downward Flow Mode.

Displacement Patterns

(a)

(b) (c)

Fig.8.18 Displacement Patterns at a Low Injection Flow Rate of Q=4.4 mL/h in All Three Different Flow Modes. (a) Horizontal Flow Mode; (b) Vertical-Upward Flow Mode; (c) Vertical-Downward Flow Mode.

8.2.2 Low Injection Flow Rates

Because of absence of the viscous forces, the interface between the two fluids was expected to be flat [Stalkup 1992]. However, this was not found in the present study (see Figs.8.17(a) and 8.18(a)). Because the capillary imbibition greatly influenced the displacement pattern at low injection flow rates, it caused a large amount of oil to become trapped in the porous medium, and the effects of the inertial (pressure gradient) forces were not sufficiently high to overcome these capillary effects. Thus, some of the oil became immobile, and a low amount of oil was recovered.

This situation could be improved when the buoyancy forces are involved in the vertical-upward displacement, as shown in Figs.8.17(b) and 8.18(b). The trapped oil could be mobilized if buoyancy forces could overcome the capillary forces in this vertical-upward flow mode. Figs.8.17(b) and 8.18(b) show that the buoyancy forces basically dominated the capillary forces, and there are not as many holes as in the horizontal flow mode. Moreover, the density of the invading fluid is higher than that of the oil; the buoyancy forces play a positive role in this displacement, which causes the invading fluid to tend to linger at the bottom of the cell, thereby producing a fairly stable interface and a higher oil recovery.

The oil recovery efficiency will be worse when the buoyancy forces play a negative role in the vertical-downward flow mode, as displayed in Figs.8.17(c) and 8.18(c). When the displacing fluid first entered the porous medium cell, it directly moved downwards rather than any other direction. In fact, the effects of the buoyancy forces in this case

Finger Shapes

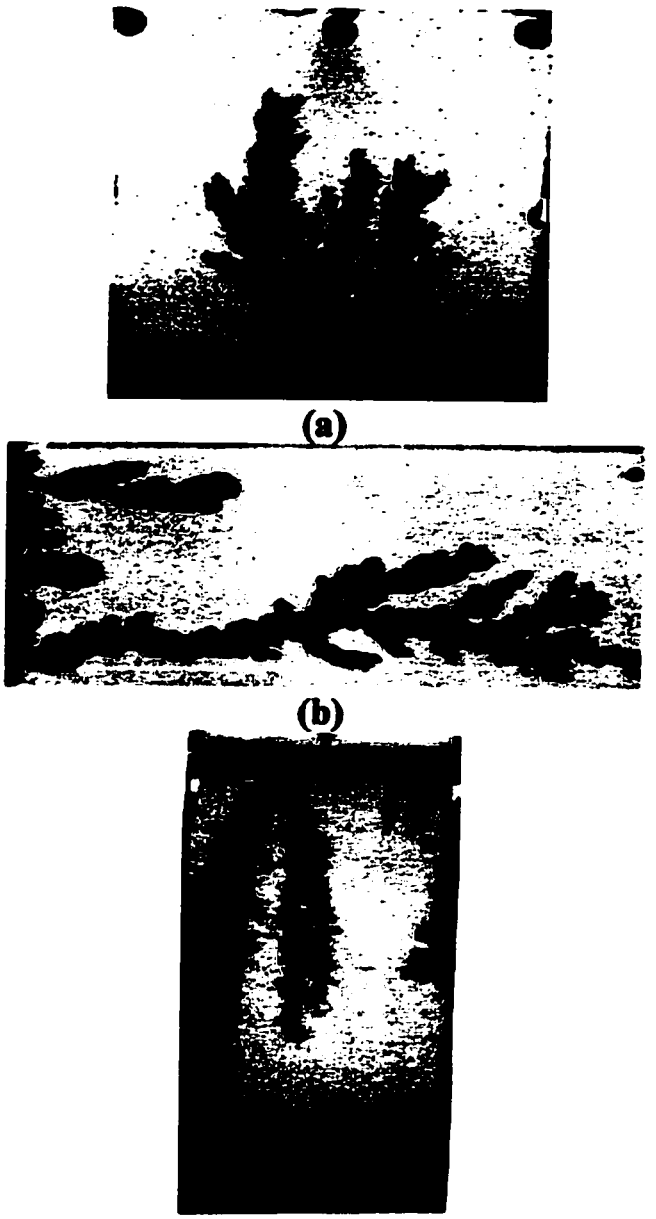

Fig.8.19 Different Finger Shapes That Occurred in the Different Flow Orientations. (a) Dendritic Shape in Miscible, Vertical-Upward Displacement; (b) Mushroom Shape in Horizontal Displacement; (c) Cactus Shape in Immiscible, Vertical-Downward Displacement.

are the same as increasing the inertial (pressure gradient) forces; the superficial velocity of the displacing fluid is much greater than in both the vertical-upward and horizontal flow mode, this could be confirmed by the following data: at the same injection flow rate, Q = 2.1 ml/h, one obtains a breakthrough time, t_{br}=6,771 s, in the vertical-downward flow mode, t_{br}=18246 s in the horizontal flow mode, and t_{br}=22,902 s in the vertical-upward flow mode. The increased velocity in the vertical-downward mode caused premature displacement breakthrough and a low oil recovery. The ***Capillary-Gravity fingers*** shown in Fig.8.19(c) differed from the viscous fingers (dentritic shape in Fig.8.19(a)) in the miscible displacement and (mushroom shape in Fig.8.19(b)) in the immiscible displacement. The shape of these capillary-gravity fingers, in Fig.8.19c, is cactus-like, small fingers like prickles imbibiting in the smaller channels in all directions, but these capillary forces were not large enough to overcome the buoyancy forces. Therefore, the main body of the invading fluid still tended to move downward, and the transverse fingers ceased to grow larger. As a consequence, a very unstable interface was produced and a lower oil recovery was obtained.

Moreover, the end effect was not very serious in both the horizontal and vertical-upward flow modes. However, it was serious in the vertical-downward flow mode. This could be explained by the fact that, because of the buoyancy (gravity) forces, the displacing fluid prefers to flow through the path with less viscous resistance. When the first entering point of the displacing fluid was established, it continued to

penetrate through this spot. In this situation, it is difficult to develop a new entering point. This is shown in Figs.8.17(c) and 8.18(c).

8.2.3 High Injection Flow Rates

The displacement patterns in all three different flow modes were quite similar to each other at high injection flow rates (see Figs.8.20 and 8.21). This indicates that both the capillary and buoyancy forces are overshadowed by the inertial forces at high injection flow rates. One could explain that the high injection flow rate is related to a high-pressure gradient, and if this pressure gradient is high enough, then both the capillary and buoyancy forces might be approximately neglected, i.e.:

$$\frac{\partial P_c}{\partial x} = \frac{\partial P_o}{\partial x} - \frac{\partial P_w}{\partial x} \to 0 \tag{8.2}$$

whence,

$$\frac{\partial P_o}{\partial x} \approx \frac{\partial P_w}{\partial x} \tag{8.3}$$

Also, because of the unity viscosity ratio, the velocity of the displacing fluid will be approximately equal to that of the displaced fluid. As a consequence, this two-phase flow is effectively a pseudo single-phase flow situation, whence a flat displacement interface could be expected to prevail. Convincing support for this assertion is provided by the very similar displacement pattern displayed in Figs.8.20 and 8.21, and by the very similar experimental results, such as t_{br}=403 s and R=79.22% for the horizontal flow mode, t_{br}=394 s and R=77.45% for the vertical-upward flow mode

and t_{br}=411 s and R=80.80% for the vertical-downward flow mode at the same flow rate of Q= 126.0 mL/h (Fig.8.21).

Displacement Patterns

(a)

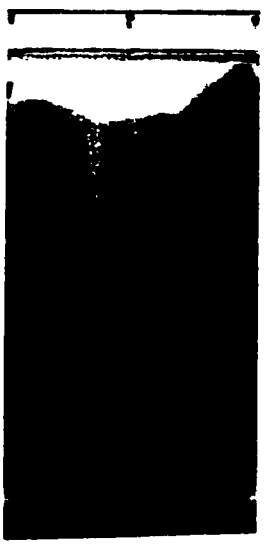

(b) (c)

Fig.8.20 Displacement Patterns at a High Injection Flow Rate of Q=59.4 mL/h in All Three Different Flow Modes. (a) Horizontal Flow Mode; (b) Vertical-Upward Flow Mode; (c) Vertical-Downward Flow Mode.

Displacement Patterns

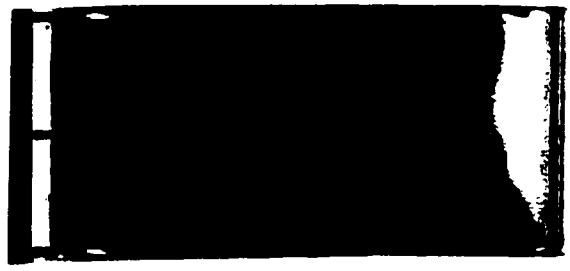

(a)

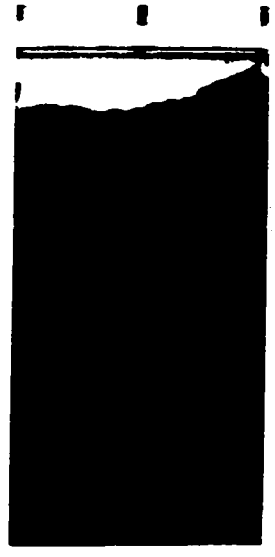

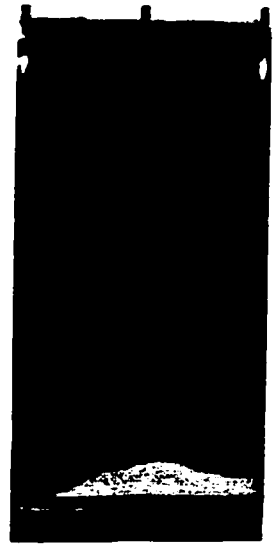

(b) (c)

Fig.8.21 Displacement Patterns at a High Injection Flow Rate of Q=126.0 mL/h in All Three Different Flow Modes. (a) Horizontal Flow Mode; (b) Vertical-Upward Flow Mode; (c) Vertical-Downward Flow Mode.

8.3 Theoretical Results

In this section, the coefficients of the expressions for R and N_{GN} from the dimensional analysis (Chapter 5) are estimated by using the experimental data. Also, comparisons of saturation profiles between the theoretical results and experimental results, and theoretical results and literature results, are made. The effects of the buoyancy forces are further discussed.

8.3.1 Regression Analysis of R and Expressions for R and N_{GN}

In Chapter 5, a dimensional analysis was utilized to determine the relationship between oil recovery and certain dimensionless groups; i.e., the gravity number, the capillary number, the viscosity ratio, and the geometrical shape factor. The model was examined for lack of fit using (i) plots of residuals of oil recovery (i.e., the observed minus the predicted values of the responses) against the predicted values (see Figs.8.22, 8.23 and 8.24), and (ii) a quantative lack-of-fit test [McLean, 1990]. The ratio is

$$R_s = \frac{\sum_{u=1}^{n}(\bar{Y}-\hat{Y})^2 / \{n-p-\sum_{i=1}^{l}(m_i-1)\}}{\hat{\sigma}_p^2} \qquad (8.4a)$$

where

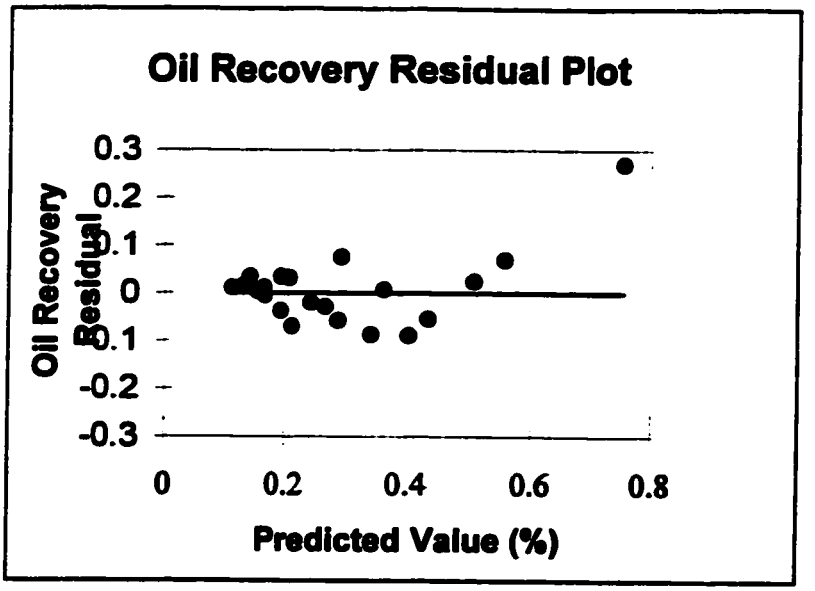

Fig.8.22 Oil Recovery Residual Plot for Horizontal Flow Mode.

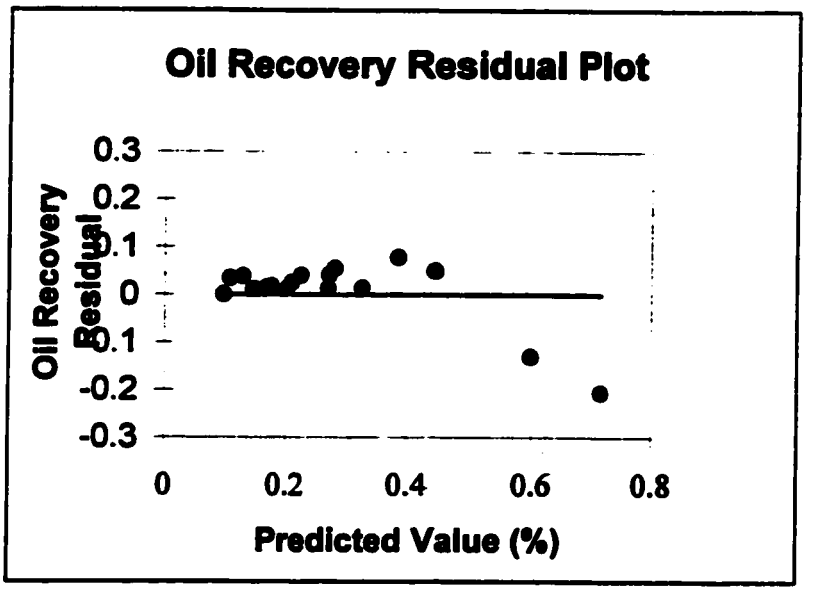

Fig.8.23 Oil Recovery Residual Plot for Vertical-Upward Flow Mode.

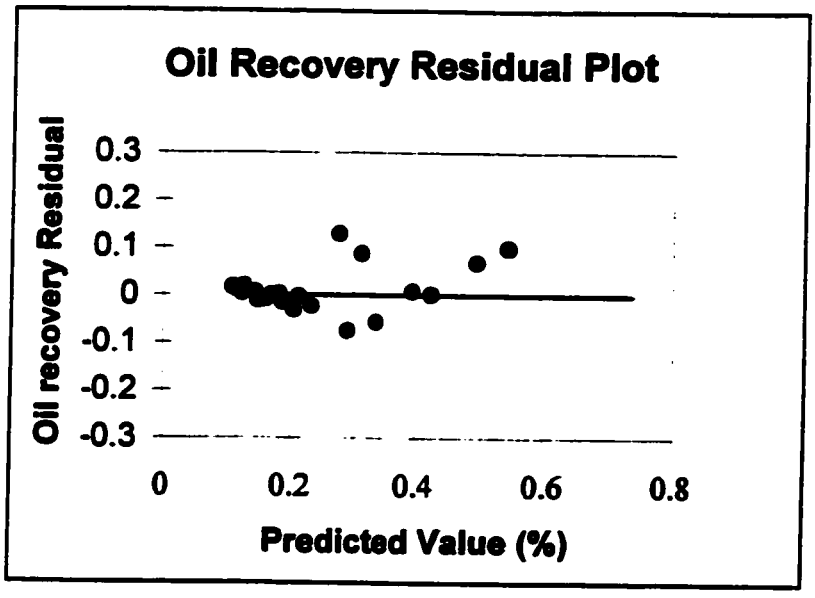

Fig.8.24 Oil Recovery Residual Plot for Vertical-Downward Flow Mode.

$$\hat{\sigma}_p^2 = \frac{\sum_{i=1}^{l}(m_i - 1)\hat{\sigma}_i^2}{\sum_{i=1}^{l}(m_i - 1)} \tag{8.4b}$$

the degree of freedom will be:

$$\nu_1 = n - p - \sum_{i=1}^{l}(m_i - 1) \tag{8.4c}$$

$$\nu_2 = \sum_{i=1}^{l}(m_i - 1) \tag{8.4d}$$

This R_s value was compared with the upper 5% abscissa value of $F_{\nu_1,\nu_2,0.05}$, and if R_s was smaller than this $F_{\nu_1,\nu_2,0.05}$ value, no lack of fit was indicated [Bates and Watts, 1988; Hopkins et al., 1987]. Table 8.3 shows the results of regression. The fitted models for the oil recovery, R, throughout the entire injection flow rate range are:

Table 8.3 Results of Regression.

Response	Significant Parameters	Parameter Values	Standard Errors	$\hat{\sigma}^2_r$	Lack-of-Fit Ratio, R_s	$F_{\nu_1,\nu_2,0.05}$	R^2_{adj}
ln(R)	lnΛ	-1.5828	0.4152	0.0054	5.8900	8.6000	0.87
⇒	β	-0.3690	0.0343				
	γ	-0.1111	0.0379				
ln(R)	lnΛ	-4.7560	1.1550	0.0252	1.6984	5.8768	0.94
⇑	α	0.2293	0.3539				
	β	-0.8190	0.1460				
	γ	-0.6350	0.3555				
ln(R)	lnΛ	-4.0024	1.3359	0.0061	5.5500	5.8360	0.93
⇓	α	0.5359	0.2699				
	β	-0.7193	0.0743				
	γ	-0.7458	0.2047				

Note: ⇒ denotes horizontal mode, ⇑ vertical-upward mode, and ⇓ vertical-downward mode.

$$R = 0.0743(\mu_r)^{-0.3690}(N_c)^{-0.1111} \tag{8.5}$$

(Horizontal Case)

$$R = 0.0086(N_g)^{0.2293}(\mu_r)^{-0.8190}(N_c)^{-0.6350} \tag{8.6}$$

(Vertical-Upward Case)

$$R = 0.0183(N_g)^{0.5359}(\mu_r)^{-0.7193}(N_c)^{-0.7459} \tag{8.7}$$

(Vertical-Downward Case)

Combining Equations (8.5), (8.6) and (8.7) with Equation (3.32) yields three equations for calculating N_{GN} in the horizontal, vertical-upward and vertical-downward cases, respectively. From Equations (8.5), (8.6) and (8.7), one can see that the exponent of the viscosity ratio is always negative, which indicates that an increase in the viscosity ratio will result in a decrease in the oil recovery [van Meurs and van der Poel 1958, Scott et al. 1965, Flock et al. 1977, Jerauld et al. 1984, Guo and Neale 1996]. Since the definition of the gravity number employed here is the same as that used elsewhere [Craig et al. 1957, Gardner et al. 1962, Araktingi and Orr 1991], the present analysis does have a good agreement with the result that the oil recovery increases as the gravity number decreases (see Fig.8.7), and that the exponent for the vertical-upward displacement is lower than that for vertical-downward displacement. This implies that, where $\rho_w > \rho_o$, the effects of buoyancy forces are favourable for oil recovery in vertical-upward displacements, whereas they are unfavourable in vertical-downward displacements.

It is also evident that the oil recovery increases with increasing capillary number when the σ remains constant. A decrease in the σ will actually increase the oil recovery [Tayal and Narayan 1990, Kiriakidis et al. 1993], whereas the present equations suggest that oil recovery decreases with decreasing IFT. However, in the present work the change of IFT necessarily causes certain other factors, such as the viscosity ratio (decreasing) and density difference (decreasing), to change. Thus, it is not obvious that R increases with decreasing σ, although the final oil recovery does increase (see

Figs.8.8a, b and c). The exponent for the capillary number in Equation (8.5) is slightly higher in the horizontal mode than for both the vertical-upward and vertical-downward mode, and this is probably due to the capillary hysterisis. As a consequence, Equations (8.5), (8.6) and (8.7) basically represent the effects of the three fundamental dimensionless groups on the oil recovery.

8.3.2 Saturation Profiles and Comparisons

The comparisons between the predicted and measured saturation profiles are shown in Figs. 8.25(I, II) & 8.26(I, II) & 8.27(I, II), 8.28(I, II) & 8.29(I, II) & 8.30(I) and 8.31(I, II) & 8.32(I, II) & 8.33(I) with the corresponding fingering patterns in Figs. 8.4 & 8.10 & 8.11, 8.5 & 8.12 & 8.13 and 8.6 & 8.14 & 8.15. The 95% confidence regions are obtained from the "Table Curve" by using the measured saturation profile with $R^2 = 0.99$. This 95% confidence region covers almost all of the predicted saturation profiles. This implies that the consistency of these results is excellent. Thus, the predicted saturation profiles can be utilized directly to analyze the effects of the buoyancy forces.

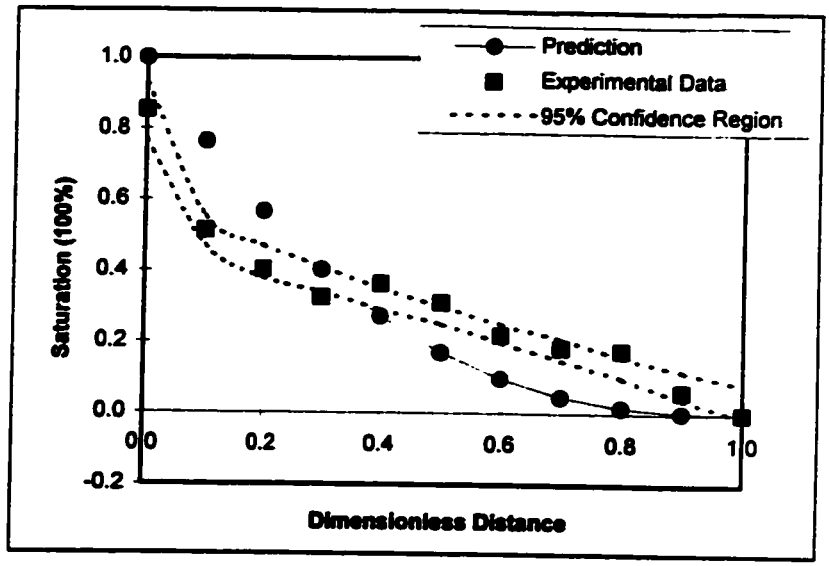

(a)

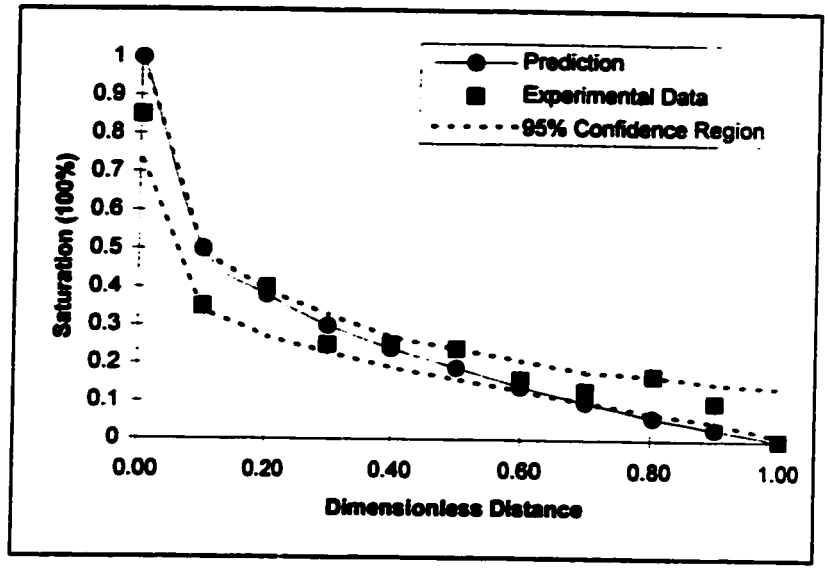

(b)

Fig.8.25(I). Comparison between Predicted and Measured Saturation Profiles in Horizontal Flow Mode. For (μ_o/μ_w=152.02, ρ_o/ρ_w=0.876), (a) Q=8.5 mL/h, (b) Q=13.2 mL/h.

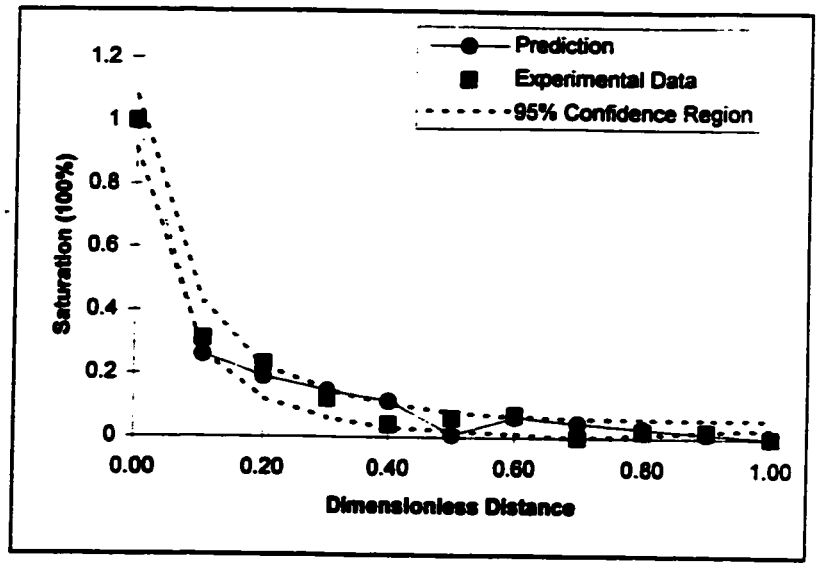

(c)

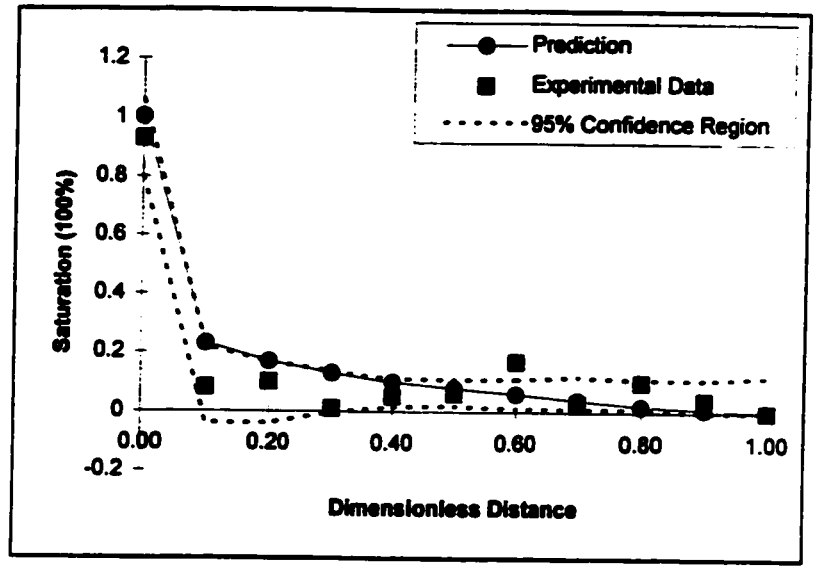

(d)

Fig.8.25(II). Comparison between Predicted and Measured Saturation Profiles in Horizontal Flow Mode. For (μ_o/μ_w=152.02, ρ_o/ρ_w=0.876), (c) Q=84.0 mL/h, (d) Q=174.0 mL/h.

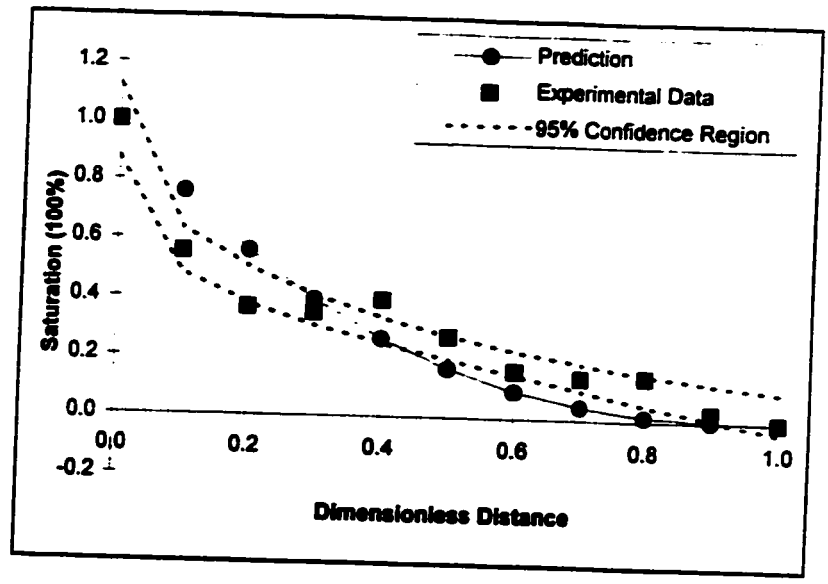

(a)

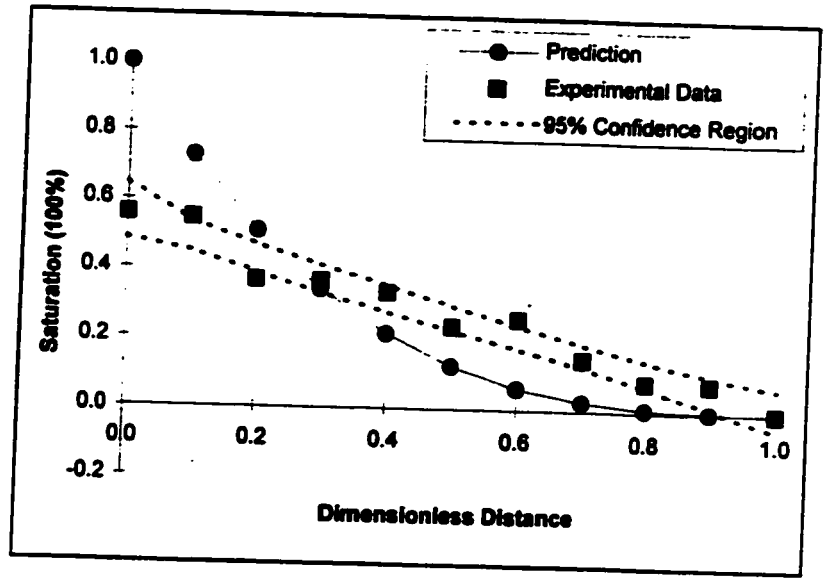

(b)

Fig.8.26(I). Comparison between Predicted and Measured Saturation Profiles in Horizontal Flow Mode. For (μ_o/μ_w=52.13, ρ_o/ρ_w=0.808), (a) Q=8.5 mL/h, (b) Q=13.2 mL/h.

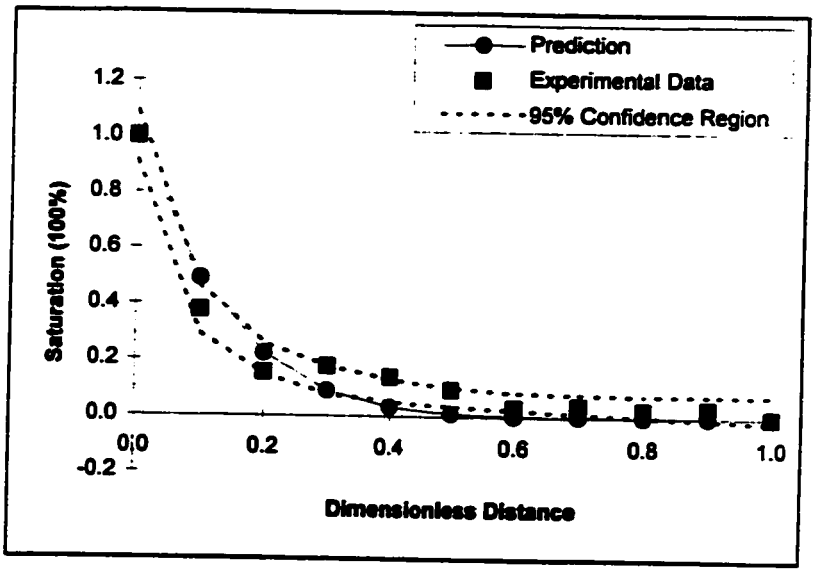

(c)

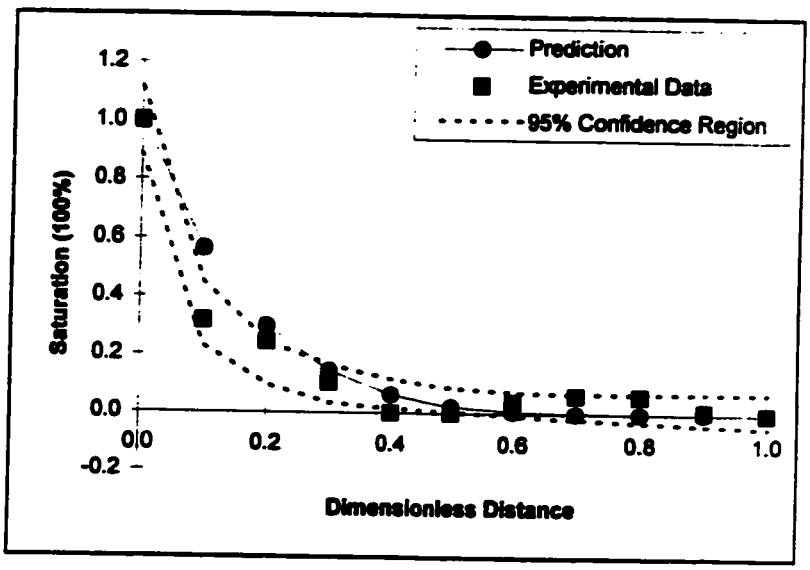

(d)

Fig.8.26(II). Comparison between Predicted and Measured Saturation Profiles in Horizontal Flow Mode. For (μ_o/μ_w=52.13, ρ_o/ρ_w=0.808), (c) Q=84.0 mL/h, (d) Q=174.0 mL/h.

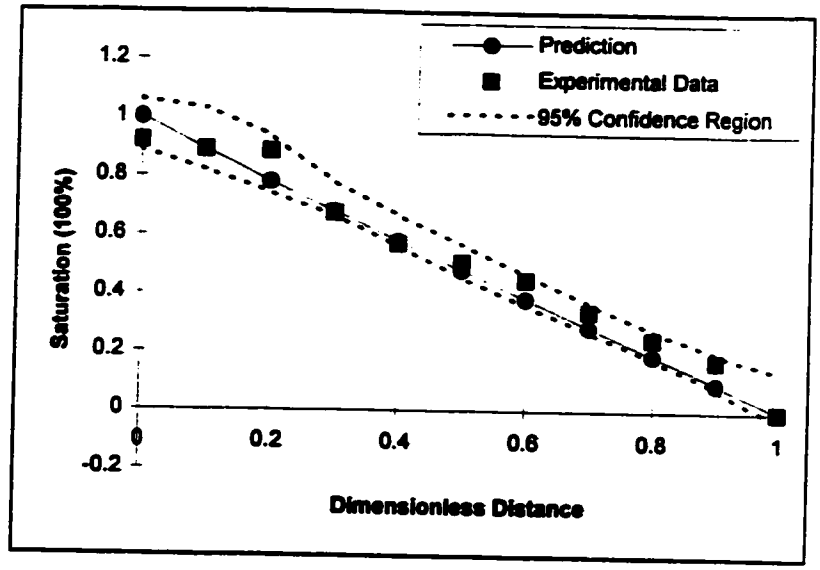

(a)

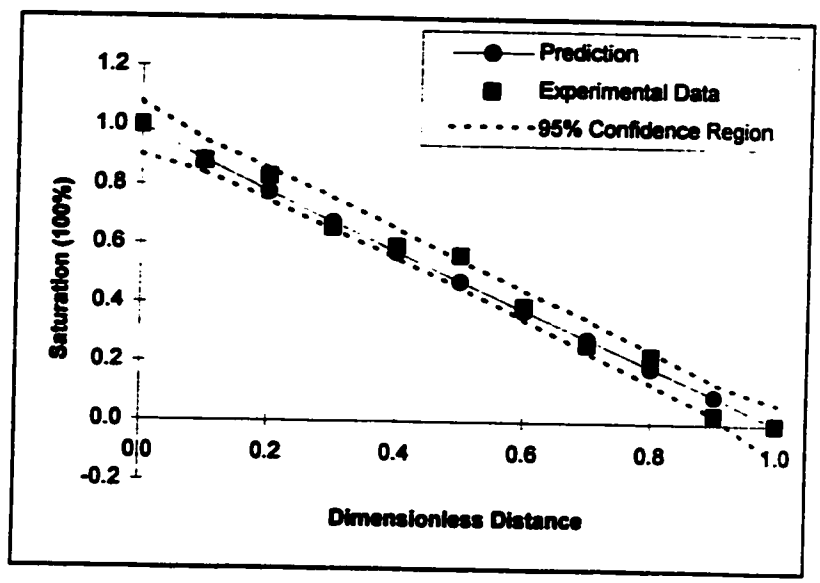

(b)

Fig.8.27(I). Comparison between Predicted and Measured Saturation Profiles in Horizontal Flow Mode. For (μ_o/μ_w=4.11, ρ_o/ρ_w=0.728), (a) Q=8.5 mL/h, (b) Q=13.2 mL/h.

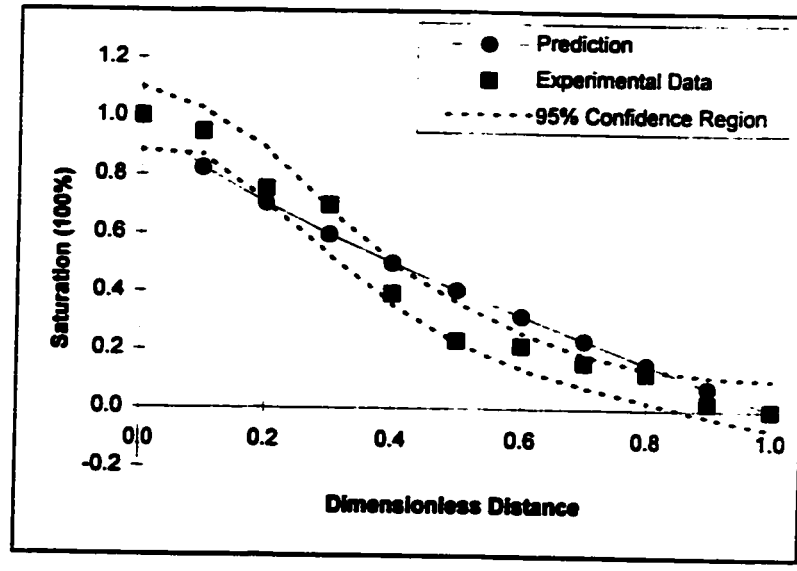

(c)

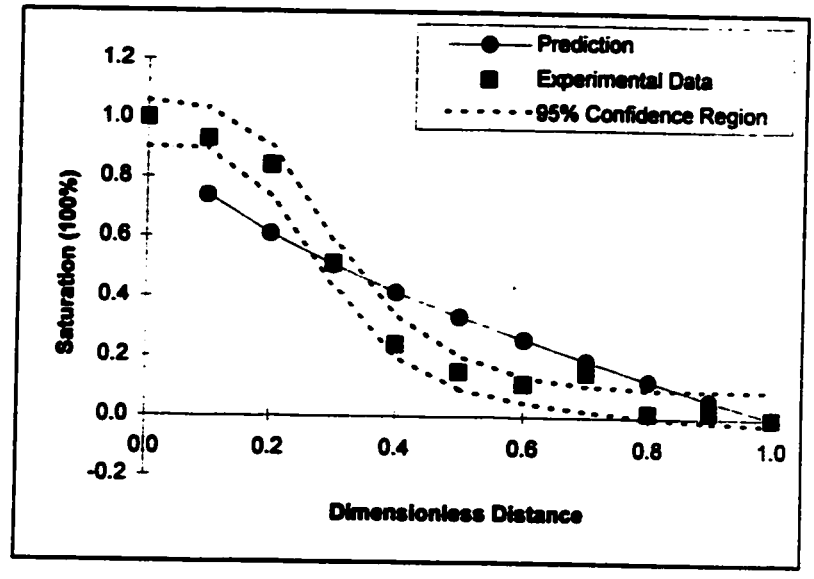

(d)

Fig.8.27(II). Comparison between Predicted and Measured Saturation Profiles in Horizontal Flow Mode. For (μ_o/μ_w=4.11, ρ_o/ρ_w=0.728), (c) Q=84.0 mL/h, (d) Q=174.0 mL/h.

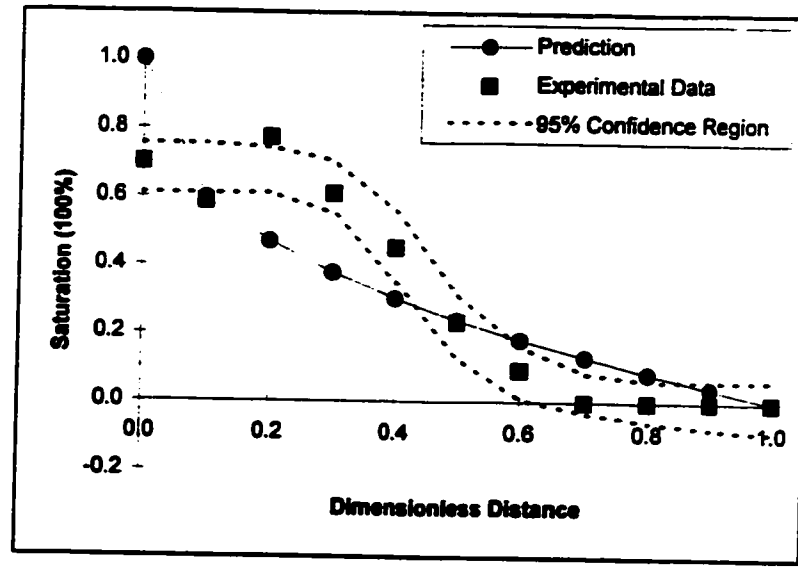

(a)

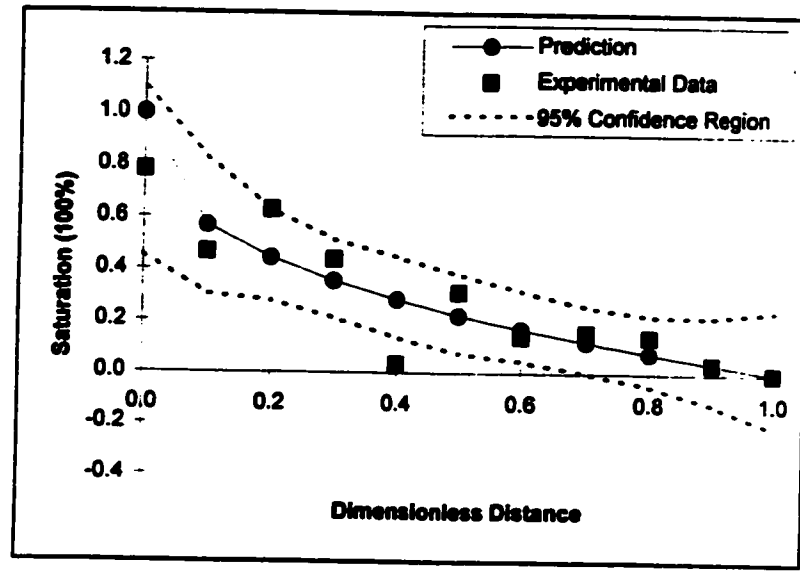

(b)

Fig.8.28(I). Comparison between Predicted and Measured Saturation Profiles in Vertical-Upward Flow Mode. For (μ_o/μ_w=152.02, ρ_o/ρ_w=0.876), (a) Q=8.5 mL/h, (d) Q=13.2 mL/h.

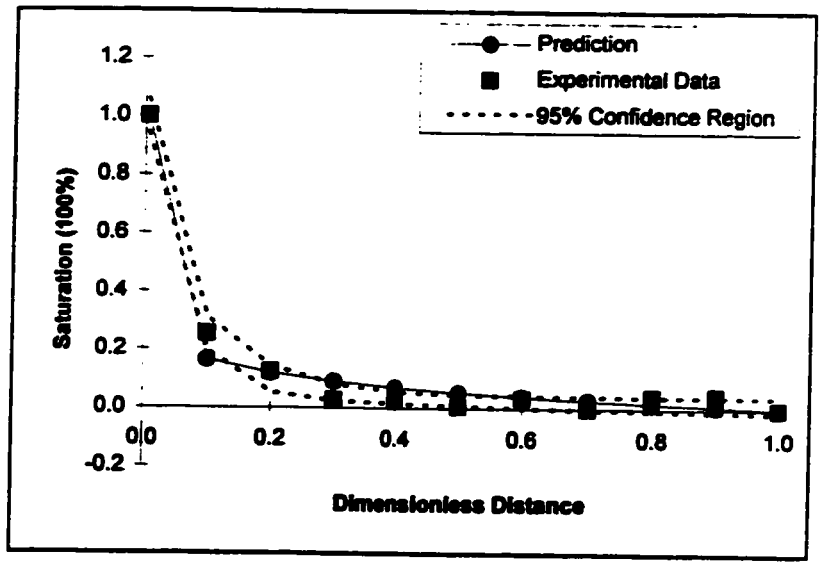

(c)

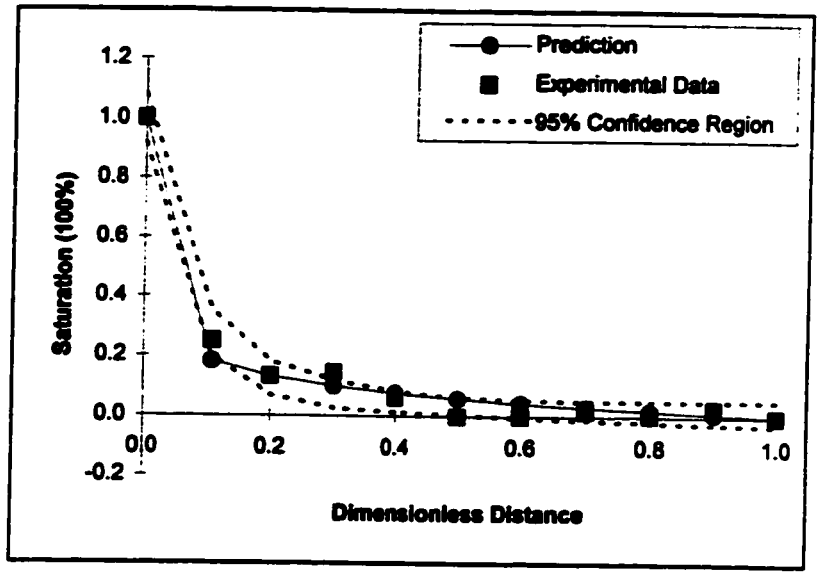

(d)

Fig.8.28(II). Comparison between Predicted and Measured Saturation Profiles in Vertical-Upward Flow Mode. For (μ_o/μ_w=152.02, ρ_o/ρ_w=0.876), (c) Q=84.0 mL/h, (d) Q=174.0 mL/h.

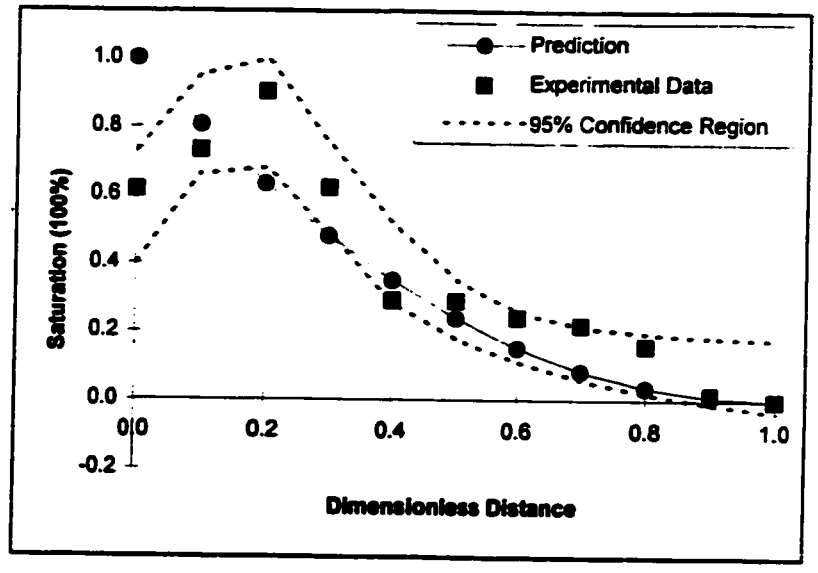

(a)

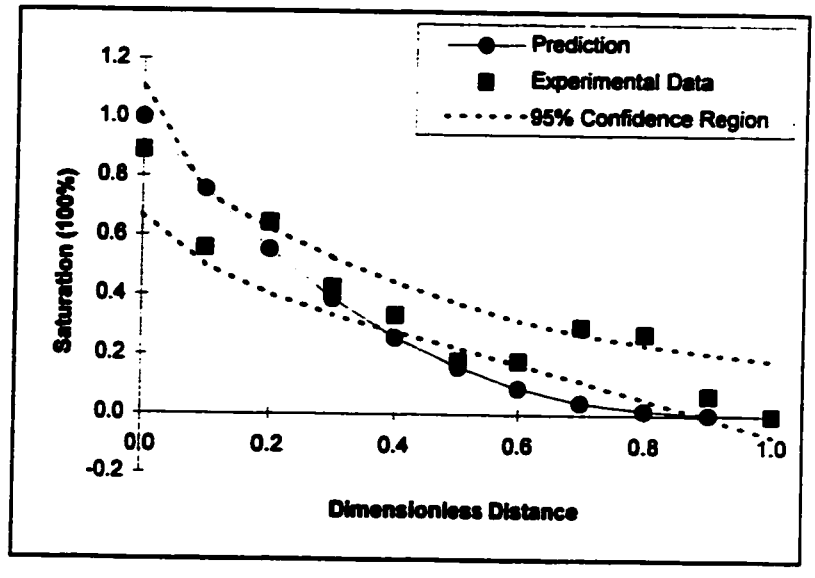

(b)

Fig.8.29(I). Comparison between Predicted and Measured Saturation Profiles in Vertical-Upward Flow Mode. For (μ_o/μ_w=52.13, ρ_o/ρ_w=0.808), (a) Q=8.5 mL/h, (b) Q=13.2 mL/h.

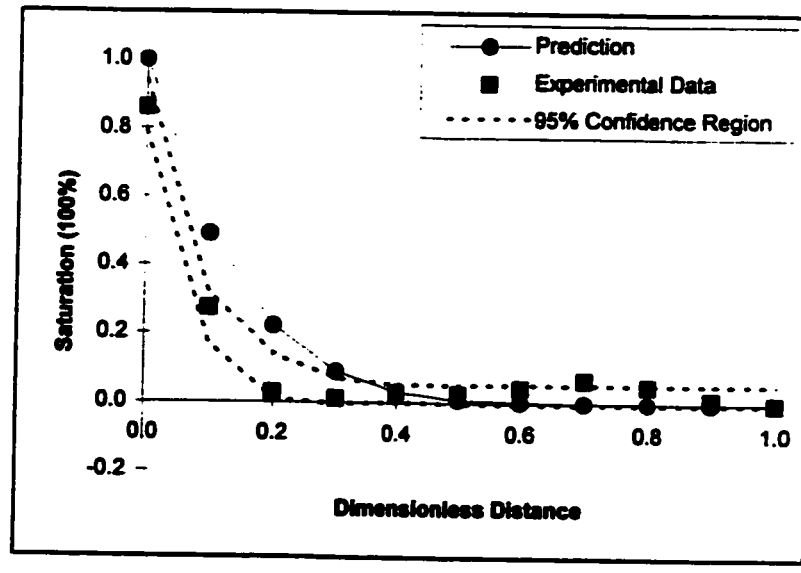

(c)

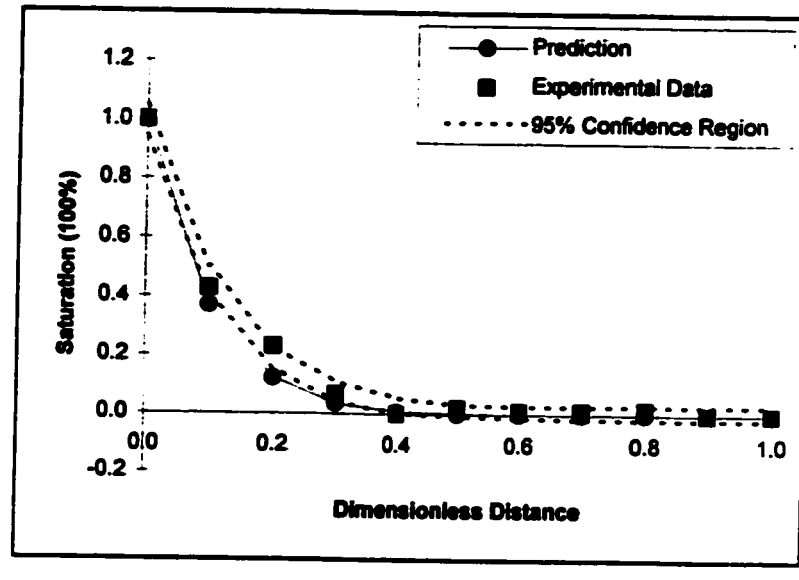

(d)

Fig.8.29(II). Comparison between Predicted and Measured Saturation Profiles in Vertical-Upward Flow Mode. For (μ_o/μ_w=52.13, ρ_o/ρ_w=0.808), (c) Q=84.0 mL/h, (d) Q=174.0 mL/h.

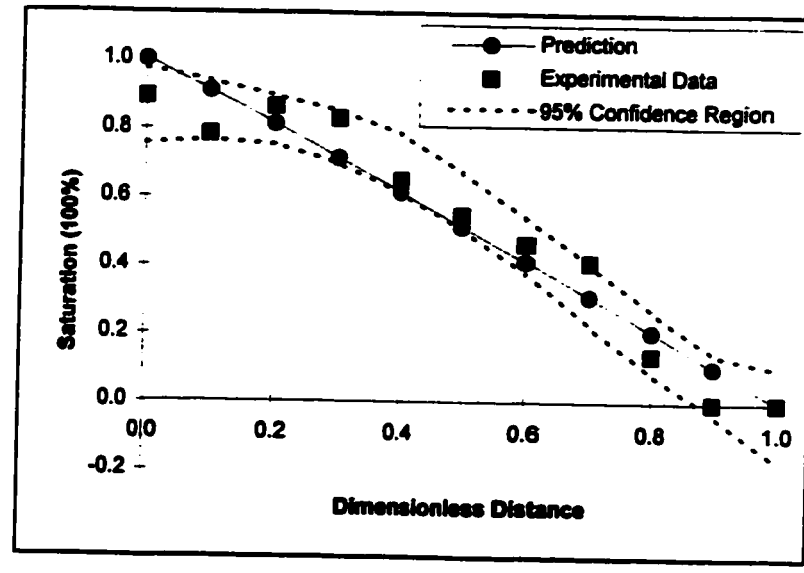

(a)

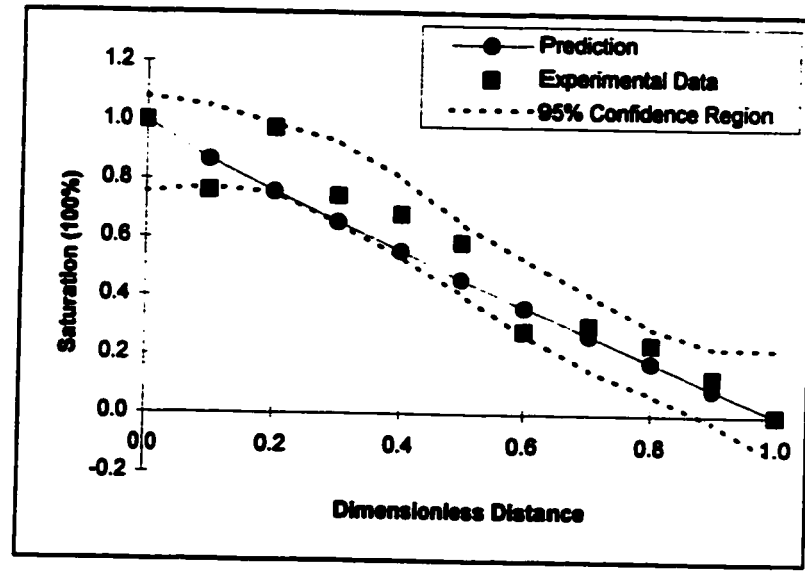

(b)

Fig.8.30(I). Comparison between Predicted and Measured Saturation Profiles in Vertical-Upward Flow Mode. For (μ_o/μ_w=4.11, ρ_o/ρ_w=0.728), (a) Q=8.5 mL/h, (b) Q=13.2 mL/h.

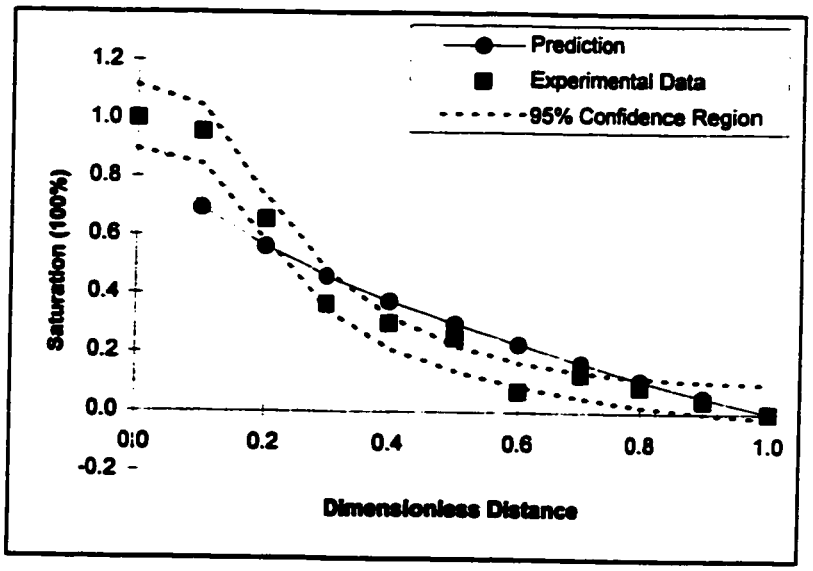

(c)

Fig.8.30(II). Comparison between Predicted and Measured Saturation Profiles in Vertical-Upward Flow Mode. For (μ_o/μ_w=4.11, ρ_o/ρ_w=0.728), (c) Q=84.0 mL/h.

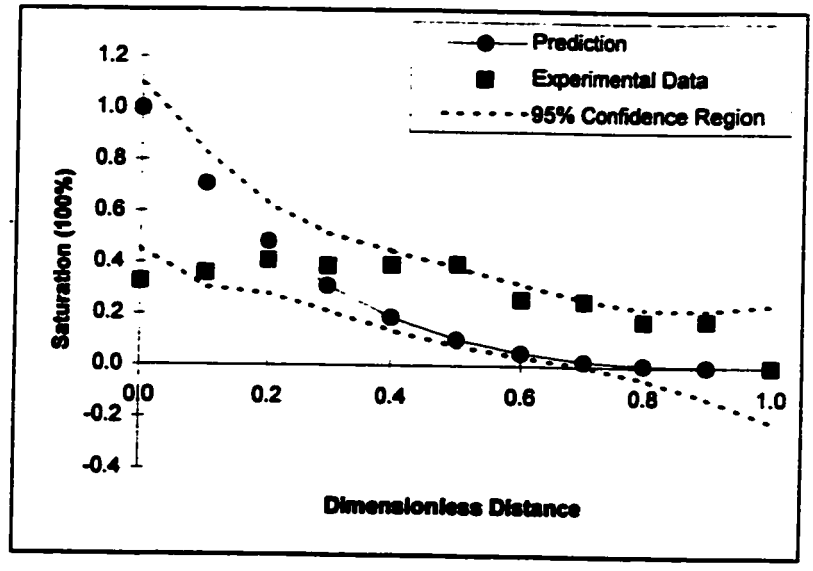

(a)

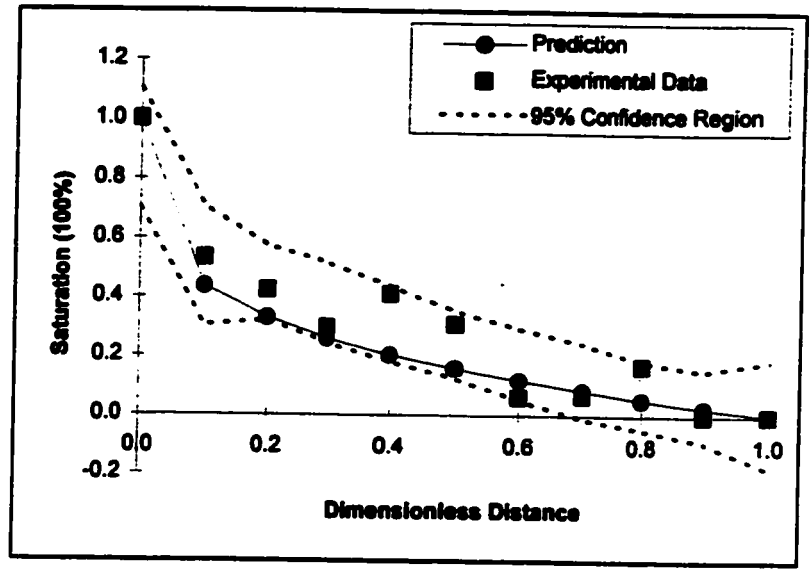

(b)

Fig.8.31(I). Comparison between Predicted and Measured Saturation Profiles in Vertical-Downward Flow Mode. For (μ_o/μ_w=152.02, ρ_o/ρ_w=0.876), (a) Q=8.5 mL/h, (b) Q=13.2 mL/h.

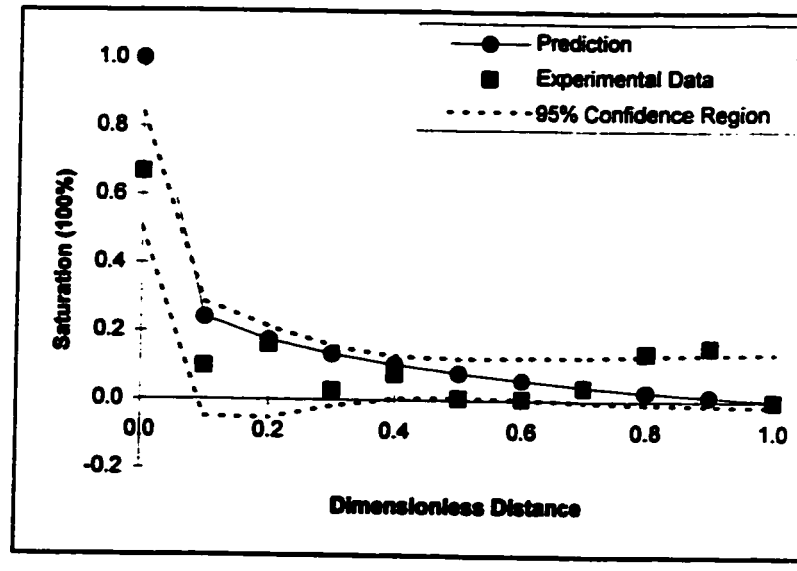

(c)

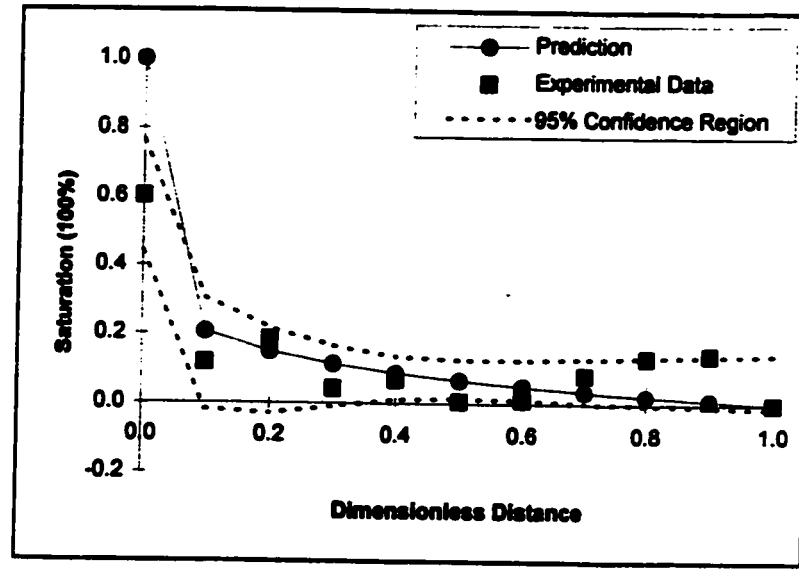

(d)

Fig.8.31(II). Comparison between Predicted and Measured Saturation Profiles in Vertical-Downward Flow Mode. For (μ_o/μ_w=152.02, ρ_o/ρ_w=0.876), (c) Q=84.0 mL/h, (d) Q=174.0 mL/h.

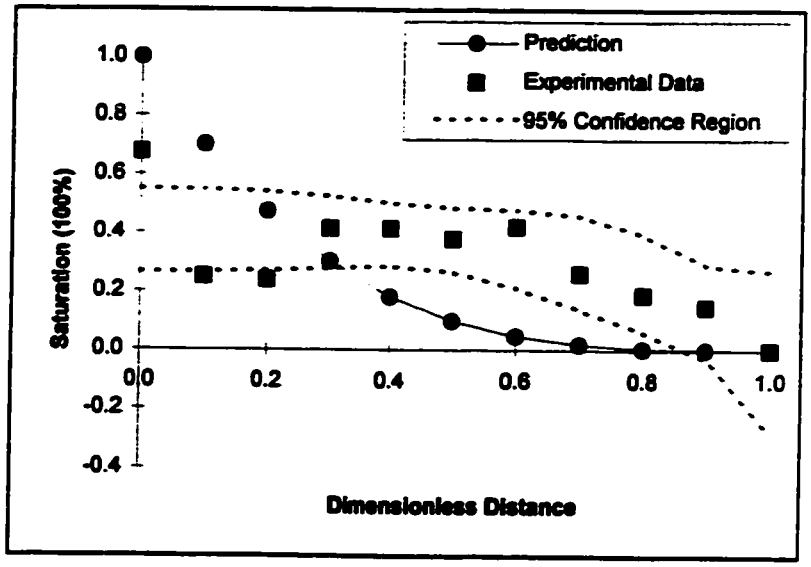

(a)

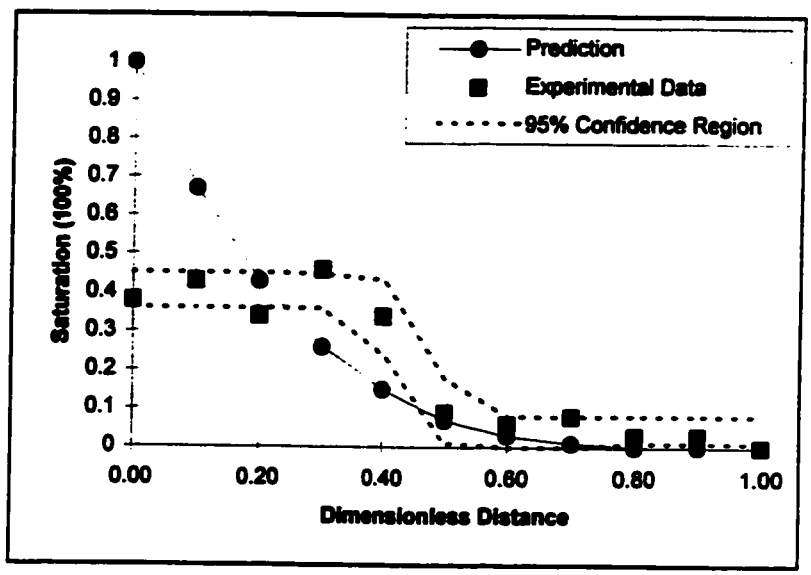

(b)

Fig.8.32(I). Comparison between Predicted and Measured Saturation Profiles in Vertical-Downward Flow Mode. For (μ_o/μ_w=52.13, ρ_o/ρ_w=0.808), (a) Q=8.5 mL/h, (b) Q=13.2 mL/h.

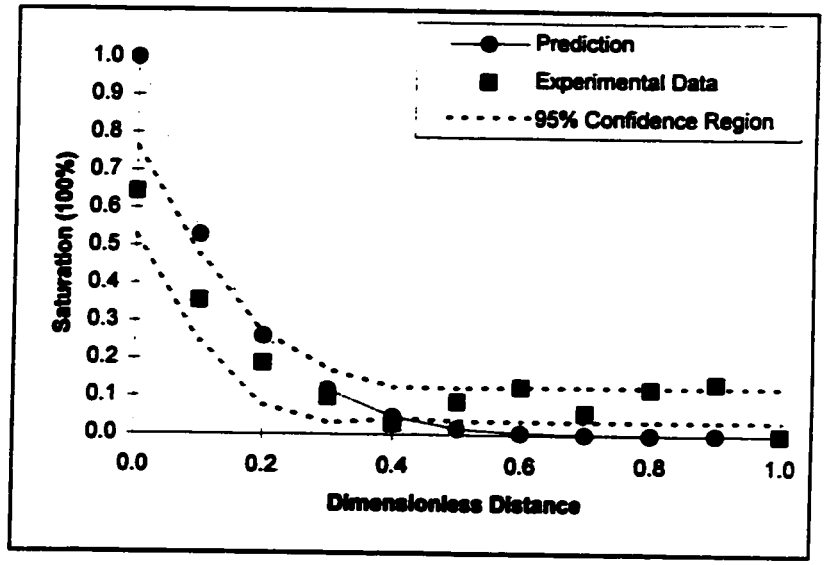

(c)

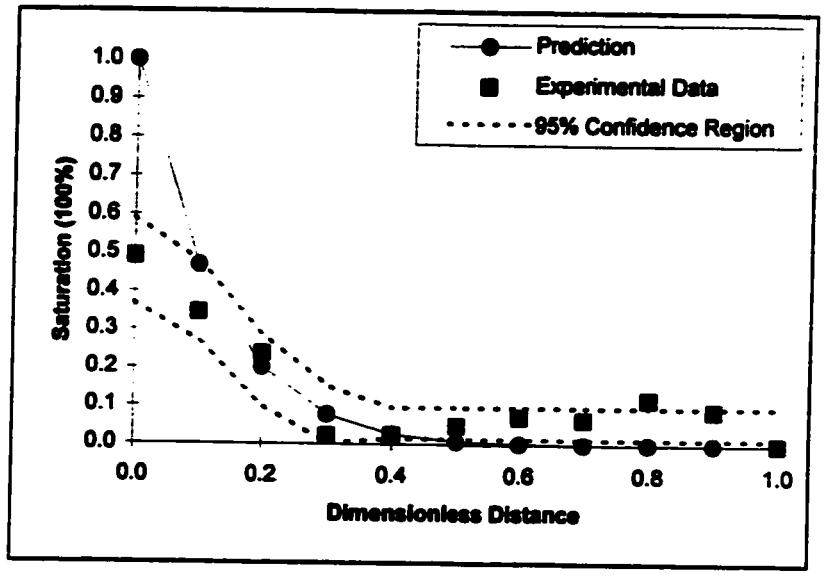

(d)

Fig.8.32(II). Comparison between Predicted and Measured Saturation Profiles in Vertical-Downward Flow Mode. For (μ_o/μ_w=52.13, ρ_o/ρ_w=0.808), (c) Q=84.0 mL/h, (d) Q=174.0 mL/h.

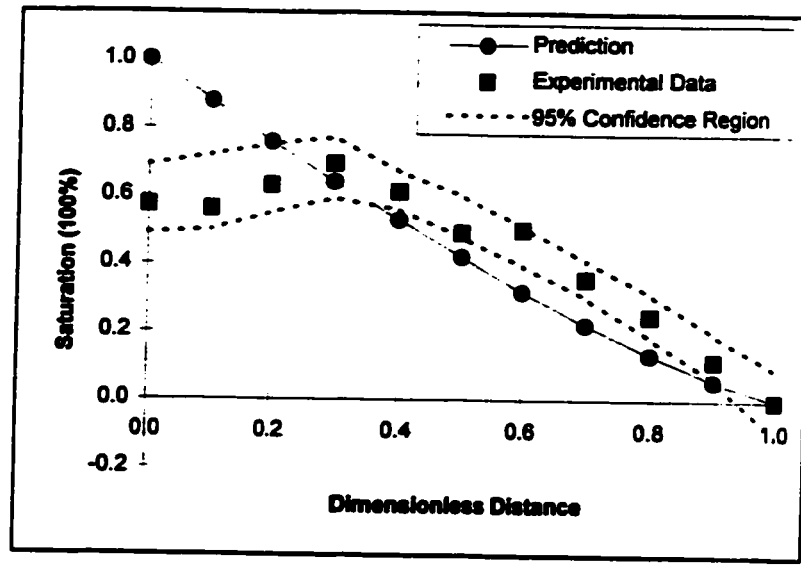

(a)

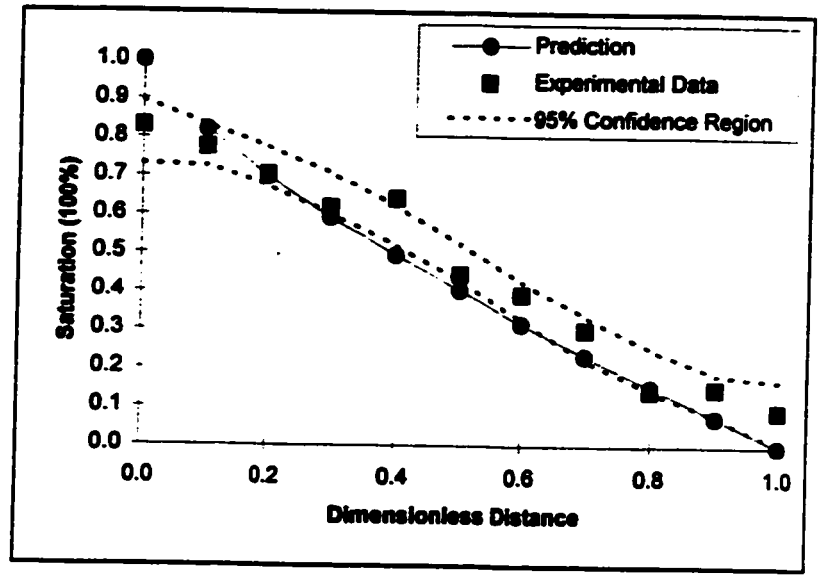

(b)

Fig.8.33(I). Comparison between Predicted and Measured Saturation Profiles in Vertical-Downward Flow Mode. For (μ_o/μ_w=4.11, ρ_o/ρ_w=0.728), (a) Q=8.5 mL/h, (b) Q=13.2 mL/h.

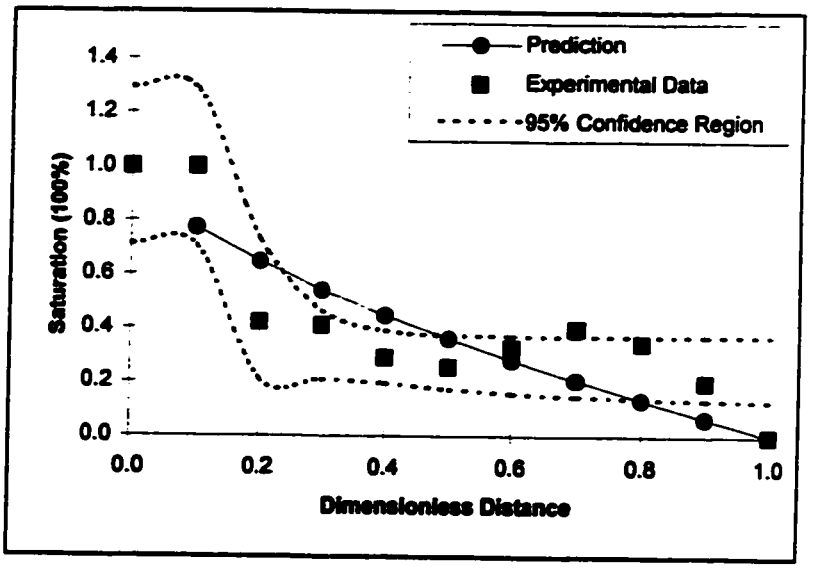

(c)

Fig.8.33(II). Comparison between Predicted and Measured Saturation Profiles in Vertical-Downward Flow Mode. For (μ_o/μ_w=4.11, ρ_o/ρ_w=0.728), (c) Q=84.0 mL/h

8.3.3 Comparison with Literature Results

Fig.8.34 depicts a comparison between the saturation profile obtained using the present theoretical analysis and the experimental saturation profile measurements of Sarma and Bentsen (1988) for the following specific conditions: μ_w = 1.0 mPa.s, μ_o = 4.7 mPa.s, σ = 36.72 mN/m, S_{wi} = 0.07, S_{or} = 0.10, thickness of core = 1.1 cm, height of core = 5.5 cm, and displacement rate = 0.0667 cm^3/s. By using Equations (8.5) and (3.33), the predicted oil recovery, R, is 56%, and the comprehensive coefficient, N_{GN}, is -1.27. The final predicted saturation profile can then be obtained using Equation (3.28).

The agreement between the predicted and experimental saturation profiles in Fig.8.34 is excellent. Moreover, the small difference between them is partly due to the fact that Sarma and Bentsen's result for t = 1200 s was measured slightly after breakthrough occurred. The 95% confidence region for Sarma and Bentsen's data includes the predicted saturation profile, which further confirms the accuracy and reliability of the present analytical solution.

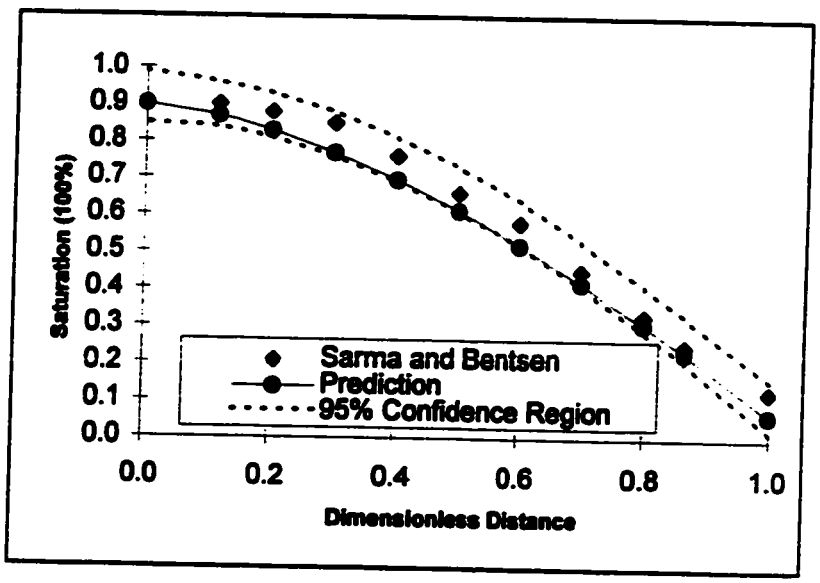

Fig.8.34 Comparison between Predicted Saturation Profile and Experimentally Measured Saturation Profile of Sarma and Bentsen.

8.3.4 Quantitative Estimation of Buoyancy Effects

In the present study, the principal objective has been to elucidate the effects of the buoyancy forces on the efficiency of the water/oil displacement processes occurring in porous media. Since the effects of the buoyancy forces can be effectively neglected in the horizontal displacement mode (see Appendix III), the experimental data obtained for this mode could be employed as a comparison with those for the vertical-upward and vertical-downward modes, as mentioned previously. In the horizontal mode, the principal controlling factors are the viscous forces and capillary forces. In both vertical cases, the principal factors involved are the buoyancy forces, viscous forces and capillary forces, although the actual *effects* of the buoyancy forces are opposite in direction for the two vertical flow modes. However, under the same experimental conditions (i.e., the same injection flow rate, fluid system, and experimental cell), we may assume that the effects of the viscous forces and the capillary forces will be the same in all three basic flow modes. Thus, by comparing each pair of experimental runs (i.e., horizontal vs. vertical-upward, and horizontal vs. vertical-downward), we can quantitatively determine the effects of the buoyancy forces on the displacements, and the amount of oil recovery increase or decrease can simply be calculated by using Equation (8.1).

Another significant difference between the displacements with and without the buoyancy forces is the average finger width at any given axial location in the porous

medium. Therefore, the ratio of finger widths, δ, can be used as an indicator of the magnitude of buoyancy forces. From Equations (3.29), (3.33) and (7.1) we obtain:

$$\delta = \frac{W_f^v}{W_f^h} = \frac{1-(\xi^v)^{\frac{R^v}{(1-R^v)}}}{1-(\xi^h)^{\frac{R^h}{(1-R^h)}}} \tag{8.8}$$

For the representative value ξ=0.5, the corresponding values for δ have been listed in Table 8.4. From these results it may be observed that:

(i) Most of the δ values for the vertical-upward flow mode are greater than 1. This is to be expected, since the buoyancy forces tend to prevent the fingers from developing upwards. In addition, because of these effects, the displacement was partially stabilized and a higher oil recovery could be attained.

Some of the δ values are less than 1, because of the end effect at the inlet of the cell. The displacing fluid does not enter the entire inlet cross-section of the porous medium, and this means that $s_{max} \neq 1$, which will dramatically influence the fingering pattern and the final oil recovery. This effect was observed in all three displacement modes.

(ii) For the vertical-downward flow mode, δ is generally less than 1. This is also to be expected, because the density of the displacing fluid is greater than that of the oil, whence the fingers tend to move downwards rather than transverse, and the width of the fingers is naturally thinner. As a result, a lower oil recovery is observed. There

are a few points out of the range, the reason also being due to the end effects at the cell inlet.

(iii) In accordance with observations (i) and (ii) above, it is apparent that the finger width in the vertical-upward flow mode will be greater than that in the vertical-downward mode, because the effects of the buoyancy forces are positive in the vertical-upward case and negative in the vertical-downward case.

Table 8.4. Results of Average Finger Width Ratio

Experimental Data Oil Recovery (100%)			Ratio $\delta_{0.5}$	Ratio $\delta_{0.5}$	Ratio $\delta_{0.5}$
H	U	D	U/H	D/H	U/D
0.3458	**0.3628**	**0.1454**	**1.0121**	**0.3626**	**2.4952**
0.2819	**0.2838**	**0.2335**	**1.0082**	**0.7990**	**1.2617**
0.2306	**0.2772**	**0.1990**	**1.1905**	**0.8433**	**1.4118**
0.1702	**0.1836**	**0.1666**	**1.0891**	**0.9763**	**1.1155**
0.1498	**0.1582**	**0.1582**	**1.0624**	**1.6024**	**1.0000**
0.1156	**0.0727**	**0.1066**	**0.6106**	**0.9164**	**0.6663**
0.1011	**0.0805**	**0.0908**	**0.7851**	**0.8918**	**0.8803**
0.3564	*0.4500*	*0.2240*	*1.1231*	*0.5689*	*1.5239*
0.2964	*0.3408*	*0.2526*	*1.1893*	*0.8247*	*1.4421*
0.2633	*0.3142*	*0.2126*	*1.2399*	*0.7778*	*1.5941*
0.1764	*0.2160*	*0.1771*	*1.2600*	*1.0045*	*1.2544*
0.1591	*0.1939*	*0.1670*	*1.2495*	*1.0556*	*1.1837*
0.1534	*0.0906*	*0.1355*	*0.5653*	*0.8722*	*0.6481*
0.1073	*0.0970*	*0.1176*	*0.8976*	*1.1038*	*0.8132*
0.4849	0.5625	0.2580	1.2045	0.4469	1.2458
0.4863	0.5099	0.4449	1.0678	0.8858	1.2054
0.4826	0.4685	0.4269	0.9602	0.8470	1.1336
0.4873	0.4932	0.4227	1.0167	0.8248	1.2326
0.4919	0.4639	0.3862	0.9228	0.7321	1.2762
0.4293	0.3377	0.3925	0.7327	0.8884	0.8247
0.3694	0.3590	0.3632	0.5753	0.9785	0.5879

Note: the **bold style** denotes IFT = 49.532 mN/m, the *italic style* denotes IFT = 39.877mN/m, and the underlined style denotes IFT = 30.895 mN/m.

8.4 Combined Effects of Capillary Number and Bond Number

Although the principal motivation for the present study was to elucidate the effects of the buoyancy forces, the effects of the capillary forces are also very important, especially at low injection flow rates, as mentioned previously. As derived in section 4.1 (Chapter 4), these forces were combined and expressed by a dimensionless number, I_{sr} (see Equation (4.3)). By setting different dip angles, ψ, the individual dimensionless number for different flow modes (horizontal, vertical-upward and vertical-downward flow modes) can be obtained, and one can employ them to analyze the interaction between those forces. Table 8.5 shows the physical parameters for calculating the dimensionless number, I_{sr}.

Table 8.5 Physical Parameters for Calculating the Dimensionless Number, I_{sr}

Parameter	Value
L_x	10 (cm)
L_y	0.3 (cm)
r	0.0225 (cm)
S_{wi}	0 (%)
S_{or}	5 (%)
C^*	306.25

By substituting numerical values for the various physical parameters into Equation (4.3), the following equations are obtained, describing the interaction between the viscous, capillary and buoyancy forces in the three different basic flow modes, i.e.:

Horizontal Flow Mode:

$$I_{sr} = 186.7122(0.9025\frac{\mu_o}{\mu_w} - 1)N_c \tag{8.9}$$

Vertical-Upward Mode:

$$I_{sr} = 186.7122(0.9025\frac{\mu_o}{\mu_w} - 1)N_c - 0.1331N_B \tag{8.10}$$

Vertical-Downward Mode:

$$I_{sr} = 186.7122(0.9025\frac{\mu_o}{\mu_w} - 1)N_c + 0.1331N_B \tag{8.11}$$

As Peters and Flock (1981) have pointed out, when the dimensionless number, I_{sr}, is greater than π^2, for a rectangular system, the displacement in the horizontal flow mode will be unstable when the viscosity ratio is unfavorable (i.e., when $\mu_w < \mu_o$). Strictly speaking, this observation relates specially to instabilities induced solely by viscous forces. However, the present work reveals that for a unity viscosity ratio, the presence of buoyancy forces can lead to unstable displacements when the dimensionless number, I_{sr}, is actually less than the critical value of π^2 for a rectangular system. We therefore introduce here the concepts of ***Capillary Instability*** (for horizontal displacements in thin porous media), and ***Capillary-Buoyancy Instability*** (for vertical displacements), which are induced, respectively,

by the capillary forces alone, or by an interaction between the capillary and buoyancy forces.

8.4.1 Horizontal Flow Mode

For the horizontal flow mode, Equation (8.9) is employed to analyze the effects of the capillary forces on the displacement, since the buoyancy forces can be effectively neglected in this mode for thin porous media. Table 8.6 lists the experimental and calculated data for this flow mode.

Table 8.6 Experimental and Calculated Data for Horizontal Flow Mode.

U (cm/s)	R (%)	N_c	I_{sr}
1.940×10^{-4}	59.78	1.06×10^{-6}	-1.93×10^{-5}
4.070×10^{-4}	59.39	2.23×10^{-6}	-4.06×10^{-5}
8.150×10^{-4}	62.18	4.47×10^{-6}	-8.14×10^{-5}
1.203×10^{-3}	67.13	6.60×10^{-6}	-1.20×10^{-4}
1.833×10^{-3}	72.75	1.00×10^{-5}	-1.82×10^{-4}
2.667×10^{-3}	75.40	1.47×10^{-5}	-2.68×10^{-4}
3.889×10^{-3}	73.78	2.13×10^{-5}	-3.88×10^{-4}
5.500×10^{-3}	74.70	3.02×10^{-5}	-5.5×10^{-4}
1.1667×10^{-2}	79.22	6.40×10^{-5}	-1.17×10^{-3}

The controlling forces in this case are the capillary forces, since the viscous forces were eliminated in this study by selecting a unit viscosity ratio. Fig.8.35 shows the variations of breakthrough oil recovery with the dimensionless number, I_{sr}, for the water-wet porous medium in the horizontal flow mode. The results indicate that the displacements are unstable at low injection flow rates (see Fig.8.17 and 18 (a)), but that they become stable at high injection flow rates (see Fig.8.20 and 21 (a)). As shown in Table 8.6, the oil recovery increases as $|I_{sr}|$ increases; i.e., as the injection flow rate increases [Tayal and Narayan 1990, Kiriakidis et al. 1993]. This indicates that at a low injection flow rate, the trapped oil is held within a porous medium by capillary forces. Reducing the magnitude of the capillary forces promotes the release of the trapped oil, thereby leading to an increased oil recovery efficiency. Point A in Fig.8.35 (which corresponds to $|I_{sr}| \approx 2.68\times10^{-4}$ and $Nc \approx 1.47\times10^{-5}$) represents the point at which the oil recovery becomes essentially independent of the capillary effects. At high injection flow rates, the pressure gradient (inertial) forces are high enough to overshadow the effects of the capillary forces, whence this two-phase flow process can be treated as a pseudo single-phase flow, as discussed previously (Equations (8.2) and (8.3)). These results are in good agreement with the conclusions of Morrow and Songkran (1981) that the residual (trapped) oil saturation is effectively constant at capillary numbers less than about 10^{-6}. A new instability scheme would be drawn as follows: $I_{sr} > -2.68\times10^{-4}$ could be the capillary region, and $I_{sr} < -2.68\times10^{-4}$ could be the stable region in this horizontal flow mode.

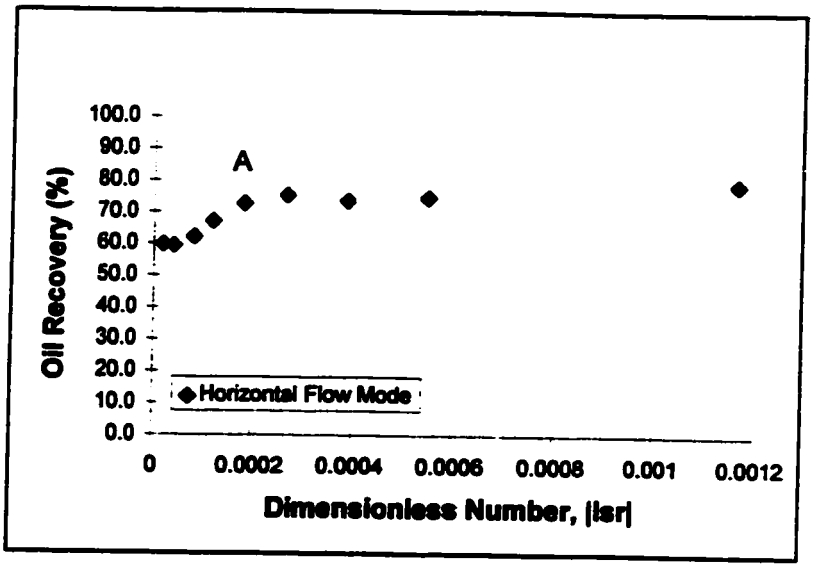

Fig.8.35 Relationship between the Dimensionless Number and Oil Recovery in the Horizontal Flow Mode.

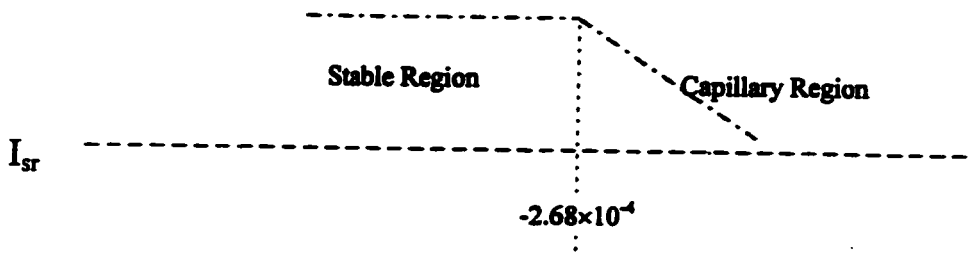

Fig.8.36 Scheme of Different Flow Regions at μ_r=1.0 in the Horizontal Flow Mode.

8.4.2 Vertical-Upward Flow Mode

For the vertical-upward flow mode, Equation (8.10) is employed to analyze the effects of interacting capillary and buoyancy forces on the displacements. Table 8.7 lists the experimental and calculated data for this flow mode.

The principal controlling factors here are the capillary forces and the buoyancy forces since the viscous forces were eliminated by selecting a unity viscosity ratio. Fig.8.37 reveals that the oil recovery is effectively independent of the combined capillary number/Bond number, I_{cr}, which indicates that the buoyancy forces are able to compensate for the deleterious effects of the capillary forces in this flow mode. The absolute value of $|I_{cr}|$ at the lowest flow rate for the horizontal flow mode (1.93×10^{-5}) is much lower than that for the vertical-upward flow mode (2.251×10^{-3}), which confirms that the buoyancy forces predominate over the capillary forces at low injection flow rates. At higher injection flow rates, the oil recovery is again essentially independent of the combined capillary number/Bond number, $|I_{cr}|$. Decreasing this number means increasing the pressure gradient (inertial) forces; decreasing this number even more means that the pressure gradient (inertial) forces take over both the capillary forces and the buoyancy forces. Again, this two-phase flow process can be treated as a pseudo single-phase flow. Over the entire flow range studied, the displacements are relatively stable (see Figs.8.17 and 18 (b) and 8.20 and 21 (b)) because of the significant stabilizing effects of the buoyancy forces in the vertical-upward displacement mode.

8.4.3 Vertical-Downward Flow Mode

For the vertical-downward flow mode, Equation (8.11) is employed to analyze the effects of the interacting capillary forces and buoyancy forces on the displacements. The experimental and calculated data for this mode are listed in Table 8.8.

Table 8.7 Experimental and Calculated Data for the Vertical-Upward Flow Mode

U (cm/s)	R (%)	N_c	N_B	I_{sr}
1.940×10^{-4}	75.04	1.06×10^{-6}	0.0169	-2.251×10^{-3}
4.070×10^{-4}	77.40	2.23×10^{-6}	0.0169	-2.252×10^{-3}
8.150×10^{-4}	79.78	4.47×10^{-6}	0.0169	-2.254×10^{-3}
1.203×10^{-3}	80.76	6.60×10^{-6}	0.0169	-2.257×10^{-3}
1.833×10^{-3}	76.70	1.00×10^{-5}	0.0169	-2.260×10^{-3}
2.667×10^{-3}	84.47	1.47×10^{-5}	0.0169	-2.265×10^{-3}
3.889×10^{-3}	77.13	2.13×10^{-5}	0.0169	-2.271×10^{-3}
5.500×10^{-3}	75.25	3.02×10^{-5}	0.0169	-2.280×10^{-3}
1.1667×10^{-2}	77.45	6.40×10^{-5}	0.0169	-2.315×10^{-3}

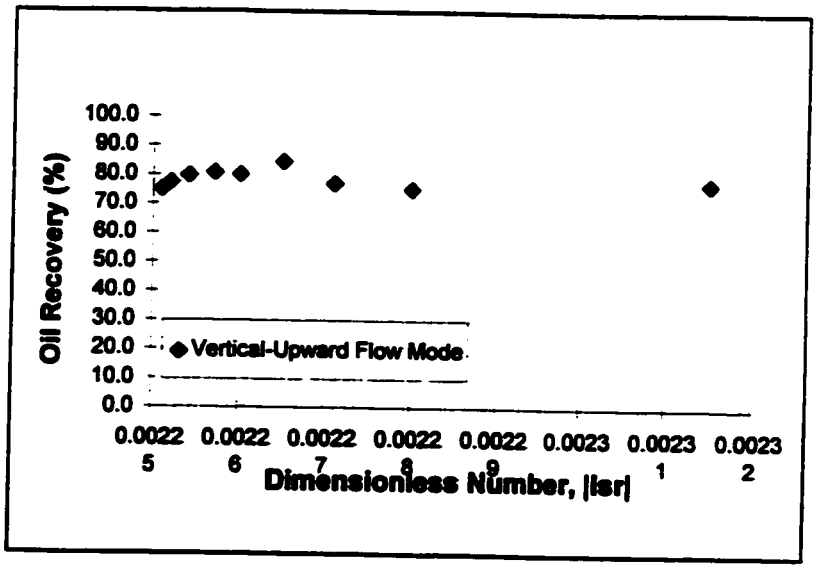

Fig.8.37 Relationship between the Dimensionless Number and Oil Recovery in the Vertical-Upward Flow Mode.

The principal controlling factors in this case are again the capillary and the buoyancy forces, although the buoyancy forces played a negative role in this case, as mentioned previously. Fig.8.38 shows the relationship between the oil recovery and the combined capillary number/Bond number, $|I_{sr}|$, for the vertical-downward flow mode. In general, decreasing the absolute value of this combined number will increase the oil recovery, since a high Bond number implies high buoyancy forces relative to the capillary forces, and leads to premature instability in this flow mode, in which the buoyancy forces are acting in the same direction as the inertial (pressure gradient) forces. This is why the oil recovery increases rapidly as the injection flow rate increases. Point A in Fig.8.38 (at which $|I_{sr}| \approx 2.24 \times 10^{-3}$) can be considered to be a critical point, since decreasing $|I_{sr}|$ below the value of 2.24×10^{-3} has a relatively small effect on the oil recovery. This is because the pressure gradient (inertial) forces are steadily increasing, and the flow system gradually approaches a pseudo

single-phase flow situation. Moreover, the fingering pattern at the high injection flow rate is very similar to the patterns for the horizontal and vertical-upward flow modes (see Figs.8.20 and 21), which further confirms that the effects of the capillary forces and the buoyancy forces are overshadowed at high injection flow rates.

Table 8.8 Experimental and Calculated Data for the Vertical-Downward Flow Mode

U (cm/s)	R (%)	N_c	N_B	I_{sr}
1.940×10^{-4}	22.18	1.06×10^{-6}	0.0169	2.249×10^{-3}
4.070×10^{-4}	32.90	2.23×10^{-6}	0.0169	2.248×10^{-3}
8.150×10^{-4}	59.81	4.47×10^{-6}	0.169	2.246×10^{-3}
1.203×10^{-3}	67.87	6.60×10^{-6}	0.0169	2.243×10^{-3}
1.833×10^{-3}	72.41	1.00×10^{-5}	0.169	2.240×10^{-3}
2.667×10^{-3}	60.93	1.47×10^{-5}	0.0169	2.235×10^{-3}
3.889×10^{-3}	69.98	2.13×10^{-5}	0.0169	2.229×10^{-3}
5.500×10^{-3}	73.77	3.02×10^{-5}	0.0169	2.220×10^{-3}
1.1667×10^{-2}	80.80	6.40×10^{-5}	0.0169	2.186×10^{-3}

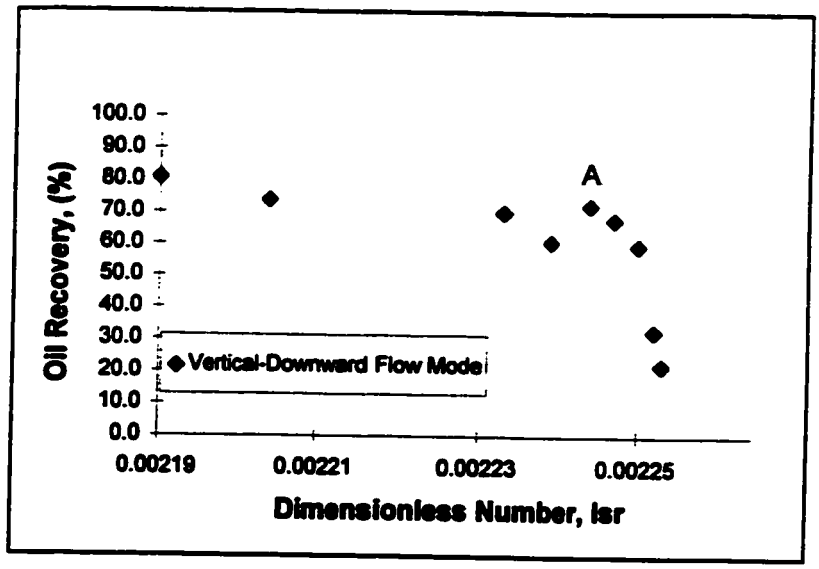

Fig.8.38 Relationship between the Dimensionless Number and Oil Recovery in the Vertical-Downward Flow Mode.

8.5 Miscible Displacements with a Unity Viscosity Ratio

In this section, we further modify the fluid system; i.e., the viscosity ratio is set to unity and the two fluids employed are miscible. Therefore, the effects of both the viscous forces and the capillary forces are effectively eliminated during this miscible displacement process. In addition, the diffusional effects are negligible [Guo and Neale 1996], whence only buoyancy (i.e., gravity) and inertial (i.e., pressure gradient) forces are present, thereby permitting a direct comparison of the effects of these two forces. Fig.8.39 depicts the general relationship between the injection flow rate and the fractional recovery of the displaced fluid for the three different flow modes. It is immediately apparent that the buoyancy forces exert a controlling influence at low injection flow rates, but have little effect at high injection flow rates. For example, the oil recovery in the vertical-upward flow mode is extremely high (95.15% at Q= 2.1mL/h) and in the vertical-downward flow mode the oil recovery is relatively very low (24.10% at Q= 2.1mL/h). This reveals that the effects of the buoyancy forces are very significant in the vertical displacements. These observations can be explained in terms of the relative magnitudes of the buoyancy forces and inertial forces, as described in more detail below.

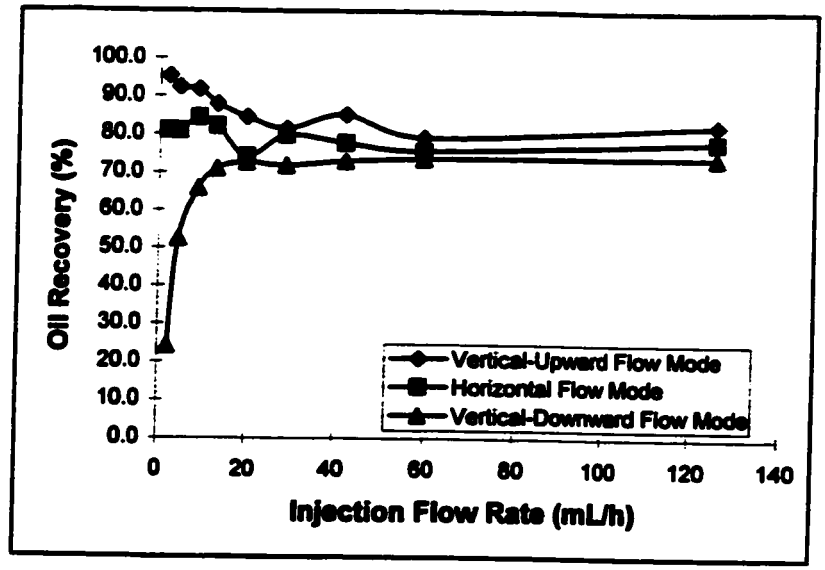

Fig. 8.39 Relationship between the Injection Flow Rate and Oil Recovery in All Different Flow Modes.

8.5.1 Horizontal Flow Mode

In view of the neglection of the buoyancy forces in the horizontal flow mode (Appendix III), which is a good assumption for thin porous media (where gravity segregation effects are minimal [Guo and Neale 1996]), the flow mechanism can be regarded as equivalent to single-phase flow in view of the complete miscibility of the fluid system and unity viscosity ratio employed. Moreover, because of the absence of viscous forces, it was expected that the displacement efficiency in the horizontal flow mode would not be significantly influenced by the injection flow rate, as confirmed by Fig.8.39. This is in good agreement with previous results [Guo and

Horizontal Miscible Displacement

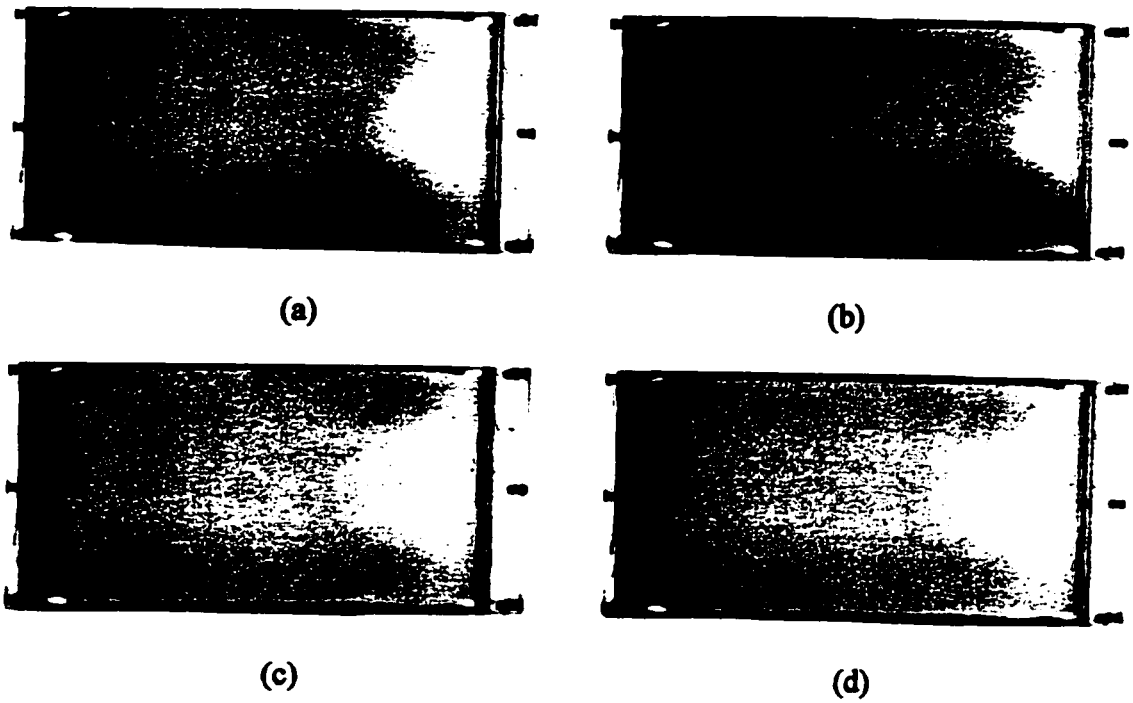

Fig.8.40 Horizontal Miscible Displacement. Dyed Tetrachloroethylene-Heavy Paraffin Oil Mixture Displacing Light Paraffin Oil (μ_o/μ_w=1.0, ρ_o/ρ_w=0.8496) at (a) Q=2.1 mL/h, R=81.06%, (b) Q=4.4 mL/h, R=80.85%, (c) Q=59.8 mL/h, R=75.76%, (d) Q=126.0 mL/h, R=78.24%.

Neale 1996]. As shown in Fig.8.40, the displacement patterns and fractional recoveries are influenced only slightly by the injection flow rate, and each experiment exhibits a nominally stable displacement front, except near the confining edges of the cell, where slight channeling effects come into play on account of the finite width of the porous medium and the associated high porosity zone near the edges. Because experiments were carried out using the same porous medium cell, the edge effects could be expected to appear, and to be of comparable magnitude, in all three of the horizontal and vertical flow modes.

8.5.2 Vertical-Upward Flow Mode

In the vertical-upward flow mode, the effects of the buoyancy forces influence the displacements, especially at very low injection flow rates, where they have adequate time to come into play and exert their full effects on the displacement process. Due to the significant density difference ($\Delta\rho$ = 0.1508 g/mL) between the two fluids, the high-density displacing fluid tends to linger at the bottom of the porous medium cell, thereby promoting a very flat horizontal displacement interface. At low flow rates, the displacing fluid invades the entire cross-section of the porous medium (see Fig.8.41 (a) and (b)), resulting in a displacement efficiency as high as 95.15%. The displacement in this case is very stable, as described previously in Chapter 4. In contrast to the corresponding displacement in the horizontal flow mode, it clearly exhibits the importance of the buoyancy forces. When the injection flow rate increases, the time available for the buoyancy forces to come into play is

Vertical-Upward Miscible Displacement

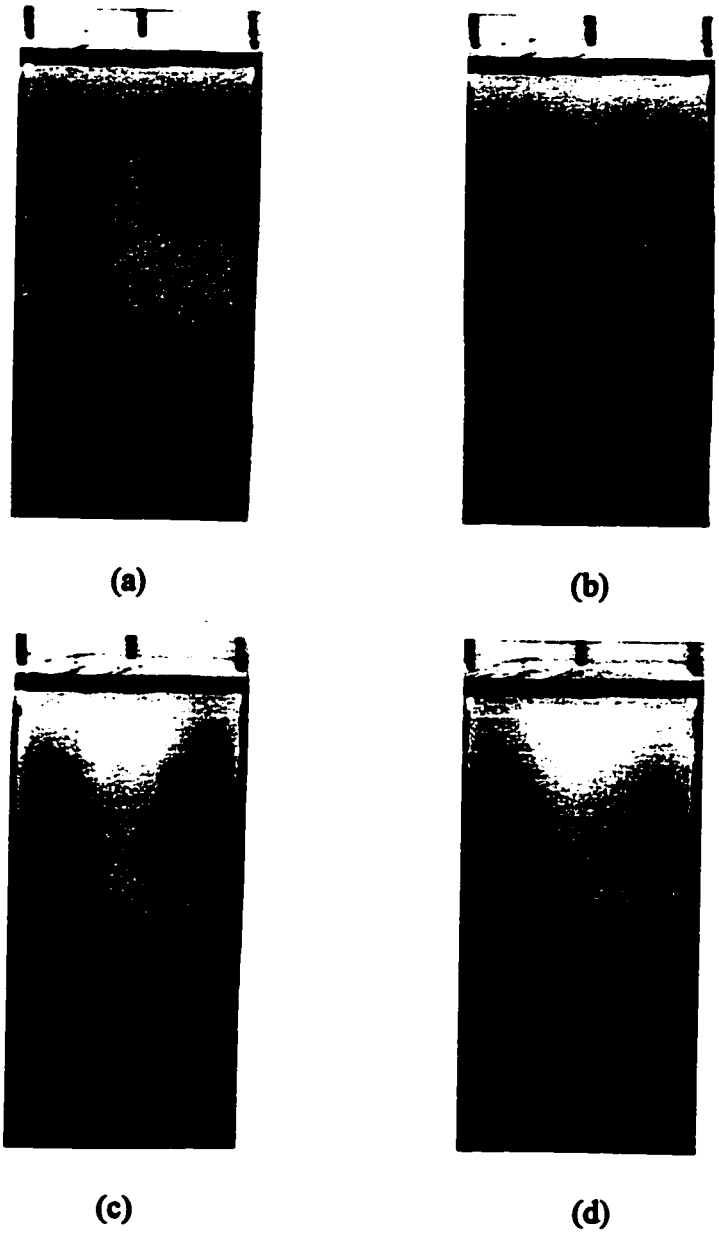

Fig. 8.41 Vertical-Upward Miscible Displacement. Dyed Tetrachloroethylene-Heavy Paraffin Oil Mixture Displacing Light Paraffin Oil (μ_o/μ_w=1.0, ρ_o/ρ_w=0.8496) at (a) Q=2.1 mL/h, R=95.15%, (b) Q=4.4 mL/h, R=92.24%, (c) Q=59.8 mL/h, R=79.21%, (d) Q=126.0 mL/h, R=82.57%.

diminished, and the displacement pattern and displacement efficiency (see Fig.8.41 (c) and (d)) approach those corresponding to the horizontal flow mode (see Fig.8.40 (c) and (d)), as would be expected that both displacement patterns and final oil recovery efficiency are close to each other (R=78.24% for the horizontal case, R=82.57% for the vertical-upward case).

8.5.3 Vertical-Downward Flow Mode

In the vertical-downward flow mode, the effects of the buoyancy forces also play a significant role in the displacement, except that in this mode they exert effects in the opposite direction to those in the vertical-upward mode. At low injection flow rates, where both buoyancy forces and inertial forces work in the same direction, the displacing fluid tends to move downwards much more rapidly (i.e., at Q=2.1 mL/h, t_{br}=7,355 s for the vertical-downward flow while t_{br}=29,042 s for the vertical-upward flow). However, when the injection flow rate is very low, i.e., Q=2.1 mL/h, the effects of the buoyancy forces are so great that the displacing fluid starts to pull away from the upper reservoir, tending to empty the reservoir faster than it is replenished with freshly injected displacing fluid. In the present experiments, some of the volatile tetrachloroethylene solvent in the displacing fluid actually vaporized under the partial vacuum condition created, as is clearly shown by the dark black region at the top of Fig.8.42 (a). Fig.8.42 illustrates convincingly that the buoyancy forces destabilized the displacement process in the vertical-downward flow mode

Vertical-Downward Miscible Displacement

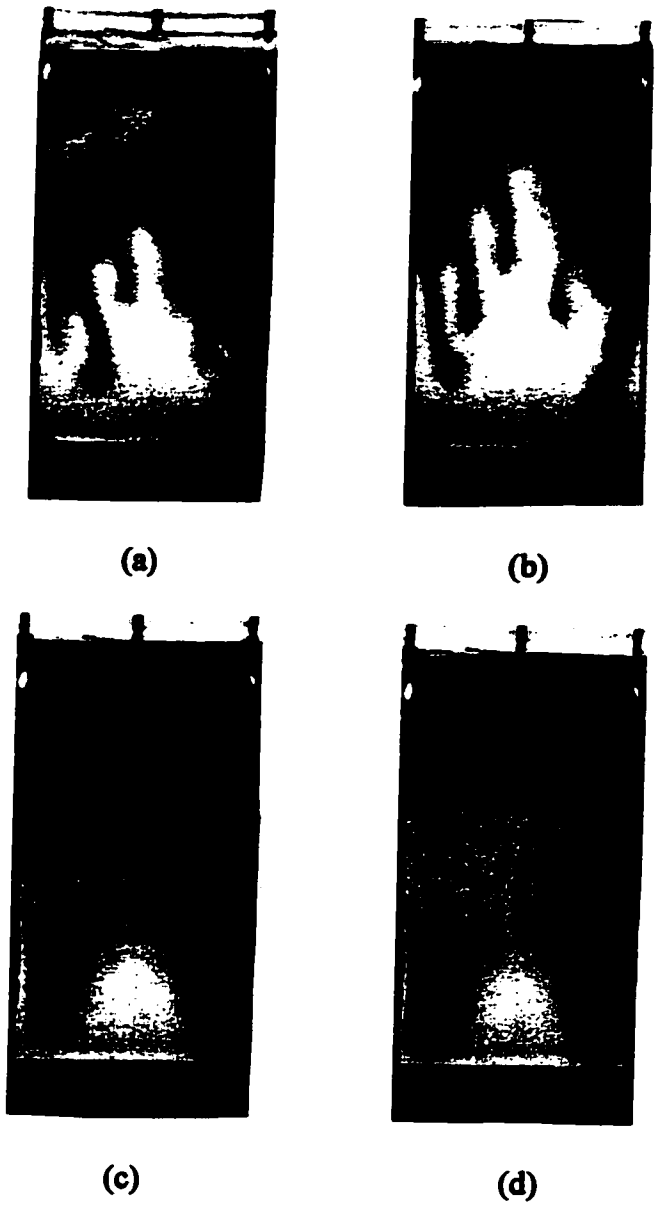

Fig.8.42 Vertical-Downward Miscible Displacement. Dyed Tetrachloroethylene-Heavy Paraffin Oil Mixture Displacing Light Paraffin Oil (μ_O/μ_W=1.0, ρ_O/ρ_W=0.8496) at (a) Q=2.1 mL/h, R=24.10%, (b) Q=4.4 mL/h, R=52.37%, (c) Q=59.8 mL/h, R= 73.71%, (d) Q=126.0 mL/h, R=74.11%.

for the case in which $\rho_1 > \rho_2$, as previously deduced analytically in Chapter 4. It is therefore apparent that "*gravitational fingers*" have been produced (see Fig.8.42 (a) & (b)). These gravitational fingers have a very smooth shape, unlike the dendritic shape of conventional viscous fingers or the cactus-like shape of purely capillary fingers. These gravitational fingers result in a large amount of displaced fluid being uncontacted, and a correspondingly low displacement efficiency (i.e., R=24.10% at Q = 2.1 mL/h). However, at a higher flow rate, the displacement pattern resembles more closely the corresponding patterns for the horizontal and vertical-upward flow. As shown in Figs.8.40(c) and (d), 8.41(c) and (d), and 8.42(c) and (d), the displacement patterns for the three different flow modes are very similar to each other at a high flow rate. This is to be expected, since at higher flow rates the buoyancy forces necessarily have less time to come into play and exert their full effects.

8.6 Immiscible Displacements with and without Connate Water

The presence of connate water in the porous medium cell isolated the oil from contacting the particles of the porous medium; therefore the size of the 'new channels' and the oil distribution became slightly different from the case that did not have connate water present (see Fig.8.43). Therefore, the capillary effects were somewhat different on the displacements. Figs.8.44, 8.46 and 8.48 depict the general relationship between the injection flow rate and breakthrough oil recovery in the presence and absence of connate water in the three different flow modes considered herein. Because of the high interfacial tension (i.e., σ=49.53mN/m referring to capillary effects), high viscosity ratio (i.e., μ_r=152.02 referring to viscous effects), and large density difference (i.e., $\Delta\rho$=0.1239 g/cm^3 referring to buoyancy effects), the oil recoveries in all displacements were less than 30% over the entire range of the injection flow rates.

8.6.1 Horizontal Flow Mode

As mentioned previously, viscous forces have little effect on the displacements when the injection flow rate is low, and capillary forces necessarily become the dominant factors, since the buoyancy forces can be effectively neglected in the horizontal flow mode.

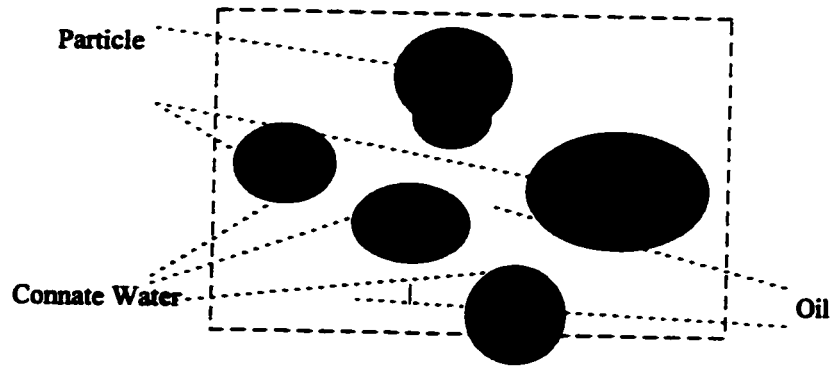

Fig.8.43 Scheme of the Connate Water Film, the Particles, and the Oil in the Porous medium.

In view of Fig.8.45 (a) and (b) of the fingering patterns at low injection flow rates, without connate water present in the porous medium cell, the injected fluid can enter the inlet of the cell at any points and at any time during the displacement process whereupon it imbibes in the channels (i.e., capillary effects). Although the connate water is present in the porous medium cell, once the first point of entering the cell is developed, it will hardly create a new entrance, since the pressure gradient at that point is lower than anywhere else, and the displacing fluid prefers to penetrate into the well-established channels (the channels containing connate water), since the viscous resistance in those channels is smaller. The effects of the capillary forces seem to be nonessential. This causes a premature breakthrough of the displacements. As a result, the oil recovery is smaller when the connate water is present (see Fig.8.44). At high injection flow rates, where the viscous forces predominate, the existence of connate water does not have as many effects on the displacements as

when connate water is not present. Thus, the fingering patterns in both cases are similar to each other (compare Fig.8.45(c) and (d)).

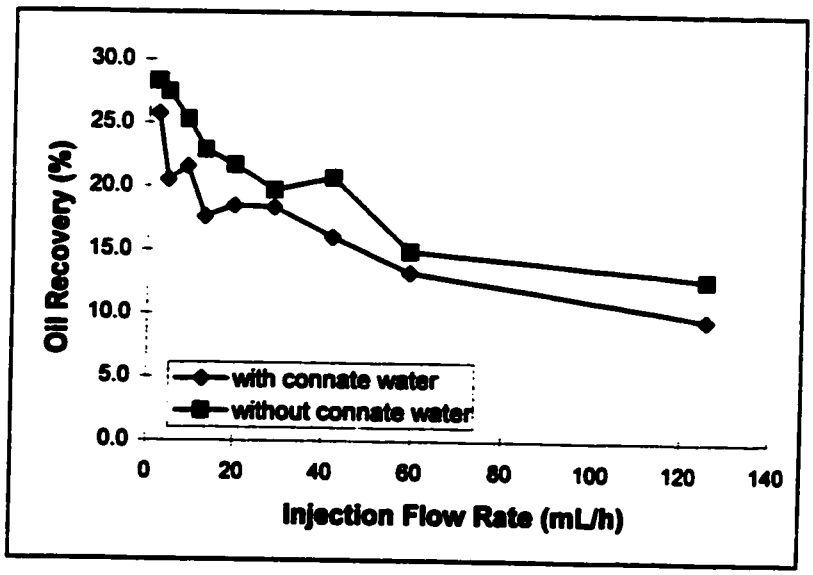

Fig.8.44 Relationship between Injection Flow Rate and Oil Recovery in the Presence and Absence of Connate Water in the Horizontal Flow Mode.

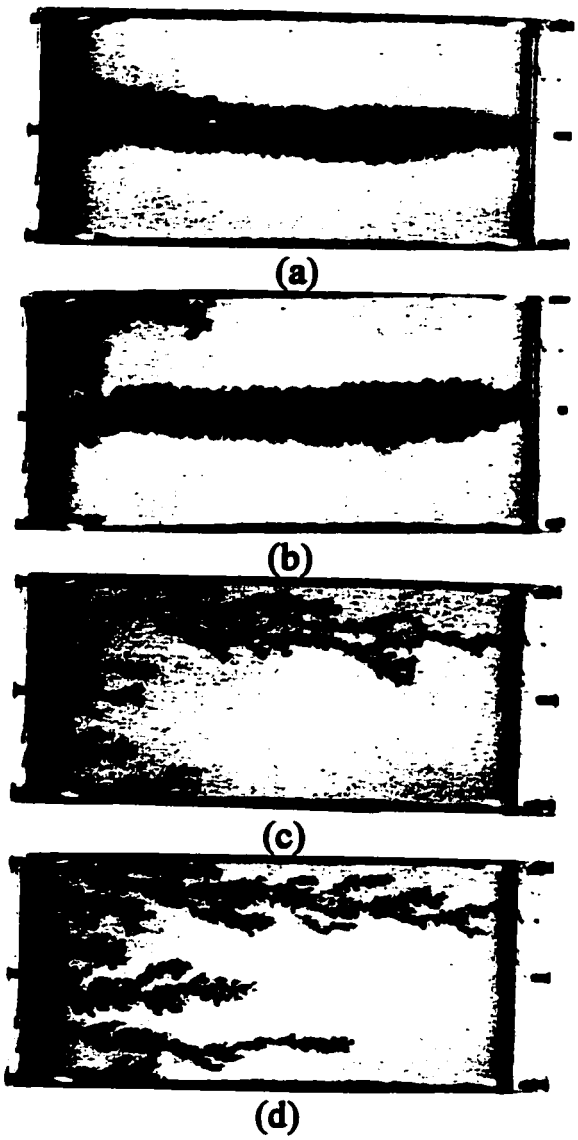

Fig.8.45 Fingering Patterns in the Horizontal Flow Modes with μ_o/μ_w=152.02, ρ_o/ρ_w=0.876 at (I) Q=2.1 mL/h. (a) t_{br}=7855 s, R=25.74%; (b) t_{br}=7080 s, R=23.20%; (II) Q=126.0 mL/h. (c) t_{br}=49 s, R=9.63%; (d) t_{br}=65 s, R=12.79%; (a and c with connate water, b and d without connate water)

8.6.2 Vertical-Upward Flow Mode

In the vertical-upward displacement processes, the viscous, capillary and buoyancy forces will exert their full effects on the displacement process. Low injection flow rates give more opportunities to exhibit the capillary effects and buoyancy effects, and the viscous forces are basically limited. When connate water is absent in the porous media, the injected fluid imbibes in the smaller channels (i.e., capillary effects), and lingers at the bottom of the cell (i.e., buoyancy effects). However, when the connate water is present, the capillary forces may not be as effective as when it is not present, since the injected fluid will join the connate water and connect them during the displacement. Hence, a network of the injected fluid and the connate water is built, which will help to displace more oil. Fig.8.47(a) and (b) shows that the colour density of the fingers for the case with connate water is darker than for the one without connate water, mostly because of the existence of connate water, and fingers grow from the accumulations. As a consequence, the breakthrough oil recovery for the case with connate water is higher than for that without connate water. On the other hand, at higher injection flow rates, the effects of both the capillary and buoyancy effects are much less significant, because the viscous forces control the displacement process. The connate water has little effect on the displacement process, and the fingering patterns for both cases are close to each other (see Fig.8.47(c) and (d)), also close to the correspondingly horizontal case (see Fig.8.45(c) and (d), and Fig.8.47(c) and (d)).

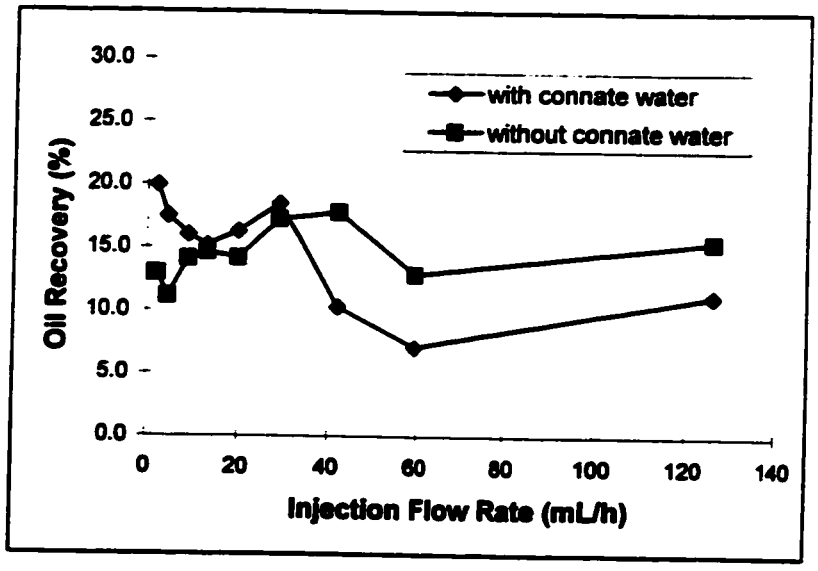

Fig.8.46 Relationship between Injection Flow Rate and Oil Recovery in the Presence and Absence of Connate Water in the Vertical-Upward Flow Mode.

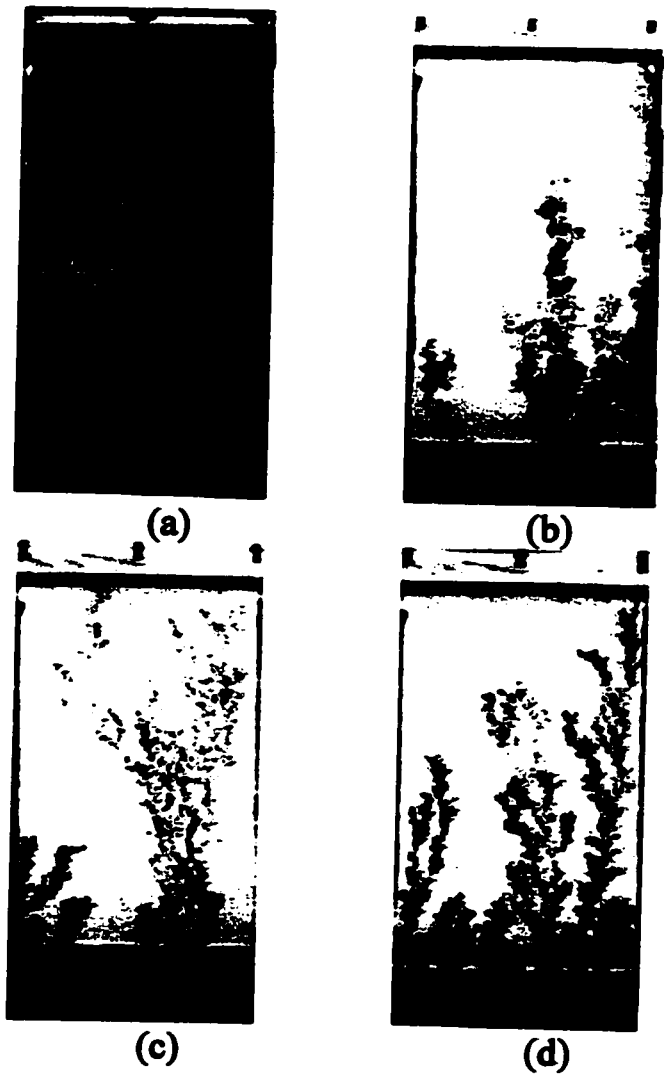

Fig.8.47 Fingering Patterns in the Vertical-Upward Flow Modes with μ_o/μ_w=152.02, ρ_o/ρ_w=0.876 at (I) Q=2.1 mL/h. (a) t_{br}=6093 s, R=19.96%; (b) t_{br}=3954 s, R=12.95%; (II) Q=126.0 mL/h. (c) t_{br}=57 s, R=11.21%; (d) t_{br}=79 s, R=15.53%; (a and c with connate water, b and d without connate water)

8.6.3 Vertical-Downward Flow Mode

The situation in the vertical-downward flow mode will be different again from previous cases, since the direction of the buoyancy forces is the same as the flow direction of the injected fluid. At low injection flow rates, the capillary forces primarily exerted the same effects as mentioned above. However, unlike the phenomenon that occurred in the vertical-upward flow mode, the effects of buoyancy forces will play a negative role in the displacement process. Due to the same direction of the buoyancy forces and the motion of the displacing fluid, the buoyancy forces will accelerate the displacing fluid downwards much faster through the cell, resulting in a low breakthrough time and hence a low oil recovery. In addition, in the absence of connate water the fingers invade not only downwards, but also transversely because of the capillary effects. In the case with connate water, the fingers are narrow (see Fig.8.49(a) and (b)) because of the well-established "new channels". When the injection flow rates are increased, the fingering patterns for both cases gradually become similar to those for the horizontal and vertical-upward flow modes (see Fig.8.45(c) and (d), Fig.8.47(c) and (d), and Fig 8.49(c) and (d)).

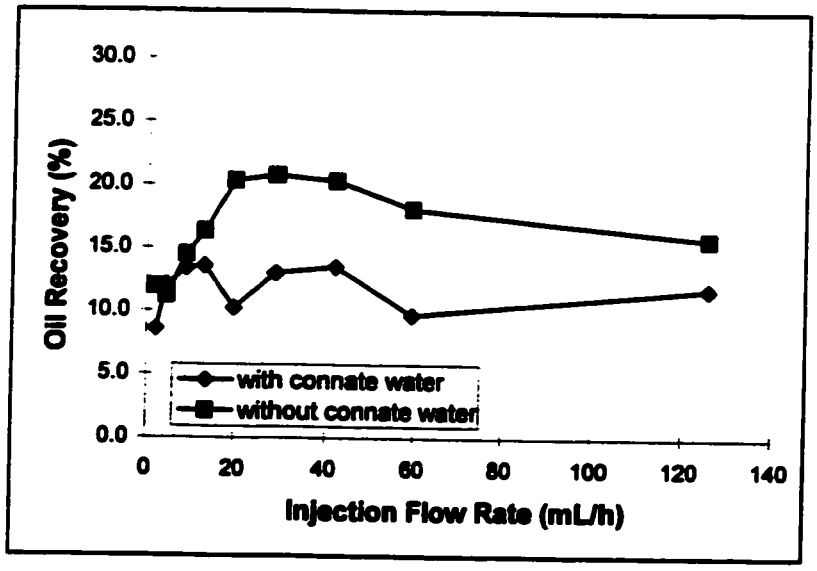

Fig.8.48 Relationship between the Injection Flow Rate and Oil Recovery in the Presence and Absence of Connate Water in the Vertical-Downward Flow Mode.

Vertical-Downward Immiscible Displacement

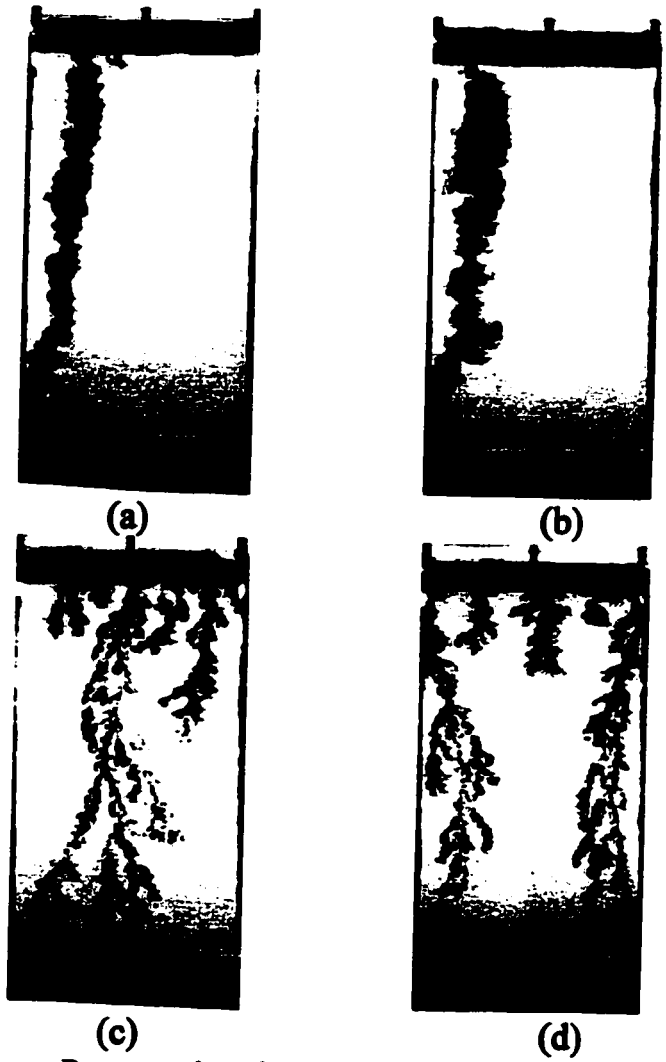

Fig.8.49 Fingering Patterns in the Vertical-downward Flow Modes with μ_o/μ_w=152.02, ρ_o/ρ_w=0.876 at (I) Q=2.1 mL/h. (a) t_{br}=2619 s, R=8.58%; (b) t_{br}=3646 s, R=11.95%; (II) Q=126.0 mL/h. (c) t_{br}=60 s, R=11.80%; (d) t_{br}=80 s, R=15.73%; (a and c with connate water, b and d without connate water)

8.6.4 Instability Analysis

As derived in Chapter 4, Equation (4.25) can be employed to calculate the critical velocity for all three different flow modes. For Equation (4.25)(b) and (c), one could easily find that the results of this critical velocity are negative, since the comprehensive coefficient, N_{GN}, is always negative. Physically speaking, this makes no sense, since the quantity of velocity cannot be negative. However, it does reveal that the inequality Equation (4.17) cannot be satisfied, which means that the pressure gradient within the oil phase cannot overcome gradients of both the capillary pressure and the pressure gradient of the water phase. This causes the water to move faster than the oil. Therefore, the irregular front of the displacement is produced. One may conclude that stability can never be reached in linear immiscible displacements aligned in horizontal and vertical-downward flow modes, even if the viscosity ratio is favorable to the displacements.

For the vertical-upward flow mode, the situation will be somewhat different from those discussed above; since the term ($\Delta\rho g$=121.422 g/cm^2 s^2) is much greater than the second term (~0.8g/cm^2 s^2) in this study. This means that the buoyancy forces can overshadow the capillary forces. If it is assumed that the viscosity of oil is much greater than that of water, Equation (4.25a) could be simplified as:

$$U_c = \frac{\Delta\rho g K}{\mu_o} \tag{8.12}$$

For the experiments presented in section 8.6, the calculated critical velocity for the vertical-upward flow mode is $U_c = 1.43 \times 10^{-6}$ cm/s. Unfortunately, the range of injection flow rates employed in this study ranged from 1.94×10^{-4} cm/s to 1.17×10^{-2} cm/s. They are all larger than this critical velocity. As a judgment of instability, all the displacements are unstable. This is confirmed by the photographs in Fig.8.47.

Chapter 9

Conclusions

9.1 Effects of Buoyancy Forces

1. In vertical, linear, immiscible displacements, buoyancy forces exert an extremely important influence on the fingering pattern. They either stabilize the displacement, resulting in a higher oil recovery, or destabilize it, leading to a lower oil recovery.

2. Buoyancy forces play a different role in the vertical-upward flow mode and the vertical-downward flow modes. In certain cases, the difference in oil recoveries ranges from 5% to 70%.

9.2 Effects of Injection Flow Rate

1. The injection flow rate is one of several key factors in the displacement process. It controls the balance between the buoyancy, viscous and capillary forces. Variation of the injection flow rate will significantly change the fingering pattern and oil recovery.

2. At low injection flow rates, both the buoyancy and capillary forces are important. For the vertical-upward flow mode, a higher oil recovery can be expected. However, in the vertical-downward flow mode, a lower oil recovery is obtained.

3. At high injection flow rates, viscous forces overshadow both the buoyancy and capillary forces. No matter which flow mode is involved, the final fingering patterns will be similar, and R about the same.

9.3 Saturation Profile

1. An analytical solution of the displacement equations has been obtained, which takes the effects of the buoyancy forces, capillary forces and viscous forces into account. The agreement between experimental results and theoretical results is good.

2. It has become possible to quantitatively predict the effects of the buoyancy forces by either (a) comparing the oil recovery in the different displacement modes, or (b) comparing the average finger widths in the different displacement modes.

3. Because of the analytical solutions obtained in this work, it is now possible to plot the saturation profiles and to compare them with ones from the literature.

Application of this solution is very simple, as long as a certain number of empirical parameters are known.

9.4 Displacement Instability

1. The viscosity ratio and density difference will greatly affect the critical velocity in the vertical flow modes. Increasing one of them will change the instability of the displacements.

2. Instabillity occurs not only at an unfavorable viscosity ratio, but also at a favorable viscosity ratio, owing to the effects of both the capillary forces and buoyancy forces.

3. A big gain in oil recovery can be obtained by increasing the capillary number. The combined capillary number and Bond number can be employed to analyze the relative interaction between the capillary forces and buoyancy forces.

4. The miscible linear displacement processes in the horizontal flow mode can be treated as a pseudo single-phase flow, and nothing should affect the displacement except wall effects of the cell. The oil recovery is basically independent of the injection flow rate, and the displacement front is stable.

5. For the vertical flow modes, the instability of the miscible linear displacement can be divided into two results at low injection flow rates with a unit viscosity ratio: (i) the displacement will be absolutely stable in the vertical-upward flow mode, and (ii) the displacement will be completely unstable in the vertical-downward flow mode.

6. Gravity fingers have their own characteristic fingering shape, unlike the viscous fingers and the gravity-capillary fingers. However, the quantitative effects of these different types of fingers on oil recovery are much the same.

7. The instability of immiscible linear displacements can be characterized in two ways: (i) the displacement will be stable in the vertical-upward flow mode if the buoyancy forces are greater than the capillary forces, and (ii) the displacement will never be stable in the horizontal and vertical-downward flow modes, due to the significant capillary effects and buoyancy effects.

Recommendations for Future Work

1. To simulate a more realistic situation, transverse displacement is recommended, since transverse flow combines the basic features of the horizontal and vertical flow modes.

2. To study instability in vertical linear immiscible displacements, a lower injection flow rate is recommended, since the buoyancy forces are extremely important at lower injection flow rates.

3. A larger experimental cell could help to provide additional information, primarily by reducing end effects and the geometry effect.

References

1. Araktingi, U. G. and Orr, F. M.: "Viscous Fingering, Gravity Segregation, and Reservoir Heterogeneity in Miscible Displacements in Vertical Cross Section", paper SPE/DOE 20176 presented at the 1991 SPE/DOE Symposium on Enhanced Oil Recovery, Tulsa, Oklahoma, April 22-25.

2. Bates, D. M. and Watts, D. G.: "*Non-Linear Immiscible Displacement in Unconsolidated Porous Media*", J. Wiley & Sons, 1988.

3. Bentsen, R. G. and Saeedi, J.: "Liquid-Liquid Immiscible Displacement in Unconsolidated Porous Media", *JCPT* (January-March 1981), **20**, 93-103.

4. Buckley, S. E. and Leverett, M. C.: "Mechanism of Fluid Displacement in Sands", *Trans. AIME* (1942), **146**, 107-116.

5. Cannon Instrument Co.: "Instructions for the Use of the Cannon-Fenske Routine Viscometer", Cannon-Fenske Instrument Corperation, P. O. Box 16, State College, PA. 16801.

6. Christie, M. A.: "High-Resolution Simulation of Unstable Flow In Porous Media", *SPERE* (August 1989), **4**, 297-308.

7. Chuoke, R. L., van Meurs, P. and van der Poel, C.: "The Instability of Slow, Viscous Liquid-Liquid Displacements in Permeable Media", *Trans. AIME* (1959), **216**, 188-194.

8. Craig, F. F., Sanderlin, J. L., Moore, D. W. and Geffen, T. M.: "A Laboratory Study of Gravity Segregation in Front Drives", *Trans. AIME* (1957), **210**, 275-282.

9. Douglas, J., Blair, P. M. and Wagner, R. J.: "Calculation of Linear Waterflood Behaviour Including the Effects of Capillary Pressure", *Trans. AIME* (1957) **210**, 96-102.

10. Dullien, F. A. L.: *Porous Media - Fluid Transport and Pore Structure*, 2nd Ed., Academic Press. Inc., New York, NY, 1979.

11. Dumoré, J. M.: "Stability Considerations in Downward Miscible Displacements", *Trans. AIME* (1964), **231**, 356-362.

12. Fayers, F. J. and Sheldon, J. W.: "The Effects of Capillary Pressure and Gravity on Two-Phase Fluid in a Porous Medium", *Trans. AIME* (1959), **216**, 147-155.

13. Fayers, F. J.: "An Approximate Model with Physical Interpretable Parameters for Representing Miscible Viscous Fingering", *SPERE* (May 1988), **3**, 551-558.

14. Flock, D. L., Peters, E. J. and Baird, H.: "The Influence of Frontal Instabilities during Viscous Oil Displacement", in *The Oil Sand of Canada-Venezuela 1977*, CIM Special Volume 17, Canadian Institute of Mining & Metallurgy, Eds. D. A. Redford and A. G. Winestock, 1977, pp. 380-385.

15. Gardner, G. H. F., Downie, J. and Kendall, H. A.: "Gravity Segregation of Miscible Fluids in Linear Models", *Trans. AIME* (1962), **225**, 95-104.

16. Gottfried, B. S., Guilinger, W. H. and Snyder, R. W.: "Numerical Solution of the Equation for One-Dimensional Multi-Phase Flow in Porous Media", *Trans. AIME* (1966), **237**, 62-72.

17. Guo, T. and Neale, G. H.: "Effects of Buoyancy Forces on Miscible Liquid-Liquid Displacement Processes in a Porous Medium", *Powder Technology* (1996), **86**, 265-273.

18. Hagoort, J.: "Displacement Stability of Water Drive in Water-Wet Connate-Water-Bearing Reservoir", *Trans. AIME* (1974), **257**, 63-74.

19. Hagoort, J.: "Oil Recovery by Gravity Drainage", *SPEJ* (June 1980), **20**, 139-150.

20. Hill, S.: "Channeling in Packed Columns", *Chem. Eng. Sci.*(1952) **1**, 247-258.

21. Hopkins, J. S., Golding, J. A. and Ritcey, G. M.: "The Critical Factors Influencing Uranium Precipitation by Hydrogen Peroxide: The Use of Experimental Design Techniques", *Hydrometallurgy* (1987), **17**, 315-334.

22. Hornof, V. and Morrow, N. R.: "Gravity Effects in the Displacement of Oil by Surfactant Solutions", *SPERE* (Nov. 1987), **2**, 627-633.

23. Hu, M. C., Hornof, V. and Neale, G. H.: "Visualization of Unstable Miscible Radial Displacement in a Consolidated Porous Medium", *Powder Technology* (1985), **41**, 265-268.

24. Jerauld, G. R., Nitsche, L. C., Teletzke, G. F., Davis. H. T. and Scriven, L. E.: "Frontal Structure and Stability in Immiscible Displacement", paper SPE 12691, available from SPE, Richardson, TX (1984).

25. Johnson, E. F., Bossler, D. P. and Naumann, V. O.: "Calculation of Relative Permeability from Displacement Experiments", *Trans. AIME* (1959), **216**, 370-376.

26. Kiriakidis, D. G., Mitsoulis, E. and Neale, G. H.: "Computer Simulations of Immiscible Displacement in a Porous Medium Containing a Region of Different Wettability", *JCPT* (1993), **32**, 21-25.

27. Koval, E. J.: "A Method for Predicting the Performance of Unstable Miscible Displacement in Heterogeneous Media", *Trans. AIME* (1963), **228**, 145-154.

28. Kyte, J. R. and Rapoport, L. A.: "Linear Waterflood Behavior and End Effects in Water-Wet Porous Media", *Trans. AIME* (1958), **213**, 423-426.

29. Leverett, M. C.: "Capillary Behaviour in Porous Solids", *Trans. AIME* (1941), **136**, 152-169.

30. McEven, C. R.: "A Numerical Solution of the Linear Displacement Equation with Capillary Pressure", *Trans. AIME* (1959), **216**, 412-415.

31. McLean, D. D.: *Strategies for Engineering Process Analysis*, Course Notes, Department of Chemical Engineering, University of Ottawa, Ottawa, Canada, May 1990.

32. van Meurs, P. and van der Poel, C.: "A Theoretical Description of Water-Drive Processes Involving Viscous Fingering", *Trans. AIME* (1958), **213**, 103-112.

33. Morel-Seytoux, H. J.: in *Flow through Porous Media*, Edited by R. J. M. deWiest, Academic Press, New York (1969), 456-516.

34. Morrow, N. R. and Songkran, B.: "Effects of Viscous and Buoyancy Forces on Non-Wetting Phase Trapping in a Porous Media", *Surface Phenomena in Enhanced Oil Recovery*, D. O. Shah(ed.) Plenum Press, New York City (1981), 387-412.

35. Muskat, M.: "The Effect of Casing Perforation on Well Productivity", *Trans. AIME* (1942), **146**, 175-187.

36. Muskat, M., Wyckoff, R. D., Botset, H.G. and Mores, M.W.: "Flow of Gas-Liquid Mixtures through Sands", *Trans. AIME* (1937), **123**, 69-96.

37. Nasr-el-Din, H., Hornof, V. and Neale, G.H.: "Radial Fingering in a Water-Wet Porous Medium", *Revue de l'Institut Français du Pétrole* (1987), **42**, 783-796.

38. Ni, L. W., Hornof, V. and Neale, G. H.: "Radial Fingering in a Porous Medium", *Revue de l'Institut Français du Pétrole* (1986), **41**, 217-228.

39. Outmans, H. D.: "Transient Interface during Immiscible Liquid-Liquid Displacement in Porous Media", *Trans. AIME* (1962a), **225**, 156-164.

40. Outmans, H. D.: "Nonlinear Theory for Frontal Stability and Viscous Fingering in Porous Media", *Trans. AIME* (1962b), **225**, 165-176.

41. Page, C. A., Brook, H. J. and Neale, G. H.: "Visualization of the Effects of Buoyancy on Liquid-Liquid Displacements in Vertically-Aligned Porous Medium Cells", *Experiments in Fluids* (1993), **13**, 472-474.

42. Paterson, L., Hornof, V. and Neale, G.H: "Visualization of a Surfactant Flood of an Oil-Saturated Porous Medium", *SPEJ* (June 1984a), **24**, 325-327.

43. Paterson, L., Hornof, V. and Neale, G.H: "Water Fingering into an Oil-Wet Porous Medium Saturated with Oil at Connate Water Saturation", *Revue de l'Institut Français du Pétrole* (1984b), **39**, 8-13.

44. Perkins, T. K., Johnson, O. C. and Hoffman, R. N.: "Mechanics of Viscous Fingering in Miscible System", *Trans. AIME* (1965), **234**, 301-317.

45. Perkins, T. K. and Johnston, O. C.: "A Review of Diffusion and Dispersion in Porous Media", *Trans. AIME* (1963), **228**, 70-84.

46. Perkins, T. K. and Johnston, O. C.: "A Study of Immiscible Fingering in Linear Model", *Trans. AIME* (1969), **246**, 39-48.

47. Peters, E. J. and Flock, D. L.: "The Onset of Instability during Two-Phase Immiscible Displacement in Porous Media", *SPEJ* (April 1981), **21**, 249-258.

48. Rachford, H. H.: "Instability in Water Flooding Oil from Water-Wet Porous Media Containing Connate Water", *Trans. AIME* (1964), **231**, 133-148.

49. Richardson, J. G. and Perkins, F. M.: "A Laboratory Investigation of the Rate on Recovery of Oil by Water Flooding", *Trans. AIME* (1957), **210**, 114-121.

50. Sarma, H. K. and Bentsen, R. G.: "A New Method for Estimating Relative Permeabilities from Unstabilized Displacement Data", Paper No.88-39-87 presented at the *39th Annual Technical Meeting of the Petroleum Society of CIM*, Calgary, Alberta, June 12-16, 1988.

51. Scott, G. R., Collins, H. N. and Flock, D. L.: "Improving Waterflood Recovery of Viscous Crude Oils by Chemical Control", paper presented at *Heavy Oil Seminar, The Petroleum Society of C.I.M.*, Calgary, Alberta, May 5, 1965, 243-251.

52. Slobod, R. L. and Howlett, W.: "The Effects of Gravity Segregation in Laboratory Studies of Miscible Displacement in Vertical Unconsolidated Porous Media", *Trans. AIME* (1964), **231**, 1-8.

53. Spivak, A.: "Gravity Segregation in Two-Phase Displacement Processes", *Trans. AIME* (1974), **257**, 619-632.

54. Stalkup Jr, F.: *Miscible Displacement*, Monograph vol.8, third printing, Henry L. Doherty Memorial Fund of AIME, Society of Petroleum Engineers, Richardson, TX, 1992.

55. Tayal, P. and Narayan, K. A.: "Visualization of Water and Surfactant Floods in Oil-Saturated Porous Media", *Experiments in Fluids* (1990), 9, 337-344.

56. Thirunavu, S.R and Neale, G.H.: "Effects of Buoyancy Forces on Immiscible Water/Oil Displacement in a Vertically-Oriented Porous Medium", *Revue de l'Institut Français du Pétrole* (1995), **50**, 517-536.

57. Vizika, O. and Lombard, J. M.: "Wettability and Spreading: Two Key Parameters in Oil Recovery with Three-Phase Gravity Drainage", *SPERE* (February 1996), **11**, 55-60.

58. Wooding, R. A. and Morel-Seytoux, H. J.: "Multiphase Fluid Flow through Porous Media", *Annual Review of Fluid Mechanics* (1976), 8, 233-274.

Appendices

Appendix I

In the absence of capillary forces, Equation (3.3) becomes:

$$U_w^V = f_w(U \mp M_o \Delta\rho g) \tag{A.1}$$

After applying the conservation of mass equation and changing this equation into dimensionless form, Equation (3.17) becomes:

$$\frac{dU^V}{ds}\frac{ds}{sz} = -\frac{L\Phi}{t_{br}} z \frac{ds}{dz} \tag{A.2}$$

Here, one can see that $\frac{dU^V}{ds} = -\frac{L\Phi}{t_{br}} z$. Whence, at a fixed time, the right-hand side of Equation (A.2) can be treated as a constant but variable z.

Appendix II

Insertion of Equation (3.10) into Equation (3.18) yields:

$$\frac{dU^V}{ds} = \frac{d(f_w U)}{ds} \pm \frac{d(f_w M_o \Delta\rho g)}{ds} \propto z \tag{A.3}$$

Whence we may conclude that:

$$\frac{d(f_w M_o)}{ds} \propto z \tag{A.4}$$

Insertion of Equation (3.10) into Equation (3.21) yields:

$$\frac{dC_c}{ds}\frac{ds}{dz} = \frac{d(f_w M_o \frac{dP_c}{ds})}{ds}\frac{ds}{dz} \tag{A.5}$$

which, upon rearrangement, yields:

$$\frac{d(f_w M_o \frac{dP_c}{ds})}{ds}\frac{ds}{dz} = \frac{dP_c}{dz}\frac{d(f_w M_o)}{ds} + f_w M_o \frac{d^2 P_c}{ds^2}\frac{ds}{dz} \tag{A.6}$$

In view of Equation (A.4), the first term of equation (A.6) will be:

$$\frac{dP_c}{dz}\frac{d(f_w M_o)}{ds} \propto \frac{dP_c}{dz} z \tag{A.7}$$

and the second term of Eqaution (A.6) will be:

$$f_w M_o \frac{d^2 P_c}{ds^2}\frac{ds}{dz} = f_w M_o \frac{d}{ds}(\frac{dP_c}{dz}) \tag{A.8}$$

As Douglas and Wagner (1958) have pointed out, at the initial condition (i.e. t=0, z=0):

$$\frac{dP_c}{dz} = \frac{LQ\mu_w}{k_w} \tag{A.9}$$

Extending their equation at t=0, z=1 yields:

$$\frac{dP_c}{dz} = -\frac{LQ\mu_o}{k_o} \tag{A.10}$$

These last two equations are also valid at any time. However, if it is assumed that the the end-point permeability is approximately equal to the absolute permeability [Paters and Flock, 1981], then these two equations may be approximated by the following equations:

at z=0:

$$\frac{dP_c}{dz} \approx \frac{LQ\mu_w}{K} \tag{A.11}$$

at z=1:

$$\frac{dP_c}{dz} \approx -\frac{LQ\mu_o}{K} \tag{A.12}$$

Equations (A.11) and (A.12) indicate that the differentials of P_c with respect to z can be treated as constants at the given limits. Hence, the conclusion can be drawn that $P_c(z)$ may be expressed by a set of straight line. Equation (A.8) will then be zero and f(z) will be proportional to the variable z as following:

$$f(z) \propto z \tag{A.13}$$

Appendix III

The neglection of the effects of buoyancy forces in the horizontal flow mode can be justified by considering the following:

The three-dimensional oil recovery for μ_o/μ_w=152.02 and Q=8.5 mL/h is 28.19%. By using the method describing in Chapter 6, the two-dimensional oil recovery shown on the relevant photograph is 30.20%. The difference between these values is 2.02%. Hence, it is reasonable to assume that the buoyancy (gravity) effects are effectively negligible in horizontal flow mode.

Appendix IV

The precision of the experimental data is a very important factor to make judgment if the experiments are reliable. Based on this point of view, some of the experiments was repeated. For each of the replication, the 95% confidence interval could be calculated, and this could be used to judge the reliability of the experiments [McLean, 1990]. The equation for calculating the confidence interval was employed as following:

$$\bar{y} \pm t_{v,0.025} \frac{s}{\sqrt{n}} \tag{A.14}$$

and

$$s = [\frac{1}{n-1} \sum_{i-1}^{n} (y_i - \bar{y})^2]^{1/2} \tag{A.15}$$

The experimental results employed were randomly selected. As one can see from Table A-1 that the 95% confidence interval is very smaller (the maximum is 0.0289 for the selected calculations). In other words, the reproducibility of the experiments is good. The precision of experimental data in present study could be considered as ±3%.

Appendix V

Performing a Calibration

This calibration sets a new scale factor for X,Y coordinate measurements. You can enter the distance in pixels between two points on the image or select two points directly by clicking on the image. The new number of calibrated units represented by the distance between the two points must then be entered: the default is 100 units.

To perform a two point calibration, the following procedure is followed:

1. Choose the *Measure* menu *Spatial Calibration* command.

2. When the *Spatial Calibration* dialog appears select the 2 Point option.

3. If you know the number of pixels in the distance you want to translate, enter the appropriate number in the *Old Distance* box.

4. If you need to use the image to determine the distance, click the Image button. The *Spatial Calibration* dialog disappears and the *Calibration Mode* dialog appears prompting you to select a calibration point. The cursor changes to a special calibration pointer. The status bar at the bottom of the image prompts you to select the first calibration point. It also displays the X,Y coordinates of the location of the pointer.

5. Click the first point, then move the pointer over the distance you want to calibrate and click the second point. The *Spatial Calibration* dialog reappears. The value in the *Old Distance* box is the distance in pixels between the two selected points.

6. Enter the value you want to use as the new measurement distance in the *New Distance* box.

7. Click OK. The pixel distance between the specified points is converted to the distance indicated in the *New Distance* box.

Table A-1. The Results of the Precision Calculations of Experimental Data

Name of the Experiments	Mean	Standard Deviation	95% Confidence Interval
Horizontal Case, μ_t=152.02, Q=27.6 mL/h	0.1787	0.0085	0.1787±0.0289
Horizontal Case, μ_t=152.02, Q=27.6 mL/h	0.1807	0.0058	0.1807±0.0197
Horizontal Case, μ_t=152.02, Q=27.6 mL/h	0.1001	0.0137	0.1001±0.0220
Horizontal Case, μ_t=152.02, Q=27.6 mL/h	0.0818	0.0048	0.0818±0.0095
Horizontal Case, μ_t=152.02, Q=27.6 mL/h	0.1740	0.0044	0.1740±0.0149

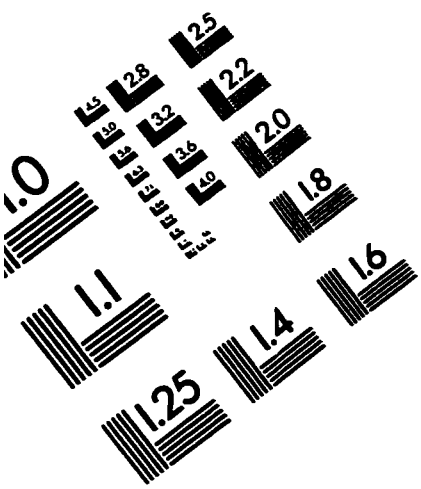

IMAGE EVALUATION TEST TARGET (QA-3)

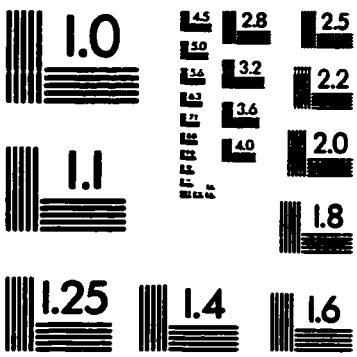

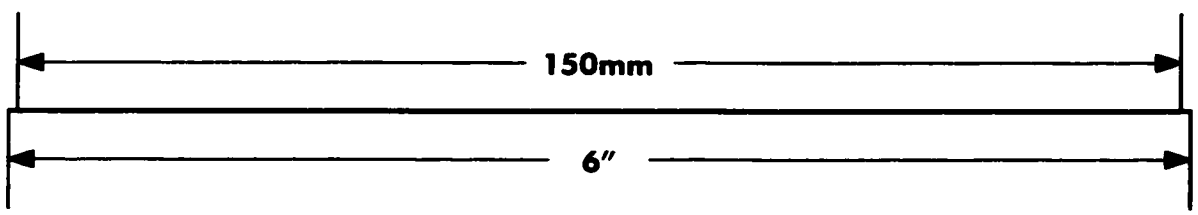

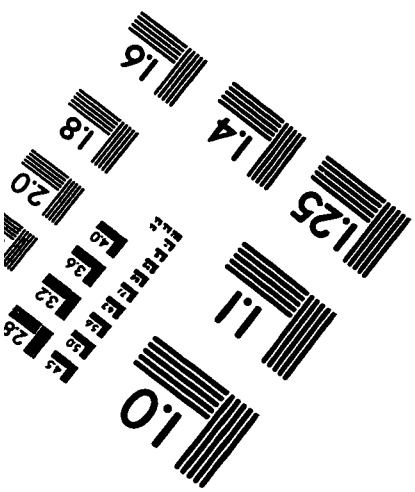

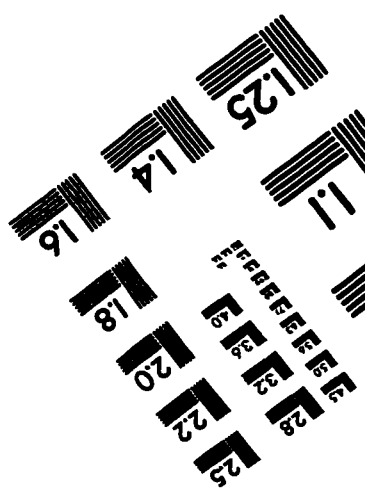

APPLIED IMAGE, Inc
1653 East Main Street
Rochester, NY 14609 USA
Phone: 716/482-0300
Fax: 716/288-5989